Tectonophysics 580 (2012) 58–87

Contents lists available at SciVerse ScienceDirect

Tectonophysics

journal homepage: www.elsevier.com/locate/tecto

From arc-continent collision to continuous convergence, clues from Paleogene conglomerates along the southern Caribbean–South America plate boundary

A. Cardona [a,b,*], C. Montes [b,c], C. Ayala [b,d], C. Bustamante [b,d], N. Hoyos [d], O. Montenegro [b,d], C. Ojeda [b,d], H. Niño [e], V. Ramirez [e], V. Valencia [f], D. Rincón [g], J. Vervoort [f], S. Zapata [b,d]

[a] Escuela de Procesos y Energía, Universidad Nacional de Colombia, Medellín, Colombia
[b] Corporación Geológica Ares, Bogotá, Colombia
[c] Geociencias, Universidad de los Andes, Bogotá, Colombia
[d] Smithsonian Tropical Research Institute, Balboa, Panamá
[e] Vicepresidencia de Exploración, Empresa Colombiana de Petroleos (ECOPETROL), Bogotá, Colombia
[f] School of Earth and Environmental Sciences, Washington State University, Pullman, WA, USA
[g] Instituto Colombiano del Petróleo (ICP-ECOPETROL), Piedecuesta, Colombia

ARTICLE INFO

Article history:
Received 27 December 2011
Received in revised form 21 August 2012
Accepted 25 August 2012
Available online 6 September 2012

Keywords:
Provenance
Paleogeography
South Caribbean margin
Orogenic collapse
Arc-continent collision

ABSTRACT

A Paleogene conglomeratic-sandy succession preserves the complex record of arc-continent collision, orogen collapse and basin opening, followed by inversion related to renewed oblique convergence. This record is unique because both arc and continental margin are now severely fragmented and only partially exposed along the southern Caribbean–South American boundary in northern Colombia. We studied these clastic sequences in the San Jacinto deformed belt using an integrated provenance study that includes conglomerate clast counting, geochemistry and U–Pb and Hf isotopic analysis in magmatic clasts, together with sandstone petrography, heavy mineral analysis and detrital zircon U–Pb geochronology. The record of events extracted from these coarse clastic rocks includes the formation and approach of an allochthonous Upper Cretaceous intra-oceanic arc active from 88 Ma until 73 Ma. This arc collides against the upper Paleozoic to Triassic continental margin after 73 Ma, but before late Paleocene times. Poorly exposed remnants of serpentinized peridotites and middle pressure metamorphic detritus are related to closure of an intervening oceanic basin between the continent and the colliding arc. This orogen was emerged in late Maastrichtian–early Paleocene, and then collapsed as recorded by the thick upper Paleocene and younger succession of the San Jacinto deformed belt where the coarse clastics, subject of this study, are exposed.
Orogenic collapse may have been the result of subduction zone flip, with incipient subduction of the buoyant Caribbean Plate under South America.

© 2012 Elsevier B.V. All rights reserved.

1. Introduction

Sediment-dominated accretionary wedges deposited in transitional to marine sedimentary environments may represent some of the thickest sediment accumulations on earth, and represent a major element of ancient and modern accretionary orogens (Cawood et al., 2009; Clift et al., 2002; Ingersoll et al., 2003). Their preservation and subsequent evolution in continental margins have major implications for crustal growth and recycling models and for the reconstruction of the kinematic and paleogeographic evolution of convergent margins (Cawood et al., 2009; Gray et al., 2007; Ingersoll et al., 2003; Kusky et al., 1997; Marsaglia, 2003; Onishi and Kimura, 1995; Snyder et al., 2002). These sediments are commonly sourced by the erosion of the adjacent uplifted margin and their substrate may be either oceanic, supra-subduction or continental crust (Foster et al., 2009; Ingersoll et al., 1995, 2003). Provenance analyses of these sedimentary deposits help elucidate the substrate where they were deposited, timing of arc-continent interactions, and identify the lithological characteristics of sutured collisional orogens. This is particularly useful as overimposed tectonic events mask the collisional and post-collisional evolution of the margins (Bahlburg et al., 2009; Cawood et al., 2009; Clift et al., 2008; Dewey and Mange, 1999; Foster et al., 2009; Hall, 2002; Mange et al., 2010; Trop et al., 2003).

The Late Cretaceous to Eocene tectonic evolution of northwestern South America has been dominated by the interaction of the South American continental margin with the margins of an allochthonous and Pacific-derived Caribbean oceanic plate (Bayona et al., 2011; Cardona et al., 2010; 2011; Jaillard et al., 2008, 2009; Pindell et al., 1998, 2005; Spikings et al., 2001, 2005; Vallejo et al., 2006, 2009; Weber et al., 2009, 2010). This scenario is expressed by a series of ocean-continent collisional orogens (either plateau-continent or

* Corresponding author at: Escuela de Procesos y Energía, Universidad Nacional de Colombia, Medellín, Colombia.
E-mail addresses: agustincardonam@gmail.com, agcardonamo@unal.edu.co (A. Cardona).

0040-1951/$ – see front matter © 2012 Elsevier B.V. All rights reserved.
http://dx.doi.org/10.1016/j.tecto.2012.08.039

arc-continent interactions), and the subsequent subduction attempts and relative eastern oblique displacement of the Caribbean oceanic plate under/against the northwestern South America continental margin (ibid).

This record of oceanic-continent collisions has been the focus of tectonostratigraphic analyses inboard, in the Colombian Andes (Fig. 1; Ayala-Calvo et al., 2010; Bayona et al., 2008; in press; Cardona et al., 2010; 2011; Gomez et al., 2005; Horton et al., 2010; Kennan and Pindell, 2009; Kerr et al., 1997; McCourt et al., 1984; Montes et al., 2005; Mora et al., 2010; Parra et al., 2009; Restrepo-Moreno et al., 2009; Weber et al., 2009, 2010; Villagómez, 2010; Villagómez et al., 2011). However, the sedimentary record closer to the sutures, and the subsequent evolution of the *fore-arc* segments of the margin, remains less well constrained (Cerón et al., 2007; Duque-Caro, 1979a,b, 1984; Flinch, 2003; Guzmán, 2007; Mantilla-Pimiento et al., 2009).

It is in this proximal position to the suture that the San Jacinto deformed belt is exposed as a discontinuous, long and narrow sedimentary wedge of Paleogene rocks deposited over magmatic substrate of oceanic affinity (Fig. 2, Duque-Caro, 1984). This belt is a morphological entity isolated from the major Andean Cordilleras and has been considered as an accretionary wedge deformed by Caribbean–South American convergence (Duque-Caro, 1984; Escalona and Mann, 2011; Mantilla-Pimiento et al., 2009; Pindell and Kennan, 2009; Pindell et al., 1998). However, the paucity of data, in particular compositional data from the siliciclastic rocks, has limited the understanding of the timing and style of interaction of the northern South America continental margin and the Caribbean plate.

Conglomerates of the San Jacinto deformed belt contain clasts that can be used to understand the plate tectonic evolution of this segment of the margin, where basement rocks are extensively covered and eroded (Clift et al., 2009; Dávila and Astini, 2007; Dupuis et al., 2009; Ferguson et al., 1996; Wanders et al., 2004).

In this contribution we present a regional provenance analysis of upper Paleocene to Eocene conglomerates and sandstones from the San Jacinto deformed belt in northern Colombia (Fig. 2). Different techniques such as conglomerate clast counting, clast geochemistry, U–Pb geochronology and zircon Hf isotopes, together with associated sandstone petrography and U–Pb detrital zircon geochronology, are used to understand the provenance of this belt. These new results together with published tectonostratigraphic constraints are used to reconstruct the tectonic evolution of the continental margin of northwestern South America from the Maastrichtian to the early Paleocene arc-continent collision, Paleocene-Eocene continental margin subsidence and related oblique convergence. When compared with the record in other segments of the Northern Andean margin and the Antilles, these results suggest that from 73 to 65 Ma there is a margin-wide collisional event in northern South American that reflects the accretion of not a single (Burke, 1988; Pindell and Kennan, 2009), but various Late Cretaceous intra-oceanic arcs that were formed at the margins of the Caribbean plate (Bustamante et al., 2011; Cardona et al., 2009; Neill et al., 2011; Vallejo et al., 2006; 2009; Weber et al., 2011; Wright and Wyld, 2011).

1.1. Geological setting

The more widely accepted model of the Caribbean–South American plate tectonic interactions suggest that the former includes a Cretaceous oceanic plateau segments formed in the Pacific plates (Burke, 1988; Cardona et al., 2010; Hughes and Pilatasig, 2002; Luzieux et al., 2006; Pindell, 1993; Pindell et al., 1998, 2005; Spikings et al., 2001, 2005;

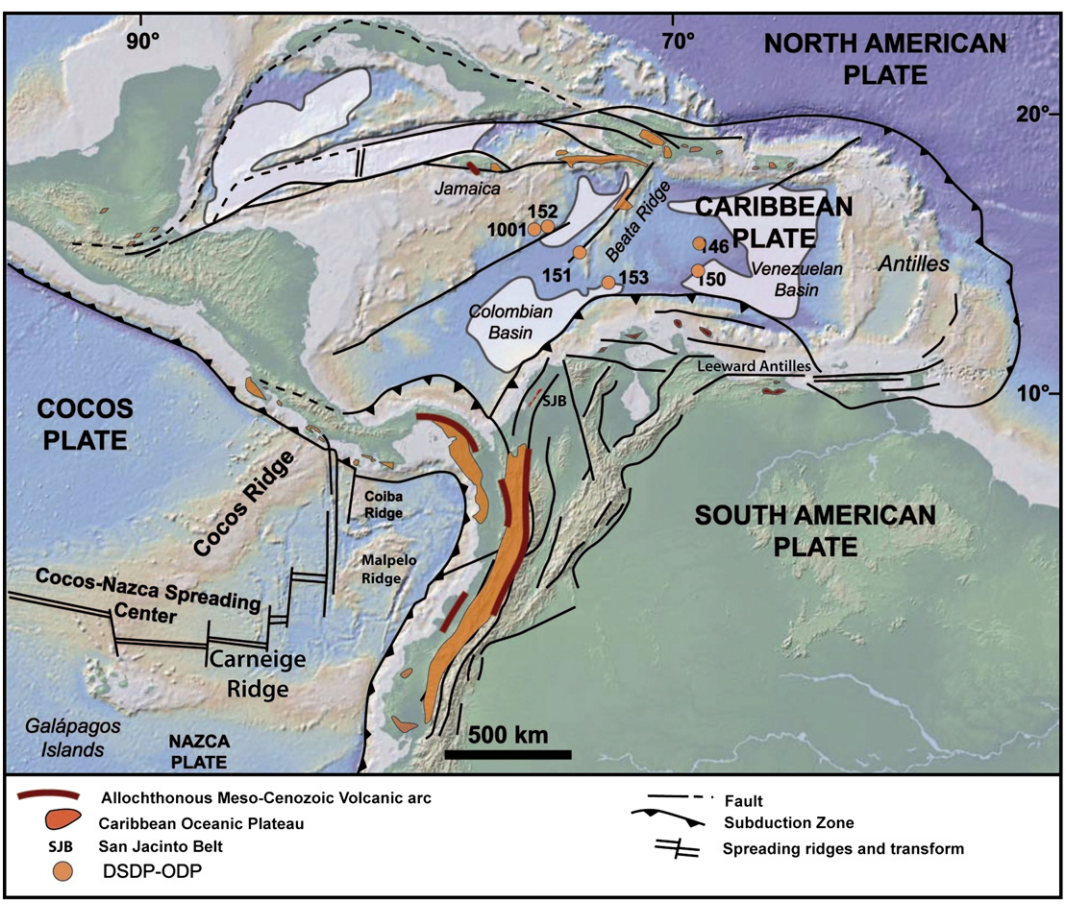

Fig. 1. Modern tectonic configuration including exposed intra-oceanic arc and plateau remnants of the northern Colombia and the Caribbean including the San Jacinto deformed belt (modified from Buchs et al., 2010).

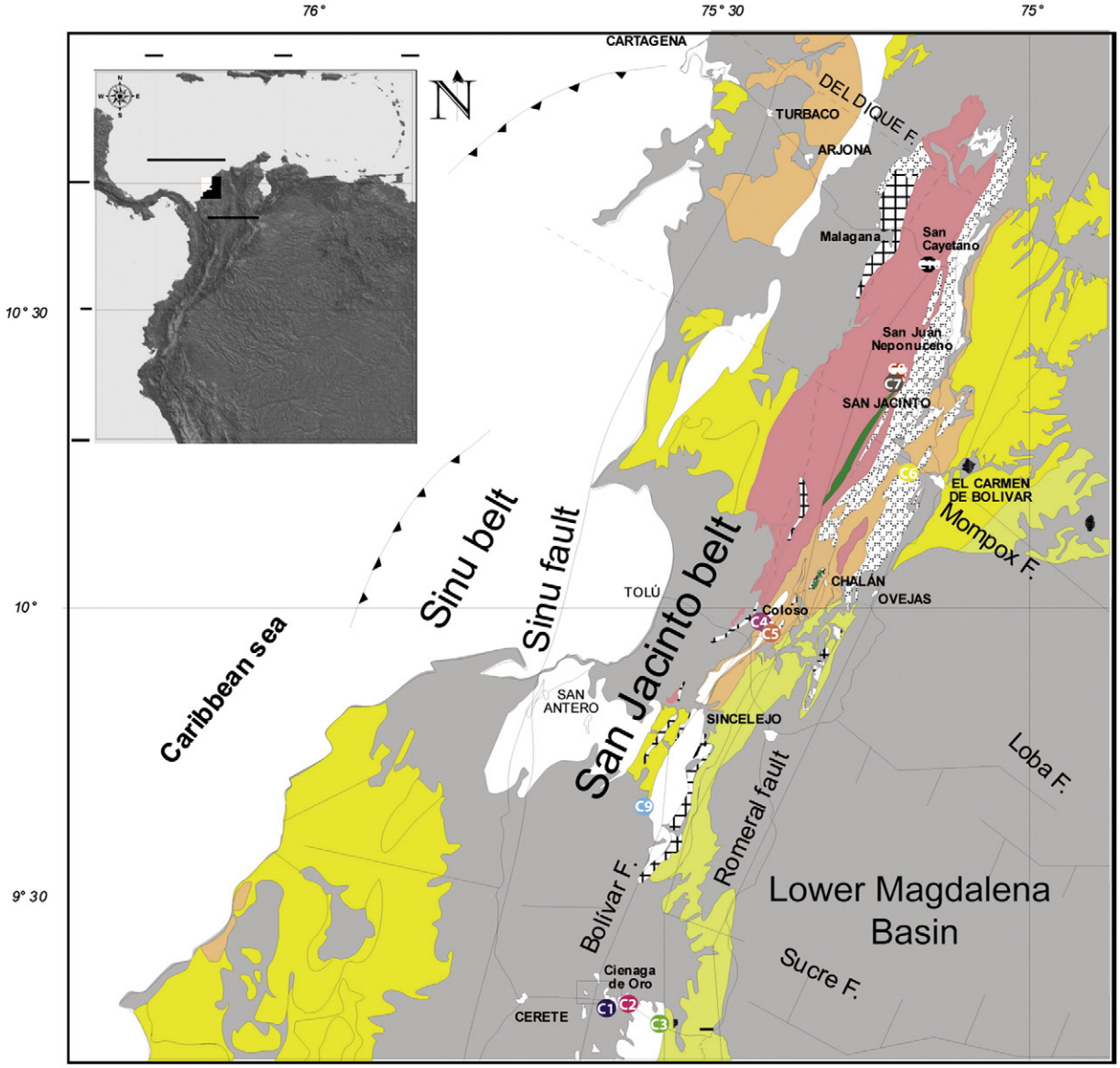

GEOLOGY

- **Cretaceous** (Fm. Cansona)
- **Late Paleocene - Early Eoceno** (Fm. San Cayetano)
- Early - Middle **Eocene** (Fm. Maco and Fm. Chengue)
- **Eoceno** (Fm. Tolú Viejo and Fm. Palenque)
- Late **Eocene** (Fm. San Jacinto, Pendales, Arroyo de Piedra and Fm. el Morro.
- **Oligocene** (Fm. Carmen, Ciénaga de Oro and Fm. Arjona)
- **Middle Miocene** (Fm. Mucacal, San Onofre, Mandatú, Alférez, Jesús del Monte, Hibácharo and Fm. Porquera)
- **Pliocene** (Fm. Tubará, Zambrano, Bayunca and Fm.Cerrito)

Station

- **C1:** **Cereté - Ciénaga de Oro** road (Fm. San Cayetano) (Analysis: **a, c, d, e**)
- **C2:** **Veraztegui - Ciénaga de Oro road** (Fm. San Cayetano) (Analysis: **a, c, d**)
- **C3:** **Ciénaga de Oro - La Ye road** (Fm. San Cayetano) (Analysis: **a, b, c, f**)
- **C4:** **Arroyo Seco** (Fm. San Cayetano) (Analysis: **a, b, c, d, e, f, g**)
- **C5:** **Arroyo Seco** (Fm. Tolú Viejo) (Analysis: **a, b, e, g**)
- **C6:** **Arroyo Alférez** (Fm. San Jacinto) (Analysis: **a, b, c, f**)
- **C7:** **Arroyo Pijiguay** (Fm. Macó) (Analysis: **a, b, c, f**)
- **C8:** **Arroyo del medio** (Fm. Macó) (Analysis: **a, b, c, e**)
- **C9:** **Tuchín (same locality of Zimmerle, 1968)** (Analysis: c)
- **C10:** **Ye del Carreto - San Cayetano road** (Fm. san Cayetano) (Analysis: **b**)

(a) Conglomerate clasts count, **(b)** Petrography, **(c)** Volcanic clast geochemistry, **(d)** Plutonic clast geochemistry, **(e)** Heavy minerals, **(f)** U-Pb detrital geochronology, **(g)** U-Pb and Hf plutonic clasts.

Fig. 2. Geological map of the San Jacinto deformed belt in northern Colombia (modified from Guzman et al., 2004; Guzmán, 2007).

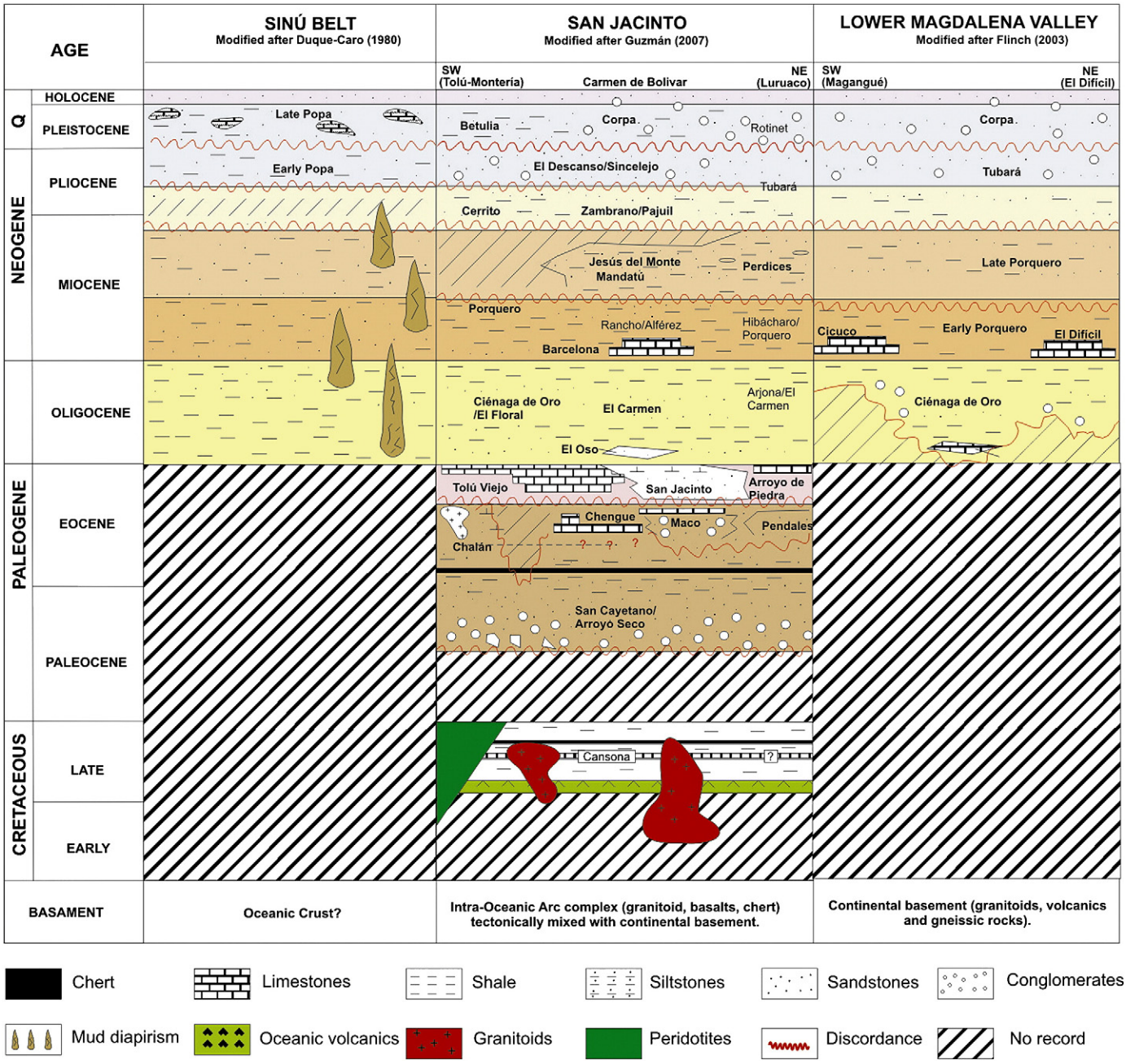

Fig. 3. Stratigraphic chart from the San Jacinto deformed belt and the adjacent Sinu belt and Lower Magdalena Valley (modified from Duque-Caro, 1980; Flinch, 2003; Geotec, 1997; Guzmán, 2007; Guzman et al., 2004).

Table 1
Results of conglomerate clasts analysis including coordinates of field localities.

Clast/station	C1	C2	C3	C4	C5	C6	C8	C10
Coordinates N	14774204	1472763	1470883	1537044	1536818	1566624	1586564	1605481
Coordinates E	823500	832107	8352112	852780	852780	881515	8794775	884051
Basalt-Andesite	28	44	35	29	NR	NR	67	40
Porphyritic Andesite	12	12	19	27	NR	NR	12	23
Granite	3	0	3	0	NR	NR	NR	10
Granodiorite	1	24	37	15	NR	NR	NR	27
Chert	12	20	5	13	38	NR	8	NR
Limestone	NR	NR	NR	10	NR	7	NR	NR
Sandstone	NR	NR	NR	4	NR	2	6	NR
Mudstone	NR	NR	NR	NR	NR	82	NR	NR
Gneiss	3	NR	1	NR	NR	NR	NR	NR
Quartzite	18	NR	NR	NR	NR	NR	7	NR
Milky quartz	23	NR	NR	2	62	9	NR	NR

Vallejo et al., 2006, 2009; Van del Lelij et al., 2010; Weber et al., 2009, 2010; Wright and Wyld, 2011). This oceanic plateau was formed south of its current position, and migrates to occupy an inter-American position by consuming a post-Pangea, proto-Caribbean oceanic crust. Within its trajectory and since the Late Cretaceous, a single or several intra-oceanic arcs were built at its margins and obliquely collided with the northwestern South America.

Several accreted oceanic basaltic and plutonic segments, found in the Andes and the northern Caribbean margins of South America, are related to this interaction (Cardona et al., 2010; Kerr et al., 1997, 2003; Luzieux et al., 2006; Marresh et al., 2009; Sisson et al., 2005; Spadea and Espinosa, 1996; Vallejo et al., 2006; Weber et al., 2009).

Following the collisional phases, the northeastern displacement of the Caribbean plate and the North–south America convergence created extensive block displacement and rotation, and the Caribbean plate began its subduction under the South American plate (Cardona et al., 2011; Montes et al., 2010; Müller et al., 1999; Pindell et al., 1998; 2005; Vallejo et al., 2006; 2009).

In northern Colombia, the Caribbean margin is marked by a series of isolated massifs and ranges, bound by Cenozoic sedimentary basins that contrast with the continuous nature of the Andean Cordillera to the south. The San Jacinto deformed belt Colombia is one of those isolated domains (Fig. 1), and is exposed as a discontinuous series of ranges formed by an extensive upper Paleocene to Oligocene sedimentary succession deposited over the remnants of a poorly known intra-oceanic and mixed oceanic/continental crust (Cerón et al., 2007; Duque-Caro, 1984; Mantilla-Pimiento et al., 2009). Regional tectonic interpretations have considered this belt as an accretionary wedge formed within the intra-oceanic Caribbean arc, or as a sedimentary wedge deposited over the migrating Caribbean plate (Duque-Caro, 1984; Escalona and Mann, 2011; Flinch, 2003; Pindell and Kennan, 2009). The deformation and accretion of this wedge to the upper continental plate took place in the Oligocene (Duque-Caro, 1984).

In the next chapter we present the tectonostratigraphic framework of the San Jacinto deformed belt in order to present and discussed the provenance data within a regional framework.

1.2. Tectonostratigraphic constraints from the San Jacinto deformed belt

The San Jacinto deformed belt is exposed as three discontinuous ranges with a N20°E trend (Figs. 1 and 2, Duque-Caro, 1979a,b). This belt records marine to transitional sedimentation between the late Paleocene to Oligocene times (Fig. 3, Duque-Caro, 1984; Flinch, 2003; Guzmán, 2007).

To the southwest, it is bound by the Romeral fault zone, which is a positive flower structure that separates it from the post-Eocene sediments of the Lower Magdalena Basin (Cerón et al., 2007; Mantilla-Pimiento et al., 2009). This basin contains a coherent continental ensialic basement of Triassic age and correlatable with the basement exposed in the Central Cordillera (Cerón et al., 2007; Mantilla-Pimiento et al., 2009; Montes et al., 2010; Rincón et al., 2007). The Romeral fault zone which is traceable along the Andean Cordilleras has been considered as the suture zone between the Caribbean and the South American continent that was remobilized by subsequent tectonic events (Duque-Caro, 1979a,b; Flinch, 2003; Mantilla-Pimiento et al., 2009).

The Lower Magdalena basin is considered as a post-late Eocene rotational basin linked to the advance of the Caribbean plate, or as a non-magmatic fore-arc basin (see reviews in Duque-Caro, 1979a,b; Flinch, 2003; Montes et al., 2010). To the northwest, the San Jacinto deformed belt is bound by a younger sedimentary accretionary prism (Sinu Belt) of Mio-Pliocene age (Duque-Caro, 1984). This younger belt has also been considered an accretionary wedge linked to the Caribbean–South American interaction, and as a major component of the South Caribbean deformed belt (Duque-Caro, 1984; Escalona and

Table 2
Sandstone framework analysis. Qm = monocrystalline quartz, Qsed = sedimentary quartz, QPF = foliated polycrystalline quartz, Qc = chert, Fk = K-Feldspar, Pl = plagioclase, Fm = microcline, Ls = sedimentary lithic, Lmm = micaceous metamorphic lithic, Lmc = chloritic metamorphic lithic, Lma = amphibolic metamorphic lithic, Lmn = gneissic lithic, Lv = volcanic lithic, Lvv = vitreous volcanic lithic, Lp = plutonic lithic, Lu = ultramafic lithic, MP = heavy mineral, Op = opaque, Mic = micas, Pe/Fo =, Gl = glauconite, Intcal = calcareous intraclast, Intsil = siliciclastic intraclast, Fos = fossils, Mtx = matrix, Cem = Cement, Org. Mat = Organic matter.

Interval	Sample	Locality	Grain size (mm)	Total points	Standard framework (without interstitial material)																									Interstitial		
					Quartz					Feldspar			Lithics									Accesories										
					Qm	Qsed	Qpf	Qpd	Qc	Fk	Pl	Fm	Ls	Lmm	Lmc	Lma	Lmn	Lv	Lvv	Lp	Lu	MP	Op	Mic	Pe/Fo	Gl	Intcal	Intsil	Fos	Mtx	Cem.	Org. Mat
Late Eoc.	7100	C1	0.1 – 0.2	497	47.28	0	0	2.62	0.6	7.04	0	0	0	0	0	0	0	0	0	0.2	0	0	0	0	0	0	2.62	0	0	0	0	39.64
Late Eoc.	7744	C6	0.3 – 1.0	335	47.76	0	2.39	15.22	5.07	4.48	8.36	0	0	2.99	0	0	0	0	1.8	0	0	0.9	0.6	0	0	0	0	0	0	0	0	10.45
Middle Eoc.	7096	C7	0.8 – 1.5	325	28	0	1.54	21.54	0	13.5	8.62	0	0	5.23	0	0	0	5.23	0	4	1.2	1.85	0	0	0	1.5	0	0	0	0	0	7.69
Middle Eoc.	7095	C7	0.3 – 1.5	364	31.32	0	1.1	12.09	4.12	4.95	16.2	0.27	4.67	0	0	0	0	3.85	0	2.2	0	1.65	0	0	0	0	0	0	0	0	0	17.58
Middle Eoc.	7753	C8	0.5 – 1.0	300	14	0	0.33	28.67	0	9	15.7	0	0	0	0.67	0	0	0.33	0	10	0	4	17	0	0	0	0.33	0	0	0	0	0
Pal-Early Eoc.	7075	C3	1.0 –1.5	300	22.67	0	2.67	37.67	3.33	11.7	8	1.33	4	1.33	0	0	2.33	1.33	0	0.67	0	3	0	0	0	0	0	0	0	0	0	0
Pal-Early Eoc.	7078	C5	0.5 – 1.5	321	22.74	0	0	4.67	35.2	2.8	2.8	0	10.6	0.31	0	0	0	8.41	0	0.93	0	0.31	0	0	0	0	0	0	0	0	0	11.21
Pal-Early Eoc.	7118	C4	0.2 – 0.5	375	14.4	0	1.33	11.47	10.4	8.53	14.4	0.27	6.67	7.73	0	0	0	2.4	0	1.6	0	0.27	0.53	0	0	0	0	0	0	0	0	20
Pal-Early Eoc.	7119	C4	0.30 – 0.5	383	10.97	0	2.61	16.97	3.92	11	18	0	1.83	5.74	0	0	0	2.87	0	1.83	0	1.83	0.78	0	0	0	0	0	0	0	0	21.67
Pal-Early Eoc.	7123	C4	1.0 – 1.5	311	14.47	0	5.14	30.55	5.14	6.11	6.75	0	9.65	7.07	0	0	2.25	3.86	0	5.47	0	0	0	0	0	0	0	0	0	0	0	3.54
Pal-Early Eoc.	7762	C1O	1.0 – 1.5	332	25	0	1.51	8.13	0	11.8	23.2	0	1.2	0	3.92	0	0	2.11	0	10.5	0	0.3	2.71	0	0	0	0	0	0	9.64	0	0

Table 3
Heavy mineral analysis.

Sample	Field locality	Rutile	Turmaline	Zircon	Garnet	Apatite	Muscovite	Chlorite	Epidote	Titanita	Kyanite	Hornblende	Zoisite	Pyroxene	Total
7685	C1	1	7	29	4	–	–	–	21	–	57	–	2	163	284
7369	C4	49	6	89	–	11	–	–	–	–	–	–	–	–	155
7004	C5	–	1	42	–	4	6	–	–	21	–	–	144	–	218
7005	C5	–	65	44	13	–	2	1	3	19	59	9	2	–	217
7006	C5	–	2	138	–	70	–	–	–	4	–	–	–	–	214
7557	C7	3	27	50	10	–	–	–	51	123	–	–	8	–	272

Mann, 2011; Pindell et al., 1998, 2005; Pindell and Kennan, 2009; Toto and Kellogg, 1992).

The stratigraphic chart of the San Jacinto deformed belt is presented in Fig. 3. Basement is constituted of highly weathered basalts intercalated with volcanic and sedimentary rocks, as well as some remnants of serpentinized peridotitic units and associated gabbros (Duque-Caro, 1984; Guzmán, 2007). 2D seismic imaging, gravimetric and magnetometric geophysical modelling, also suggests that a basaltic volcano-sedimentary units tectonically intermixed with continental crust (Cerón et al., 2007; Mantilla-Pimiento et al., 2009).

The older and lowest sedimentary sequence which is the substrate of the Paleogene sediments includes an intercalation of mudstones, siltstones, cherts and some tuffs grouped within the Cansona Formation (Duque-Caro, 1972; Geotec, 1997; Guzmán, 2007; Guzman et al., 2004). This 600–1200 m thick unit seems to locally overly basalts and agglomerates. Micropaleontological constrains suggest a Santonian to Maastricthian depositional age (Dueñas and Gómez, 2011; Duque-Caro, 1972; Geotec, 1997; Guzman et al., 2004).

Overlying the Cansona Formation are the correlative San Cayetano and Arroyo Seco formations, which are widely distributed along the San Jacinto deformed belt and may reach 350–500 m of stratigraphic thickness (Duque-Caro, 1972; Guzmán, 2007; Fig. 2). They include a prominent fining-upward siliciclastic sequence that varies from conglomerates, conglomeratic sandstones to fine-grained sandstones and mudstones. Micropaleontological material recovered from these sequences, including benthonic foraminifera, suggests a late Paleocene to early Eocene age (Bürgl, 1961; Duque-Caro, 1979a,b; Duque-Caro et al., 1991, 1996; Geotec, 1997; Guzmán, 2007; Guzman et al., 2004; Rubio et al., 2009). These units have been interpreted to have accumulated in deep to bathyal turbiditic environments (Duque-Caro et al., 1996; Geotec;, 1997; Guzmán, 2007; Rubio et al., 2009).

The laterally equivalent Maco, Chengue and Pendales formations overly the San Cayetano–Arroyo Seco formations and include sandstones and conglomeratic sandstone that laterally grade, or are intercalated with mudstones, limestone and marls, formed in fan deltas and shallow platforms. Foraminiferal constraints on these units indicate a middle Eocene age (Duque-Caro, 1968, 1972; Duque-Caro et al., 1996).

Overlying this units are the Tolu Viejo, San Jacinto and Arroyo de Piedra formations which are composed of limestones intercalated with silstones and mudstone and have a stratigraphic thickness of at least 800 m (Duque-Caro et al., 1996). These units were formed in a shallow environment of bioherms and fan deltas formed during late Eocene-early Oligocene times (Bürgl, 1961; Geotec, 1997; Rubio et al., 2009).

2. Methods

2.1. Conglomerates and sandstone analysis

Conglomerate clasts analyses were carried in accessible localities following the ribbon count method (Howard, 1993). Those clasts <2 cm in size were excluded from the analysis. Results are presented in Table 1.

Eleven sandstones interspersed with the conglomerates were collected and point-counted to determine their composition and provenance. Sandstones were stained for feldspar recognition. Thin sections were scanned as a 1800 dpi high resolution image and open as a grid with Image J software. This software from the National Institute of Health was used as an automatic sandstone framework counter. Results can be export and used directly in any graphic or spreadsheet application.

Petrographic procedure followed framework analysis after Dickinson (1985) and Folk (1980) and included the identification of different categories of igneous and metamorphic lithics (Table 2).

2.2. Heavy minerals

Sandstone samples were crushed, sieved and hydraulically concentrated in the <400 μm fraction. Subsequently sodium polytungstate was used to obtained the >2.89 g/cm^3 fraction. Grains were mounted using the Meltmount ® resin with a refraction index of 1.539. Mineral identification of ca. 300 translucent grains were done following the ribbon method (Mange and Maurer, 1991). Results are presented in Table 3.

2.3. U–Pb geochronology

U–Pb-Th geochronology was conducted at the Washington State University at Pullman following procedures established by Chang et al. (2006). Zircon crystals were extracted from samples by traditional methods of crushing and grinding, followed by separation with a Wilfley table, heavy liquids, and a Frantz magnetic separator. Samples were processed such that all zircons were retained in the final heavy mineral fraction. Picking of zircon crystals was done on plutonic samples which in general are characterized by relatively low zircon abundance. A split of zircons grains was selected from the grains available in the detrital samples and photographed. Zircons were incorporated into a 1″ epoxy mount together with standard zircons. The mounts were sanded down to a depth of ~20 μm, polished, and cleaned prior to isotopic analysis.

In the case of the zircons recovered from plutonic rocks, most of the analyses were done at the zircon tips in order to constrain the late zircon crystallization history (Valencia et al., 2005). In detrital samples, the cores of the grains were analyzed to avoid complex zircon histories (Gehrels et al., 2006).

All LA-ICP-MS U–Pb analyses were conducted at Washington State University using a New Wave Nd: YAG UV 213-nm laser coupled to a ThermoFinnigan Element 2 single collector, double-focusing, magnetic sector ICP-MS. Laser spot size and repetition rate were 30 μm and 10 Hz, respectively. He and Ar carrier gases delivered the sample aerosol to the plasma. Each analysis consisted of a short blank analysis followed by 300 sweeps through masses 204, 206, 207, 208, 232, 235, and 238, taking approximately 35 s.

LA-ICP-MS isotopic analyses are affected by two forms of interelement fractionation that must be corrected (Kosler and Sylvester, 2003). Time-dependent fractionation results from the more efficient

Table 4
U–Pb LA-ICP-MS analytical and age results from the analyzed plutonic clasts.

Sample name	238U 206Pb	1 sigma % Error	207Pb 206Pb	1 sigma % Error	206/238 Age (Ma)	1 sigma err (Ma)	207/206 Age (Ma)	1 sigma err (Ma)	Selected Age (Ma)	1 sigma err (Ma)
Sample 7005 (C5)										
7005_30	85.91694	2.44%	0.04559	2.47%	74.6	1.8	0.0	34.4	74.6	1.8
7005_29	85.29838	2.65%	0.05560	2.76%	75.1	2.0	436.4	60.3	75.1	2.0
7005_28	84.77677	2.26%	0.04714	2.20%	75.6	1.7	56.6	51.7	75.6	1.7
7005_27	82.90943	2.76%	0.04827	2.75%	77.3	2.1	112.3	63.6	77.3	2.1
7005_26	79.88820	2.54%	0.07222	2.58%	80.2	2.0	992.1	51.6	80.2	2.0
7005_25	80.23942	2.64%	0.10433	2.75%	79.8	2.1	1702.6	49.8	79.8	2.1
7005_24	83.03603	2.50%	0.05043	2.35%	77.2	1.9	214.8	53.6	77.2	1.9
7005_23	85.26149	2.51%	0.04961	2.36%	75.2	1.9	176.7	54.1	75.2	1.9
7005_22	85.11549	2.58%	0.05143	2.26%	75.3	1.9	260.3	51.1	75.3	1.9
7005_21	82.24912	2.41%	0.05195	2.25%	77.9	1.9	283.4	50.8	77.9	1.9
7005_20	82.83085	2.14%	0.04828	1.83%	77.4	1.6	112.8	42.5	77.4	1.6
7005_19	83.55528	2.37%	0.05459	2.67%	76.7	1.8	395.3	58.9	76.7	1.8
7005_18	81.68980	2.30%	0.04917	2.42%	78.4	1.8	156.1	55.6	78.4	1.8
7005_17	84.40753	2.44%	0.05154	2.62%	75.9	1.8	265.1	59.1	75.9	1.8
7005_16	86.87814	2.54%	0.04705	2.47%	73.8	1.9	51.7	58.0	73.8	1.9
7005_15	88.87562	2.22%	0.04997	2.06%	72.1	1.6	193.4	47.2	72.1	1.6
7005_14	86.29472	2.28%	0.05007	2.14%	74.3	1.7	198.2	48.9	74.3	1.7
7005_13	82.73420	2.33%	0.04837	2.17%	77.5	1.8	117.5	50.4	77.5	1.8
7005_12	86.67606	2.30%	0.04948	2.34%	73.9	1.7	170.6	53.8	73.9	1.7
7005_11	88.99103	2.43%	0.05119	2.66%	72.0	1.7	249.3	60.0	72.0	1.7
7005_10	88.87621	2.64%	0.04223	2.62%	72.1	1.9	0.0	0.0	72.1	1.9
7005_9	79.53407	2.27%	0.04646	2.35%	80.5	1.8	21.4	55.6	80.5	1.8
7005_8	88.40201	2.49%	0.04803	2.39%	72.5	1.8	100.9	55.5	72.5	1.8
7005_7	88.94947	2.24%	0.04869	2.41%	72.1	1.6	132.8	55.6	72.1	1.6
7005_6	87.90856	2.31%	0.05170	2.30%	72.9	1.7	272.2	51.8	72.9	1.7
7005_5	85.73429	1.98%	0.05195	1.67%	74.8	1.5	283.3	37.7	74.8	1.5
7005_4	82.20087	2.25%	0.04669	1.75%	77.9	1.7	33.3	41.5	77.9	1.7
7005_3	88.10638	2.09%	0.05147	1.74%	72.8	1.5	262.2	39.4	72.8	1.5
7005_2	85.72424	2.13%	0.04822	1.76%	74.8	1.6	110.3	41.1	74.8	1.6
7005_1	85.64944	2.08%	0.05258	2.34%	74.8	1.5	310.9	52.4	74.8	1.5
Sample 7006 (C5)										
7006_24	85.00431	2.11%	0.04694	1.43%	75.39	1.58	46.06	33.72	75.39	1.58
7006_23	82.78871	2.19%	0.04881	1.78%	77.40	1.68	138.67	41.31	77.40	1.68
7006_22	84.31704	2.14%	0.04849	1.52%	76.00	1.62	123.35	35.45	76.00	1.62
7006_21	76.34695	2.08%	0.04857	1.42%	83.89	1.73	126.96	33.12	83.89	1.73
7006_20	83.77884	2.15%	0.04877	1.39%	76.49	1.64	136.63	32.37	76.49	1.64
7006_19	88.05154	2.48%	0.05302	2.58%	72.80	1.79	329.70	57.60	72.80	1.79
7006_18	81.10771	2.21%	0.05085	1.41%	78.99	1.73	233.94	32.12	78.99	1.73
7006_17	86.86562	2.47%	0.04975	2.29%	73.79	1.82	183.20	52.44	73.79	1.82
7006_16	86.31753	2.15%	0.04988	1.31%	74.25	1.58	189.39	30.18	74.25	1.58
7006_14	86.60489	2.17%	0.04814	1.38%	74.01	1.60	105.97	32.20	74.01	1.60
7006_13	86.69060	2.65%	0.04943	2.58%	73.94	1.95	168.31	59.24	73.94	1.95
7006_12	75.33610	2.29%	0.04833	1.71%	85.01	1.93	115.57	39.92	85.01	1.93
7006_11	85.27833	2.28%	0.04755	1.95%	75.15	1.70	76.87	45.67	75.15	1.70
7006_10	83.50518	2.22%	0.04685	1.68%	76.74	1.69	41.69	39.72	76.74	1.69
7006_9	84.09624	2.24%	0.05574	1.80%	76.20	1.70	442.07	39.54	76.20	1.70
7006_8	84.16131	2.17%	0.04794	1.35%	76.14	1.64	96.20	31.73	76.14	1.64
7006_7	84.78095	2.26%	0.05044	2.00%	75.59	1.70	215.50	45.63	75.59	1.70
7006_6	84.95560	2.35%	0.04786	1.83%	75.44	1.76	92.19	42.80	75.44	1.76
7006_5	86.97693	2.16%	0.04724	2.13%	73.69	1.58	61.24	49.99	73.69	1.58
7006_4	83.85033	2.11%	0.04829	2.13%	76.43	1.60	113.39	49.57	76.43	1.60
7006_3	85.86213	2.23%	0.04865	2.43%	74.64	1.66	130.87	56.15	74.64	1.66
7006_2	84.24715	2.23%	0.04554	2.46%	76.07	1.69	0.00	31.32	76.07	1.69
7006_1	83.45249	2.41%	0.04803	2.72%	76.79	1.84	100.95	63.02	76.79	1.84
Sample 7003 (C4)										
7003_41a	88.65327	3.41%	0.04380	2.60%	72.3	2.5	0.0	0.0	72.3	2.5
7003_40a	87.20588	3.47%	0.04497	2.88%	73.5	2.5	0.0	8.8	73.5	2.5
7003_39a	88.95534	3.35%	0.05595	2.32%	72.1	2.4	450.4	50.7	72.1	2.4
7003_38a	90.03362	3.10%	0.04974	1.35%	71.2	2.2	182.8	31.1	71.2	2.2
7003_37a	89.19860	3.49%	0.05117	2.98%	71.9	2.5	248.4	67.2	71.9	2.5
7003_36a	86.23430	3.34%	0.04878	2.56%	74.3	2.5	137.4	59.0	74.3	2.5
7003_35a	89.85279	3.36%	0.04961	2.34%	71.3	2.4	176.8	53.7	71.3	2.4
7003_33a	89.80708	3.38%	0.04513	2.49%	71.4	2.4	0.0	8.7	71.4	2.4
7003_32a	88.50538	3.41%	0.04978	2.72%	72.4	2.5	184.9	62.1	72.4	2.5
7003_30a	88.79587	3.42%	0.04918	2.99%	72.2	2.5	156.6	68.4	72.2	2.5
7003_29a	88.19503	3.37%	0.04756	3.03%	72.7	2.4	77.3	70.5	72.7	2.4
7003_28a	87.60551	3.27%	0.05358	2.45%	73.2	2.4	353.6	54.4	73.2	2.4
7003_27a	85.15077	3.32%	0.04831	2.68%	75.3	2.5	114.6	61.9	75.3	2.5
7003_25a	92.82441	4.16%	0.05763	4.68%	69.1	2.9	515.8	99.6	69.1	2.9
7003_26a	88.75889	3.40%	0.04916	2.68%	72.2	2.4	155.5	61.5	72.2	2.4
7003_24a	88.38614	3.31%	0.05283	2.79%	72.5	2.4	321.6	62.1	72.5	2.4

Table 4 (*continued*)

Sample	238U	1 sigma	207Pb	1 sigma	206/238	1 sigma	207/206	1 sigma	Selected	1 sigma
name	206Pb	% Error	206Pb	% Error	Age (Ma)	err (Ma)	Age (Ma)	err (Ma)	Age (Ma)	err (Ma)
7003_23a	89.94038	3.39%	0.04892	2.76%	71.3	2.4	144.0	63.4	71.3	2.4
7003_21a	91.38111	3.37%	0.04817	2.63%	70.2	2.3	107.6	60.8	70.2	2.3
7003_19a	88.90837	3.56%	0.04674	3.46%	72.1	2.6	37.7	79.0	72.1	2.6
7003_20a	87.50883	3.35%	0.04733	2.79%	73.2	2.4	66.5	64.6	73.2	2.4
7003_19a	88.90837	3.56%	0.04674	3.46%	72.1	2.6	37.7	79.0	72.1	2.6
7003_17a	86.47723	3.76%	0.04950	3.87%	74.1	2.8	171.6	88.0	74.1	2.8
7003_16a	88.36750	3.45%	0.05251	2.67%	72.5	2.5	307.8	59.6	72.5	2.5
7003_15a	86.17969	3.31%	0.05530	2.27%	74.4	2.4	424.5	49.9	74.4	2.4
7003_14a	90.72013	3.29%	0.04593	2.16%	70.7	2.3	2.7	44.7	70.7	2.3
7003_13a	90.27814	3.36%	0.05017	2.22%	71.0	2.4	202.8	50.7	71.0	2.4
7003_12a	87.65162	3.34%	0.04946	2.57%	73.1	2.4	169.9	58.9	73.1	2.4
7003_10a	86.82341	2.76%	0.04873	2.23%	73.8	2.0	134.7	51.6	73.8	2.0
7003_6a	94.17460	2.94%	0.04897	2.99%	68.1	2.0	146.3	68.7	68.1	2.0
7003_5a	89.79141	2.70%	0.04647	2.29%	71.4	1.9	22.5	53.8	71.4	1.9
7003_4a	88.59839	2.91%	0.04813	2.98%	72.4	2.1	105.7	69.0	72.4	2.1
7003_3a	87.68034	3.03%	0.05732	3.11%	73.1	2.2	503.8	67.0	73.1	2.2
7003_1a	89.44171	2.76%	0.04895	2.25%	71.7	2.0	145.6	52.0	71.7	2.0
7003_9a	80.04409	2.80%	0.04970	2.23%	80.0	2.2	180.9	51.2	80.0	2.2
7003_8a	70.78166	2.69%	0.04811	2.11%	90.4	2.4	104.5	49.0	90.4	2.4
7003_34a	73.16860	3.23%	0.04810	1.97%	87.5	2.8	104.2	45.9	87.5	2.8
7003_11a	80.19782	2.81%	0.04386	2.40%	79.9	2.2	0.0	0.0	79.9	2.2

volatilization of Pb over U as the laser excavates successively deeper levels in the ablation pit during an analysis, which in turn leads to an increase in $^{206}Pb/^{238}U$ and $^{207}Pb/^{235}U$ ratios with time (Eggins et al., 1998). By definition, time-dependent fractionation is zero at the beginning of the analysis. Regression of time series data to the intercept at $t=0$, therefore, yields the point at which time-dependent fractionation equals zero.

Time-independent (or static) fractionation is the largest source of uncertainty in LA-ICP-MS U–Pb geochronology and results from mass and elemental static fractionation in the plasma and also poorly understood laser-matrix effects (Kosler and Sylvester, 2003). It is corrected by normalizing U/Pb and Pb/Pb ratios of the unknowns to the zircon standards (Chang et al., 2006). For this study we used two zircon standards: Peixe, with an age of 564 Ma (Dickinson and Gehrels, 2003), and FC-1, with an age of 1099 Ma (Paces and Miller, 1993). Peixe was used to correct the $^{238}U/^{206}Pb$ and $^{235}U/^{207}Pb$ ratios and FC-1 was used to correct the $^{207}Pb/^{206}Pb$ ratios.

Common Pb can represent a proportionally large contribution to the total Pb in Mesozoic and younger U-poor zircons. However, common Pb is typically not significant in LA-ICP-MS analyses, most likely because it is concentrated in cracks and inclusions, which can be avoided. When this is not possible, the influence of common Pb is easy to recognize on Tera-Wasserburg diagrams because analyses tend to line up on a steep linear trajectory that can be anchored at a reasonable $^{207}Pb/^{206}Pb$ common lead composition (y-intercept) (DeGraaff–Surpless et al., 2002). Common Pb corrections were made on these analyses using the ^{207}Pb method (Williams, 1998). Uranium-lead data were reduced using Isoplot (Ludwig, 2007). The final crystallization ages that we report are Concordia or intercept ages, which were determined by using the following procedure. In most of our samples, the majority of analyses form a single dominant cluster around a single spot on or just above concordia in Tera-Wasserburg space, which we interpret to be the approximate age of the sample. Analyses that gave $^{207}Pb/^{206}Pb$ ages overlapping in uncertainty with their $^{206}Pb/^{238}U$ ages were judged to be concordant. The reported error ages followed two uncertainties: the first is derived from the concordant or intercept age calculation alone (time dependent), and the second represents our systematic uncertainty during that session (time independent), with the error from the standards quadratically added to the analytical error.

U–Pb zircon crystallization ages were estimated and plot using Isoplot 3.62 (Ludwig, 2007). The uncertainty of the age is determined as the quadratic sum of the weighted mean error plus the total systematic error for the set of analyses. The systematic error, which includes contributions from the standard calibration, age of the calibration standard, composition of common Pb, and U decay constants, is generally ~1–2% (2-sigma). For the detrital samples probability plots were also obtained with the ISOPLOT 3.62 (Ludwig, 2007). Representative age populations were considered when more than three grains overlap in age (Gehrels et al., 2006). This statistical assumption relies on the fact that individual grains may sometimes represent lead-loss trajectories. Analytical results are presented in Tables 4 and 6.

2.4. Geochemistry

Bulk whole-rock chemical analysis of 21 samples was determined by inductively coupled plasma-mass spectrometry (ICP-MS) at Acme Analytical Laboratories Ltd. in Vancouver, Canada. A 0.2 g aliquot is weighed into a graphite crucible and mixed with 1.5 g of LiBO2 flux. The crucibles are placed in an oven and heated to 1050° C for 15 min. The molten sample is dissolved in 5% HNO3. Calibration standards and reagent blanks are added to the sample sequence. Sample solutions are aspirated into an ICP emission spectrograph (Jarrel Ash Atom Comb 975) for determining major oxides and certain trace elements (Ba, Nb, Ni, Sr, Sc, Y and Zr), while the sample solutions are aspirated into an ICP-MS (Perkins-Elmer Elan 6000) for determination of the trace elements, including rare earth elements. Results are presented in Table 5.

2.5. Hf isotope LA-ICP-MS geochemistry

Hf isotope determinations were performed on magmatic zircon crystals already analyzed for their U–Pb ages. The Hf spots were positioned with the U–Pb laser spots as avoiding cracks, inclusions, and zones displaying unusual cathodoluminescence. Hf isotopic measurements were performed using a ThermoFinnigan Neptune™ MC-ICP-MS equipped with 9 faraday collectors interfaced with a New Wave™ 213 nm UP Nd-YAG laser housed at Washington State University. The laser was operated at a pulse of rate 10 Hz and a fluence of 10–12 J/cm^2. Laser spot size was 40 μm except for some smaller grains where a 30 μm spot was used. Carrier gas consisted of purified He plus small quantities of N2 to minimize oxide formation and increase Hf sensitivity. The total Hf signal achieved was

Table 5
Whole-rock geochemical analysis from the plutonic and volcanic clasts. C refers to the different localities.

Rock	Locality	Sample	SiO2	Al2O3	Fe2O3	MgO	CaO	Na2O	K2O	TiO2	P2O5	MnO	Cr2O3	Sc	LOI	Sum	Co	Cs	Hf	Nb	Rb
Diorite	C1	7722	63.97	16.94	5.05	1.74	2.62	5.23	0.8	0.5	0.14	0.08	0.003	9	2.8	99.89	6.8	2.2	3.4	2.3	16.5
Diorite	C2	7728	63.19	15.67	4.79	1.73	3.36	3.53	3.86	0.53	0.2	0.07	0	9	2.9	99.8	9.6	2.2	6.8	8.9	161
Diorite	C3	7732	57.42	15.67	7.26	4.89	5.94	4.27	0.78	0.71	0.14	0.1	0.014	23	2.6	99.81	24.5	0	2.2	4	15
Granodiorite	C4	7740	59.17	16.8	5.75	1.8	6.6	3.79	1.78	0.65	0.44	0.15	0	10	2.9	99.78	11.1	2.4	3.3	3.3	43.5
Granodiorite	C8	7755	63.12	16.74	5.26	1.6	5.34	3.46	1.95	0.32	0.17	0.14	0	10	1.7	99.8	9.1	0.8	2.3	2.3	41.6
Andesite	C9	190001	58.81	15.63	7.49	4.38	5.82	2.86	1.57	0.67	0.14	0.1	0.014	23	2.3	99.76	21.1	0.5	2.4	4.9	35.3
Andesite	C9	190002	59.22	16.16	7.63	4.17	6.83	3.91	0.32	0.56	0.06	0.11	0.009	31	0.9	99.85	19		2.6	1.2	2.7
Andesite	C9	190004	53.67	14.49	9.28	5.98	5.53	3.45	0.87	0.81	0.12	0.15	0.026	30	5.4	99.77	27.9	0.2	2.1	3.9	19.2
Andesite	C9	190006	58.25	15.99	8.03	3.84	4.58	4.13	1.24	0.82	0.15	0.14	0.005	20	2.6	99.75	18.1	0.3	2.6	5.1	26.6
Andesite	C9	190007	60.06	15.01	6.44	4.49	3.54	4.22	1.29	0.77	0.14	0.06	0.016	23	3.7	99.78	17.6	0.2	2.3	5.5	27
Andesite	C9	190008	56.38	15.35	7.91	5.35	5.97	3.23	1.18	0.71	0.12	0.12	0.021	26	3.4	99.76	28.6	0.2	2.4	5.7	23.1
Andesite	C9	190009	61.08	13.63	5.61	2.32	4.32	2.21	0.76	0.42	0.14	0.09	0.002	20	9.2	99.78	10.2	0.4	1.8	3.8	16.3
Andesite	C9	190010	60.7	15.76	6.06	1.76	6.11	2.89	2.72	0.51	0.16	0.17	0.003	21	2.9	99.77	15.1	0.8	2.6	2.5	56.9
Andesite	C9	190011	57.05	16.16	8.03	4.71	4.83	3.65	1.39	0.78	0.14	0.15	0.015	24	2.9	99.79	20.1	0.2	2	3.9	23.4
Andesite	C9	190012	57.41	13.56	7.29	4.83	5.88	2.97	0.51	0.49	0.09	0.15	0.013	22	6.6	99.85	21.9	0.2	1.5	2.4	6.2
Andesite	C9	190017	58.44	15.79	7.08	4.7	6.09	3.23	0.62	0.74	0.13	0.14	0.014	24	2.8	99.79	22.5	0.2	2.4	4.6	10.8
Andesite	C1	7719	61.27	16.89	5.64	2.61	3.07	4.87	1.68	0.61	0.18	0.08	0.002	12	2.9	99.82	12.1	0.7	3.9	10.7	19.2
Andesite	C2	7725	57.09	15.16	7.99	1.42	4.26	4.86	2.36	0.64	0.46	0.12	0	13	5.4	99.72	25	0.7	2.9	2.3	33.4
Andesite	C2	7730	64.97	15.54	5.01	0.72	1.51	4.27	4.88	0.59	0.15	0.1	0	9	2.1	99.81	2.8	0.6	6.9	9.7	108.5
Andesite	C3	7733	46.76	16.34	9.89	6.8	11.85	2.95	0.21	0.93	0.08	0.19	0.035	37	3.8	99.82	40.9	0	1.5	0.5	2.2
Andesite	C3	7734	55.42	15.8	8.76	5.21	5.7	3.45	1.03	0.83	0.13	0.14	0.01	26	3.3	99.78	26	0.2	2.3	4	18.1
Andesite	C4	7737	58.75	16.54	6.23	1.92	2.57	5.02	3.86	0.64	0.44	0.09	0.002	15	3.6	99.71	18.6	0.2	4.5	3.5	57.5
Andesite	C4	7739	55.87	18.11	6.29	2.01	5.04	4.32	3.04	0.5	0.38	0.1	0	13	4	99.69	14.3	0.3	3.1	2.6	47.5
Andesite	C7	7747	50.49	15.9	11.2	5.66	5.52	2.11	0.68	0.7	0.17	0.15	0.01	38	7.2	99.74	30.3	0.1	2.8	0.5	10.2
Andesite	C8	7756	56.46	17.85	6.99	1.89	5.79	4.77	1.05	0.57	0.24	0.15	0	16	4.1	99.82	14.1	0.3	2.3	3.3	20.8
Andesite	C8	7757	54.96	16.54	9.12	3.04	4.86	5.12	1.24	0.81	0.29	0.17	0.002	28	3.6	99.79	20	0.2	2.4	1.1	21.7

between 5 and 10 V. The data were acquired in static mode with 60 one second integrations. Details of analytical procedures and data treatment are after (Vervoort et al., 2004; DuFrane et al., 2007).

For the calculation of Hf-depleted mantle model ages (Hf_{TDM}) we used $^{176}Hf/^{177}Hf$ and $^{176}Lu/^{177}Hf$ for the individual zircon samples to determine their $^{176}Hf/^{177}Hf(i)$ ratios at their crystallization ages. Projection back from zircon crystallization was calculated using $^{176}Lu/^{177}Hf_{crust,\ today} = 0.0093$ (Amelin et al., 2000; Vervoort and Patchett, 1996). The depleted mantle Hf evolution curve was calculated from present-day depleted mantle values of $^{176}Hf/^{177}Hf_{DM(0)} = 0.283225$ and $176Lu/177Hf_{DM(0)} = 0.038512$ (Vervoort and Blichert-Toft, 1999). Results are presented in Table 6

3. Results

3.1. Sampling

We have analyzed conglomerates and associated sandstones from 8 localities (Locality = C) of upper Paleocene to late Eocene strata in the southern and central segments of the San Jacinto Belt (Fig. 2). Although not all the sampled units present biostratigraphic control, lateral facies correlations can be used to established temporal limits to the analytical data (Figs. 2 and 3).

Paleontological constraints within some of the analyzed sections include biostratigraphic data from the San Cayetano–Arroyo Seco Formation within the Arroyo Seco creek (C4) which includes *Stensioina beccariformis, Ischyposporites problematicus, Polypodiisporites inangahensis, Proxapertite operculatus* that can be related to the late Paleocene to early Eocene (Rubio et al., 2009). In the Carreto–San Cayetano road (C10) the presence of radiolarium such as *Zehakina* and *Spiroplectamina* is characteristic of the late Paleocene (GEOTEC, 1997). For the Cerro Maco Formation Guzman et al. (2004) near C7 and C8 report foraminifera associations such as *Globorotalia bullbrooki, Globorotalia broedermani, Clavigerinella akersi* which are representative of the middle Eocene.

3.2. Conglomerate clast counting

Clast counting results from the different field localities are presented in Table 1.

Most of the conglomerates are matrix-supported and of polymictic character, with clasts sizes varying from 3 to 10 cm (Fig. 4). Shapes are predominantly sub-angular to weakly rounded.

Upper Paleocene conglomerates (San Cayetano–Arroyo Seco Formation, Fig. 2) are exposed in 1.0–4.6 m beds. Clasts include abundant plutonic fragments of granodiorite to granite composition, together with mafic to intermediate volcanics some of them highly porphyritic (Figs. 4A and 5A). Sedimentary clasts include chert with minor calcareous and siliciclastic (sandstone and mudstone). Although more restricted, metamorphic lithics include quartzite and milky quartz.

The two middle Eocene conglomerates from the Maco Formation (Fig. 2) also show the same major igneous associations and scarce metamorphic lithics (Figs. 4B and 5B).

A major contrast is recorded in upper Eocene to Oligocene strata (San Jacinto and Tolu Viejo Formations, Fig. 2) where igneous clasts are absent and sedimentary lithics, both siliciclastic and chemical (chert and limestone) types are extremely abundant (Figs. 4C and 5C).

3.3. Sandstone petrography and heavy minerals

Petrographic and heavy mineral results are presented in Tables 2 and 3.

Upper Paleocene–early Eocene sandstones interspersed within conglomerates are medium- to coarse-grained, with angular to subangular grains and poor to very poor sorting. Compositionally they vary from lithic arkose to lithoarenites, and include very fresh K-Feldspar and plagioclase (Figs. 4a and 6a). Lithics include sedimentary (siliciclastic and chert), igneous (volcanic and plutonic) as well as minor metamorphic fragments of predominantly micaceous character and more limited amphibolitic and gneissic fragments (Fig. 4b and 6a). Within the Dickinson (1985) sandstone discrimination diagram they plot mainly in the transitional to dissected arc field (Fig. 6b), which confirms the importance of a mix shallow and deeper magmatic source with an associated basement.

Upper Eocene sandstones are also texturally immature and of medium grain size and are characterized by higher quartz and feldspar contents, and classified as subarkose and lithic arkose (Figs. 4c and

Sr	Ta	Th	U	V	Zr	Y	La	Ce	Pr	Nd	Sm	Eu	Gd	Tb	Dy	Ho	Er	Tm	Yb	Lu	Cu	Pb	Ni
374.8	0.1	1.1	0.8	65	112.5	14.2	7.2	17.9	2.35	10.8	2.33	0.76	2.37	0.41	2.42	0.48	1.48	0.24	1.62	0.25	8.3	2	23.7
362.4	0.6	18.7	5.9	100	240.1	19.3	25.3	57.1	6.62	25.7	4.9	0.87	3.99	0.61	3.38	0.66	1.97	0.31	2.06	0.31	49.1	4.7	6.9
305.5	0.2	1.3	0.4	227	90.1	14.1	9.3	18.2	2.32	9.5	2.27	0.78	2.54	0.42	2.48	0.49	1.49	0.23	1.46	0.22	12.5	0.5	30.7
725.5	0.2	3.7	1.1	138	112.6	17.2	15.9	34.9	4.48	19.2	3.95	1.36	3.6	0.55	3.07	0.6	1.75	0.27	1.8	0.27	29.8	1.7	2.4
569.9	0.1	2.1	1.5	104	69.9	10.2	5.9	12.7	1.82	7.6	1.77	0.62	1.69	0.27	1.62	0.36	1.07	0.17	1.11	0.2	81.3	2.2	2.5
239.2	0.3	1.2	0.5	180	90.1	13.5	7.6	17	2.15	9.4	2.15	0.69	2.37	0.39	2.28	0.47	1.4	0.22	1.39	0.22	151	2.2	106
204.7		0.3	0.2	224	92.6	19.4	3	10	1.54	7.9	2.52	0.65	3	0.53	3.22	0.71	2.12	0.35	2.15	0.34	5	0.7	70
239.4	0.2	1.2	0.3	229	75.2	12.9	5.6	12.8	1.72	7.7	2.09	0.63	2.39	0.41	2.3	0.49	1.38	0.23	1.47	0.21	60	1	83
217	0.3	1.1	0.4	196	97.4	15.4	7.7	17.9	2.35	11.1	2.55	0.81	2.88	0.47	2.73	0.56	1.67	0.26	1.65	0.26	273.2	1	74
185.3	0.3	1.1	0.6	180	87	24.5	8.1	19.3	2.73	13.3	3.95	1.08	4.61	0.81	4.68	0.94	2.59	0.39	2.35	0.33	115.3	1.8	72
273.3	0.4	1.1	0.5	208	87.7	13.8	7	15.9	2.01	9.2	2.18	0.79	2.5	0.42	2.46	0.5	1.58	0.24	1.49	0.24	94.7	1.1	113
469.8	0.2	0.6	0.3	97	61.6	14.3	4.3	10.6	1.46	6.8	1.9	0.58	2.29	0.42	2.44	0.53	1.57	0.24	1.55	0.23	57.3	2.5	44
407.8	0.2	3.9	1.3	171	87.7	15.6	10.4	22.8	3	13	2.98	0.79	2.78	0.46	2.62	0.56	1.65	0.27	1.71	0.27	96.1	2.7	31
261.2	0.2	1.4	0.4	211	86.8	13.7	7.1	16	2.1	9.6	2.34	0.8	2.53	0.42	2.36	0.5	1.46	0.23	1.41	0.21	67.1	2.1	82
172.2	0.2	0.7	0.2	139	54.9	10	4.4	9.7	1.25	5.6	1.51	0.52	1.76	0.29	1.68	0.34	1	0.16	0.99	0.16	57.3	2.1	72
256	0.3	1.1	0.5	207	89.9	14.3	7.2	16.4	2.04	8.5	2.25	0.78	2.53	0.43	2.57	0.5	1.53	0.24	1.44	0.24	78.5	1.5	86
437.1	0.6	4	1.6	119	159.7	18.9	17.6	39.5	4.89	20.1	3.92	1.04	3.54	0.56	3.06	0.61	1.87	0.3	1.94	0.3	16.1	1.6	10.2
913.4	0	3.1	1.5	158	92.6	19.8	15.8	38.9	5.22	24.4	4.9	1.3	4.2	0.64	3.61	0.69	1.98	0.32	2	0.31	67.4	9.9	10.3
317.8	0.5	11	3.6	24	242.3	26.6	32.1	72.8	9.27	36	6.97	1.28	5.46	0.83	4.87	0.94	2.67	0.43	2.88	0.44	16.9	4.3	2.6
187.4	0	0	0	272	58.2	30.7	2.7	6.6	1.35	7	2.48	1.11	3.82	0.73	4.88	1.08	3.3	0.47	2.98	0.48	29.5	0.4	77.4
236.3	0.2	1	0.4	252	87	16.7	7.1	16	2.21	10.1	2.5	0.85	2.89	0.49	2.97	0.61	1.81	0.27	1.79	0.26	81	0.9	35.3
479.7	0.2	5.7	1.9	161	144.4	22	20.2	47.4	6.39	27.4	5.35	1.44	4.54	0.66	3.67	0.74	2.19	0.34	2.18	0.35	164.8	11.2	10.4
656.8	0.1	5	1.7	145	104.9	17.4	18.1	38.8	5.23	22.1	4.33	1.22	3.63	0.54	2.94	0.59	1.74	0.27	1.87	0.3	222.9	5.3	3.9
446.7	0	1.1	0.4	321	87.8	19.3	6	14.1	2.2	10.7	2.77	0.93	3.22	0.54	3.28	0.65	2.02	0.31	2.06	0.32	146.6	3.2	19.1
397.5	0.2	2.8	0.9	106	73.9	22.2	11.1	24.5	3.54	16.1	3.71	1.14	3.89	0.63	3.65	0.78	2.34	0.37	2.32	0.37	76.7	1.9	2
209.4	0	1.9	0.7	265	69.5	25.5	8.6	20.1	3.02	14.5	3.83	1.21	4.34	0.71	4.24	0.86	2.61	0.4	2.55	0.4	135	2.3	5.6

Table 6
Hf analytical results from zircons of the analyzed plutonic clasts.

Sample	$^{176}Hf/^{177}Hf$	2s	$^{176}Lu/^{177}Hf$	2s	$^{176}Yb/^{177}Hf$	Age (Ma)	eHf (0)	2s	eHf(t)	2s
7003 (C4)										
7003-12	0.283134	±0.000057	0.000931	±0.000051	0.035072	70	12.34	±2.00	13.85	±2.00
7003-11	0.283149	±0.000058	0.000820	±0.000081	0.030056	70	12.87	±2.06	14.39	±2.06
7003-10	0.283116	±0.000045	0.000869	±0.000055	0.033383	70	11.70	±1.59	13.22	±1.59
7003-9	0.283160	±0.000049	0.001044	±0.000085	0.041202	70	13.27	±1.72	14.77	±1.72
7003-8	0.283127	±0.000085	0.001921	±0.000175	0.072839	70	12.08	±2.99	13.55	±2.99
7003-7	0.283133	±0.000040	0.000644	±0.000019	0.023656	70	12.32	±1.40	13.85	±1.40
7003-6	0.283145	±0.000052	0.000723	±0.000052	0.027255	70	12.72	±1.83	14.24	±1.83
7003-5	0.283123	±0.000064	0.000890	±0.000017	0.036496	70	11.94	±2.26	13.46	±2.26
7003-4	0.283119	±0.000082	0.000804	±0.000037	0.030269	70	11.83	±2.90	13.35	±2.90
7003-3	0.283148	±0.000080	0.001024	±0.000042	0.038144	70	12.83	±2.82	14.34	±2.82
7003-2	0.283114	±0.000062	0.000889	±0.000063	0.036076	70	11.62	±2.21	13.14	±2.21
7003-1	0.283099	±0.000050	0.000787	±0.000029	0.029269	70	11.12	±1.77	12.64	±1.77
7005 (C5)										
7005-10	0.283151	±0.000059	0.001048	±0.000072	0.044271	70	12.93	±2.08	14.44	±2.08
7005-9	0.283181	±0.000065	0.001266	±0.000072	0.052509	70	13.99	±2.29	15.49	±2.29
7005-8	0.283181	±0.000066	0.001256	±0.000067	0.051686	70	14.02	±2.33	15.52	±2.33
7005-7	0.283178	±0.000051	0.001379	±0.000081	0.058921	70	13.90	±1.82	15.40	±1.82
7005-6	0.283180	±0.000054	0.000962	±0.000063	0.039829	70	13.98	±1.91	15.49	±1.91
7005-5	0.283123	±0.000064	0.000890	±0.000017	0.036496	70	11.94	±2.26	13.46	±2.26
7005-4	0.283184	±0.000037	0.001236	±0.000050	0.050978	70	14.11	±1.30	15.61	±1.30
7005-3	0.283138	±0.000054	0.000768	±0.000090	0.034783	70	12.49	±1.91	14.01	±1.91
7005-2	0.283219	±0.000054	0.001093	±0.000071	0.044697	70	15.33	±1.92	16.84	±1.92
7005-1	0.283098	±0.000040	0.000984	±0.000037	0.040747	70	11.05	±1.41	12.56	±1.41
7006 (C5)										
7006-12	0.283100	±0.000037	0.000637	±0.000017	0.021210	70	11.14	±1.29	12.67	±1.29
7006-11	0.283111	±0.000032	0.000835	±0.000033	0.027891	70	11.53	±1.13	13.04	±1.13
7006-10	0.283113	±0.000034	0.000739	±0.000055	0.024503	70	11.59	±1.19	13.11	±1.19
7006-9	0.283121	±0.000041	0.000756	±0.000018	0.025958	70	11.88	±1.44	13.40	±1.44
7006-8	0.283143	±0.000035	0.000857	±0.000029	0.029173	70	12.65	±1.25	14.16	±1.25
7006-7	0.283137	±0.000042	0.000573	±0.000024	0.018810	70	12.46	±1.49	13.99	±1.49
7006-6	0.283106	±0.000034	0.000695	±0.000018	0.022430	70	11.35	±1.20	12.88	±1.20
7006-5	0.283130	±0.000035	0.000829	±0.000072	0.026996	70	12.20	±1.23	13.72	±1.23
7006-4	0.283117	±0.000039	0.000606	±0.000020	0.020011	70	11.75	±1.38	13.28	±1.38
7006-3	0.283126	±0.000030	0.000984	±0.000120	0.032608	70	12.07	±1.07	13.58	±1.07
7006-2	0.283123	±0.000041	0.000537	±0.000004	0.017854	70	11.95	±1.46	13.49	±1.46
7006-1	0.283129	±0.000029	0.001210	±0.000140	0.041005	70	12.18	±1.04	13.68	±1.04

6c). In the Dickinson (1985) diagram, they plot in the quartzose recycled to cratonic fields.

Heavy minerals from the upper Paleocene to lower Eocene strata include both ultrastable (tourmaline, zircon and apatite) and diverse middle to lower stability heavy minerals of igneous and metamorphic origin (Fig. 7). In contrast, upper Eocene sandstone is made of only ultrastable minerals such as zircon, apatite and tourmaline (Fig. 7).

3.4. Sandstones U–Pb detrital zircon geochronology

We have analyzed five sandstones samples associated to the upper Paleocene to late Eocene conglomerates (Fig. 2). Analytical results are presented on Table 1.

One hundred ninety-eight zircon crystals from two upper Paleocene–lower Eocene sandstones (Figs. 7b and 8a) yield major age-peak populations of Late Cretaceous (80–72 Ma) and Permo-Triassic (230 Ma and 245 Ma). Older ages are less representative and include single zircons of Carboniferous, and Neoproterozoic to Paleoproterozoic ages (Fig. 8a). The youngest detrital zircon ages are of 71.3 ± 1.3 Ma (sample 6998) and 68.7 ± 1.4 Ma (sample 7001).

The middle Eocene sample (6999) includes prominent 88.2–72.9 Ma age peaks and a single Permian (270 Ma) age (Fig. 8c). The youngest detrital zircon age for this sample is of ca. 66.6 ± 0.79 Ma.

One hundred ninety-eight zircons from the two upper Eocene samples include similar Late Cretaceous age peaks of 93 Ma and 76.1 Ma (Fig. 8d), and Permian to Carboniferous age peaks, with more limited early Paleozoic and Precambrian zircons. The youngest detrital zircons ages are of 68.6 ± 4.4 Ma (sample 7557) and 70.4 ± 1.5 Ma (sample 7000).

3.5. U–Pb zircon geochronology of plutonic clasts

Three granitoid clasts were selected for U–Pb geochronology (Two from locality C4 and one from C5). Zircons are prismatic with length/width ratio of 3 to 1. Cathodoluminiscence patters are characterized by oscillatory zoning and rims characterized by embayed shapes. Some crystals are characterized by textural discontinuities in the oscillatory zoning pattern, which resemble resorbed zircons (Corfu et al., 2003). U–Pb weight average ages of the zircons range between 76 and 73 Ma and are considered as the crystallization ages from the magmatic rocks (Fig. 9a–c).

3.6. Geochemistry of volcanic clasts

We analyzed 21 volcanic clasts from three upper Paleocene-Eocene localities and three samples from a single locality of a middle Eocene conglomerate. Analytical results are presented in Table 3. SiO_2 values vary between 50.49% and 64.96%, with Al_2O_3 between 13.5% and 18.1% and MgO between 0.8% and 6%. TiO2 have a narrow range with weight percent between 0.5 and 0.9% (Table 2). Immobile trace elements relations such as the Zr/Ti versus Nb/Y (Pearce, 1996; Winchester and Floyd, 1977) and the Th–Co plot of Hastie et al. (2007) samples are classified as calc-alkaline basalts and basaltic andesites. Two samples are classified as dacites (Fig. 10a and b).

All the samples have enriched light rare earth (LREE) chondrite normalized patterns (Fig. 10c), with $(La/Yb)_N$ values between 1.87 and 7.53. Heavy rare earth (HREE) values display a narrow and low (Gd/Yb)N ratios that varies between 1.0 and 1.67 that shows a relatively flat pattern. The other two samples have a weak depletion of LREE patterns with $(La/Yb)_N$ ratios of 0.94 and 0.61.

Within mantle normalized multielemental diagrams all samples show a well defined LILE enrichment when compared with HFSE (Fig. 10d), the later also characterized by a weak depletion when compared with MORB values (not shown). Well defined Nb-Ta and Ti anomalies are also characteristic of the entire suite of rocks.

3.6.1. Petrotectonic setting

Th enrichment and Nb, Ta and Hf depletion are considered as markers of subduction-related settings (Pearce and Peate, 1995; Wood, 1980). In the same tectonic discrimination diagrams the conglomerate clasts plot within the field of calc-alkaline arc-related rocks (Fig. 10e and f).

Contents of Ti and V in mafic magmas are also related to oxygen activity during magmatic evolution, and therefore can be used to identify water induced melting which is commonly in subduction settings Rollinson, 1993; Shervais, 1982). Within this discrimination diagram the samples plot within the arc field (Fig. 10f).

The weak MREE and HREE depletion on the normalized plots (Fig. 10b) are inconsistent with the presence of residual garnet in the source. These samples are therefore the result of standard arc melt generation in the spinel peridotite stability field (Pearce, 1996). The Nb/Y vs. Zr/Y ratios have been used to discriminate between mafic rocks derived from depleted MORB mantle and mantle plumes. In the Caribbean realm these ratios are useful tracers of arc rocks derived from depleted mantle wedge formed after plume-enriched sources (Fitton et al., 1997; Hastie et al., 2010; Kerr et al., 2009; Neill et al., 2011). Volcanic clasts from the San Jacinto deformed belt plot within the conventional arc field (Fig. 10g).

3.7. Geochemistry of plutonic clasts

Whole-rock geochemical data from five plutonic clasts recovered from an upper Paleocene–lower Eocene and an upper Eocene conglomerate exposure (Fig. 2) indicate that SiO_2 values vary between 57.42% and 63.97%, with Al_2O_3 between 15.67% and 16.94% and MgO between 1.74% and 4.89%. In the TAS classification scheme after Cox et al. (1979), the rocks are classified as diorites and quartzdiorites (Fig. 11a). In the A/CNK vs. ANK diagram all the rocks are subalkaline, with A/CNK values below one, which is typical of meta-aluminous and I type granitoids (Fig. 11b, Chappell and White, 1992). One single sample is characterized by higher A/CNK values which may be related to lower K20 and CaO values. REE chondrite normalized patterns are enriched in LREE (Fig. 11c), with (La/Yb)N = 3–8.3 and flat to weakly enriched relations between MREE and HREE ($(Gd/Yb)_N$ values between 1.17 and 1.59. Eu anomaly varies from weakly positive to negative with Eu/Eu* values 0.6–1.1.

Trace elements normalized to the primitive mantle are characterized by a relative enrichment in the alkali elements (K, Rb, Ba) and Th, with a weak depletion in high field strength elements (Hf, Sm, Y, Yb) and well defined Nb, Ta and Ti anomalies (Fig. 11d).

3.7.1. Petrotectonic setting

The well defined Nb, Ta and Ti anomalies together with the enrichment of alkali elements (K, Rb, Ba), Tha and LREE support an origin of the clasts from granitoids formed as subduction-related magmas. In the Rb–Nb–Y diagram of Pearce et al. (1984) they also show a volcanic arc field affinity (Fig. 11e).

Brown et al. (1984) have suggested that Rb/Zr versus Nb versus elemental ratios followed a positive correlation in which their values increase with arc maturity. When plotted in this diagram the clasts plot within the field of more primitive island arc and continental arcs (Fig. 11f).

3.8. Hf isotopes

Ten to 12 zircon crystals were analyzed in each of the three selected granitoid clasts. Samples yield $_{Hf}$ (73) of 13.7 ± 0.6, 14.8 ± 0.9 and 13.4 ± 0.4. These isotopical signatures resembles the depleted mantle evolution curve which is characterize by εHf values of + 14 to + 18 (Vervoort and Blichert-Toft, 1999; Fig. 12) and markedly contrast with contemporaneous granitoids in the Central Cordillera of the Colombian Andes (Restrepo-Moreno et al., 2009; Fig. 12).

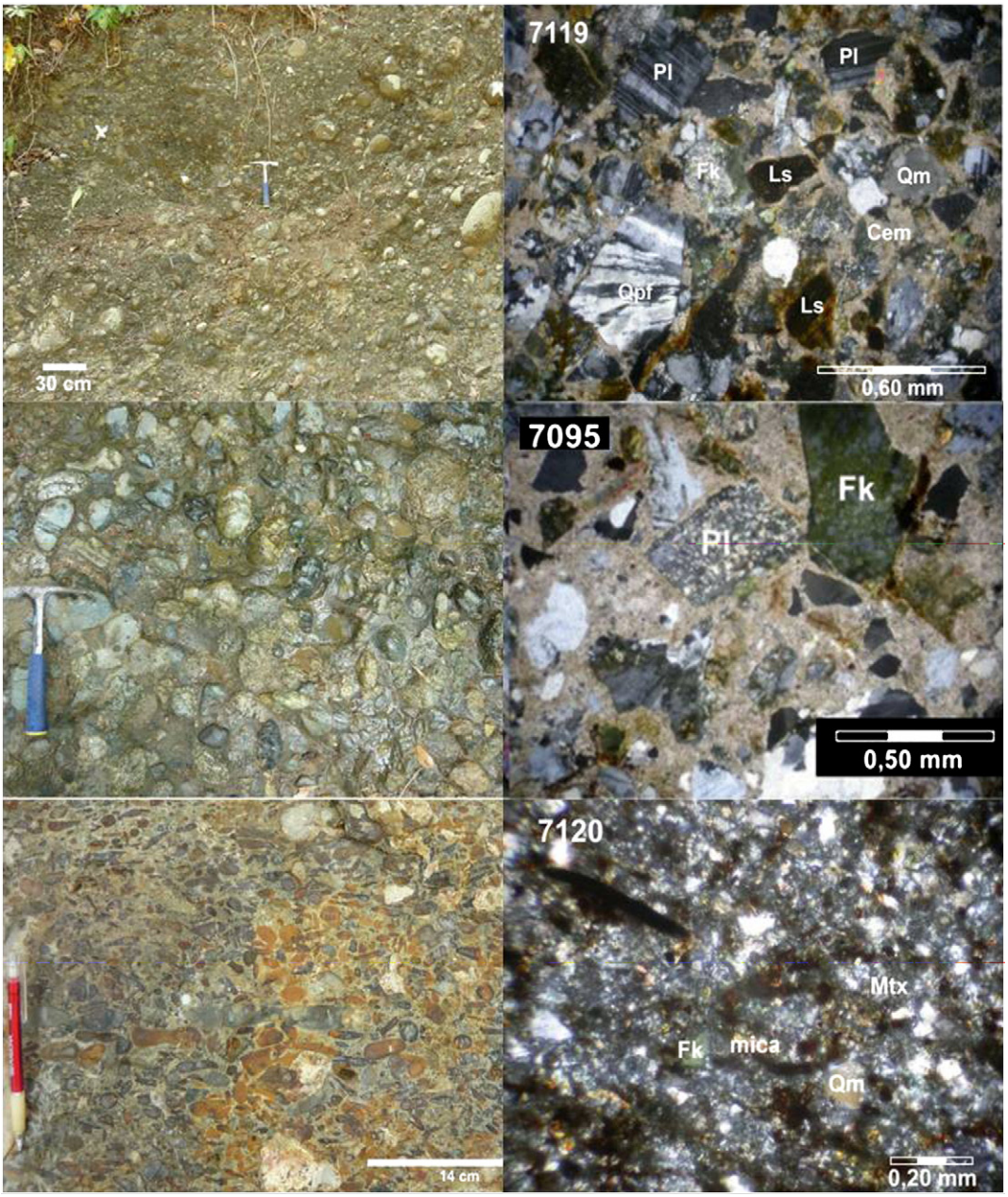

Fig. 4. Representative conglomerates and sandstones from the San Jacinto belt. A. Upper Paleocene conglomerate (C4) and sandstone (C2). B. Middle Eocene conglomerate (C8) and sandstone (C8). C. Upper Eocene conglomerate (C6) and sandstone (C5). Qm = Monocrystalline quartz, Qpf = Diffuse polycrystalline quartz, Mica = Mica, Fk = K-Feldspar, Pl = Plagioclase, Mtx = Matrix, Cem = Cement and LS = Sedimentary lithic.

4. Provenance

The wide distribution of contemporaneous conglomeratic units along strike of the San Jacinto belt may the existence of several transversal fan delta depositional systems as has been also suggested from stratigraphic analysis (Guzmán, 2007).

The angular to sub-angular shape of the upper Paleocene to lower Eocene conglomerate clasts and sandstones together with the preservation of extremely unstable material (volcanic clasts, fresh feldspars, amphibole, pyroxene and biotite) suggest that the source area was proximal, the material was rapidly buried, and have experienced limited residence time within an active sedimentary system.

The higher proportion of igneous (mafic to intermediate) and metamorphic lithics together with the high feldspar contents, and the presence of heavy minerals such as hornblende, pyroxene and titanite together with garnet, kyanite and muscovite suggest that they main source areas included a volcano-plutonic terrane of intermediate to mafic character, and a schist and gneissic metamorphic domain. The presence of chert, sandstones and mudstone with minor serpentinite lithics also suggests sedimentary and serpentinized peridotite sources.

Geochemical constraints on the analyzed magmatic clasts suggest that some of the volcano-plutonic rocks are related to an intra-oceanic calc-alkaline magmatic arc. This arc was still active until at least ca. 75–73 Ma as suggested by magmatic crystallization ages of the analyzed clasts and Late Cretaceous detrital zircons populations (70–90 Ma) in the associated sandstones. The positive, and near depleted mantle, Hf values from the magmatic clasts also confirm that some of these Late Cretaceous magmatic sources were formed in an intra-oceanic arc setting. Late Cretaceous juvenile magmatic rocks exposed in the northwestern Andes and the Caribbean margin of Colombia have been identified in allochthonous 92–75 Ma intra-

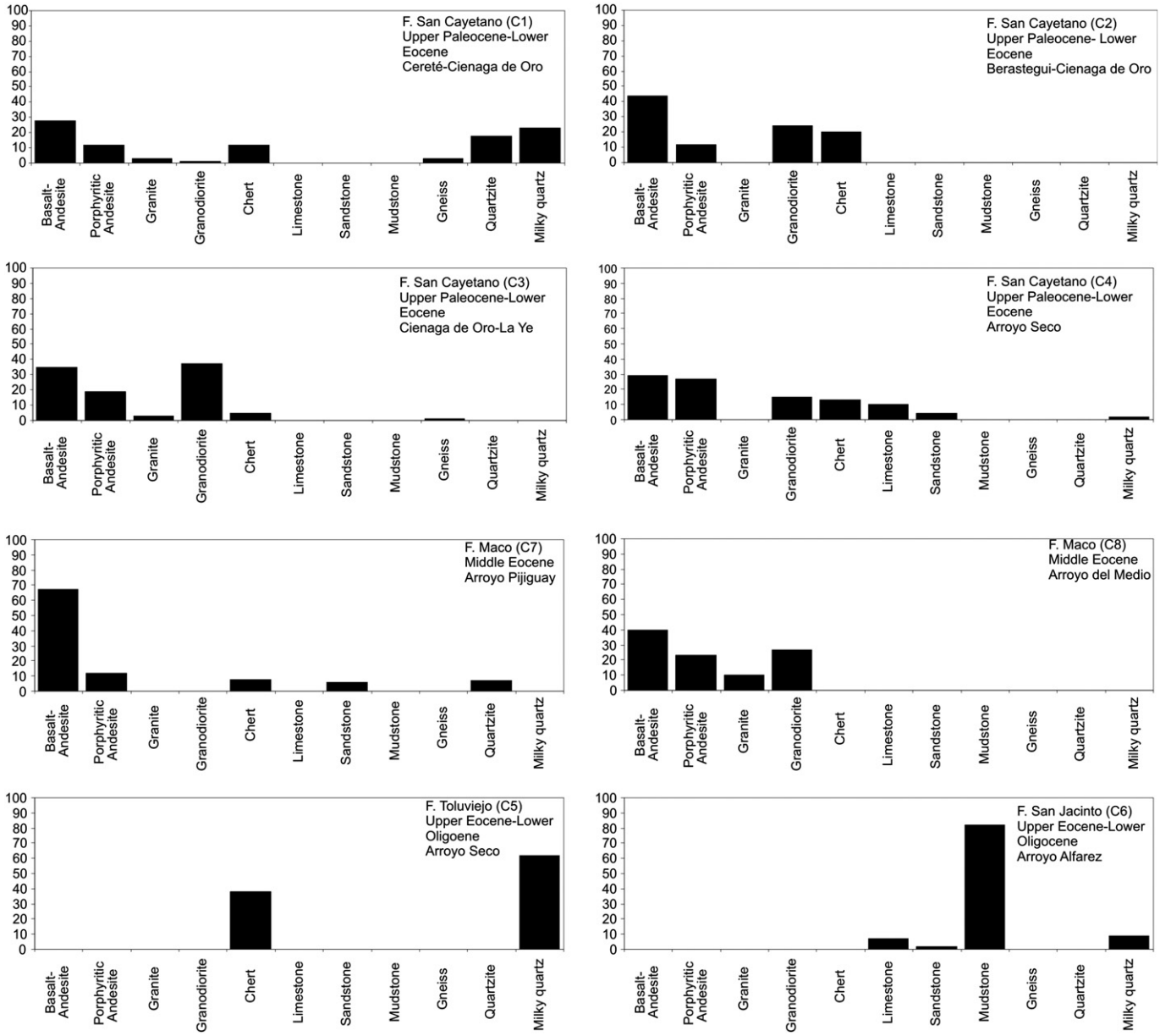

Fig. 5. Conglomerate clast counting from the selected localities of the San Jacinto deformed belt. A. San Cayetano and Arroyo Seco formations. B. Maco Formation. C. San Jacinto and Tolu Viejo formations.

oceanic volcano-plutonic suites found in the Western Cordillera, the Sierra Nevada de Santa Marta and Guajira massifs (Cardona et al., 2009, 2010, 2011; Kerr et al., 1997; Villagómez et al., 2011; Weber et al., 2009, 2011).

Late Cretaceous magmatism is also exposed in the Central Cordillera as part of the Antioqueño Batholith which consists of a composite batholith with ages between 94 and 72 Ma that intrude Late Permian to Triassic deformed granitoids and associated schists (Ibañez-Mejia et al., 2007; Leal-Mejía, 2011; Restepo-Moreno et al., 2007; Villagómez, 2010).

However the geochemical data from plutonic and volcanic clasts together with the highly positive εHf values on the analyzed zircons contrast with the more radiogenic values found on the Late Cretaceous Central Cordillera granitoids (Restepo-Moreno et al., 2007). Although an additional contribution from the Late Cretaceous continental source area of the Central Cordillera is not excluded we suggest that intra-oceanic arc sources potentially correlative with those found in the Western Cordillera and those from northern Colombia Santa Marta and Guajira regions accreted Caribbean domains are probably one of the major source areas for the Late Paleocene to Eocene conglomerates.

Moreover, recent paleogeographic reconstructions have suggest that during the Eocene the segment that include the Late Cretaceous Antioqueño Batolith in the Central Cordillera was located in a southern position, limiting their input to the San Jacinto belt (Bayona et al., 2012; Lamus-Ochoa et al., 2012).

The Permo-Triassic U–Pb detrital zircon population is comparable to the main basement units of Northern Colombia Central Cordillera, the Sierra Nevada de Santa Marta and the basement of the Lower Magdalena Basin (Cardona et al., 2010; Ibañez-Mejía et al., 2010; Montes et al., 2010; Ordóñez-Carmona and Pimentel, 2002; Vinasco et al., 2006). These areas include low- to middle-grade micaceous schists and an extensive belt of deformed two-mica granitoids of Permo-Triassic age (Ibañez-Mejía et al., 2010; Martens et al., 2011; Villagómez et al., 2011; Vinasco et al., 2006). The micaceous character

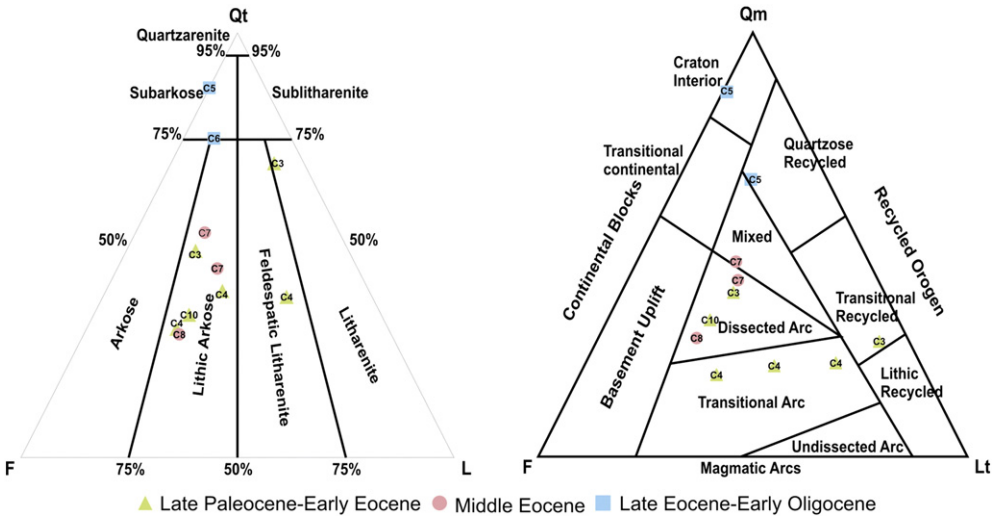

Fig. 6. A. Sandstone classification after Folk (1980). B. Sandstone provenance and tectonic setting (Dickinson, 1985).

of this granitoids (Vinasco et al., 20006) also indicates that that the intermediate and mafic volcanics and the amphibole, pyroxene and titanite sources are unrelated to this suite. Instead, we suggest that they are related to Late Cretaceous magmatic sources. Sedimentary sources may be related to Cretaceous continental or arc sediments such as those found in the Cansona Formation (Geotec, 1997; Guzmán, 2007).

A major provenance shift is recorded by the upper Eocene conglomerates of the San Jacinto and Tolu Viejo Formations. These formations are characterized by conglomerates with high proportion of sedimentary lithics, including some intraclasts that can be related to basin instability whereas extrabasinal clasts may reflect the reworked nature of some of the older sequence also related to tectonic instability. Sandstones are characterized by a major increase in quartz and feldspar. The more limited occurrence of magmatic sources in the conglomerates together with their more limited expression in the associated sandstone suggest a depletion of the more proximal volcanic sources.

4.1. Caribbean tectonics and paleogeography

The Late Cretaceous to Paleocene tectonic evolution of the northern Andes and the Caribbean margin of northern South America have been linked to oceanic-continent collision, followed by oblique convergence (Bayona et al., 2011; Cardona et al., 2010, 2011; Escalona and Mann, 2010; Jaillard et al., 2008; 2009; Pindell and Kennan, 2009; Luzieux et al., 2006; Marresh et al., 2009; Pindell et al., 1998, 2005; Spikings et al., 2001, 2005; Vallejo et al., 2006, 2009; Weber et al., 2009, 2010). This model suggests that the northeastern migration of the Caribbean oceanic plateau formed in a southwestern Pacific position is responsible for the formation different arc-continent or plateau-continent collisional orogens along the South American margin.

The provenance results of upper Paleocene to upper Eocene strata from the San Jacinto deformed belt provide new details on the nature and timing and different tectonic stages recorded by the northwestern margin of the South American continent. The presence of Late Cretaceous intra-oceanic, arc-related sources mixed with the Permo-Triassic continental basement, suggests that the intra-oceanic arc and the South American margin were already sutured in late Paleocene times. This intra-oceanic arc was still active at least until 73 Ma as suggested by the youngest plutonic clast age (Fig. 13a), and must have collided before the accumulation of the San Cayetano–Arroyo Seco Formation (late Paleocene) which can be considered as an overstep sequence that mix both the allocthonous arc and the continental margin material (Fig. 13b).

Although intra-oceanic Albian–Aptian arc remnants are exposed in western Colombia as part of the Quebradagrande Complex (Nivia et al., 2006; Villagómez et al., 2011). In the current study we have not found detrital zircons of this age, limiting their contribution as a sedimentary source.

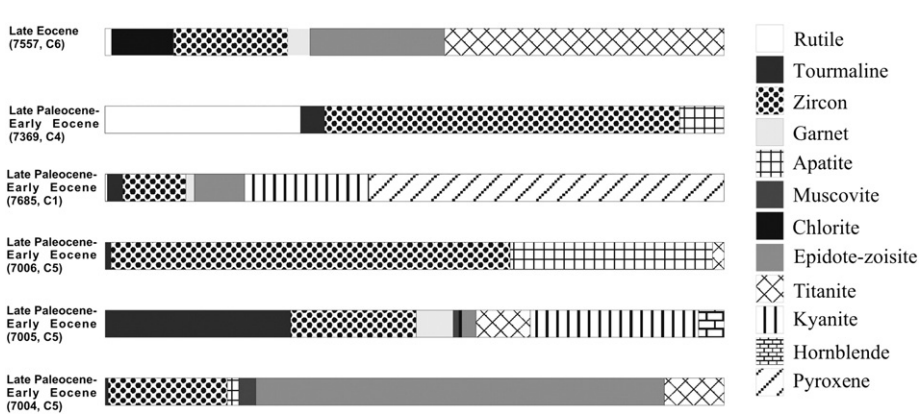

Fig. 7. Heavy minerals proportions from the analyzed sandstones of the San Jacinto deformed belt.

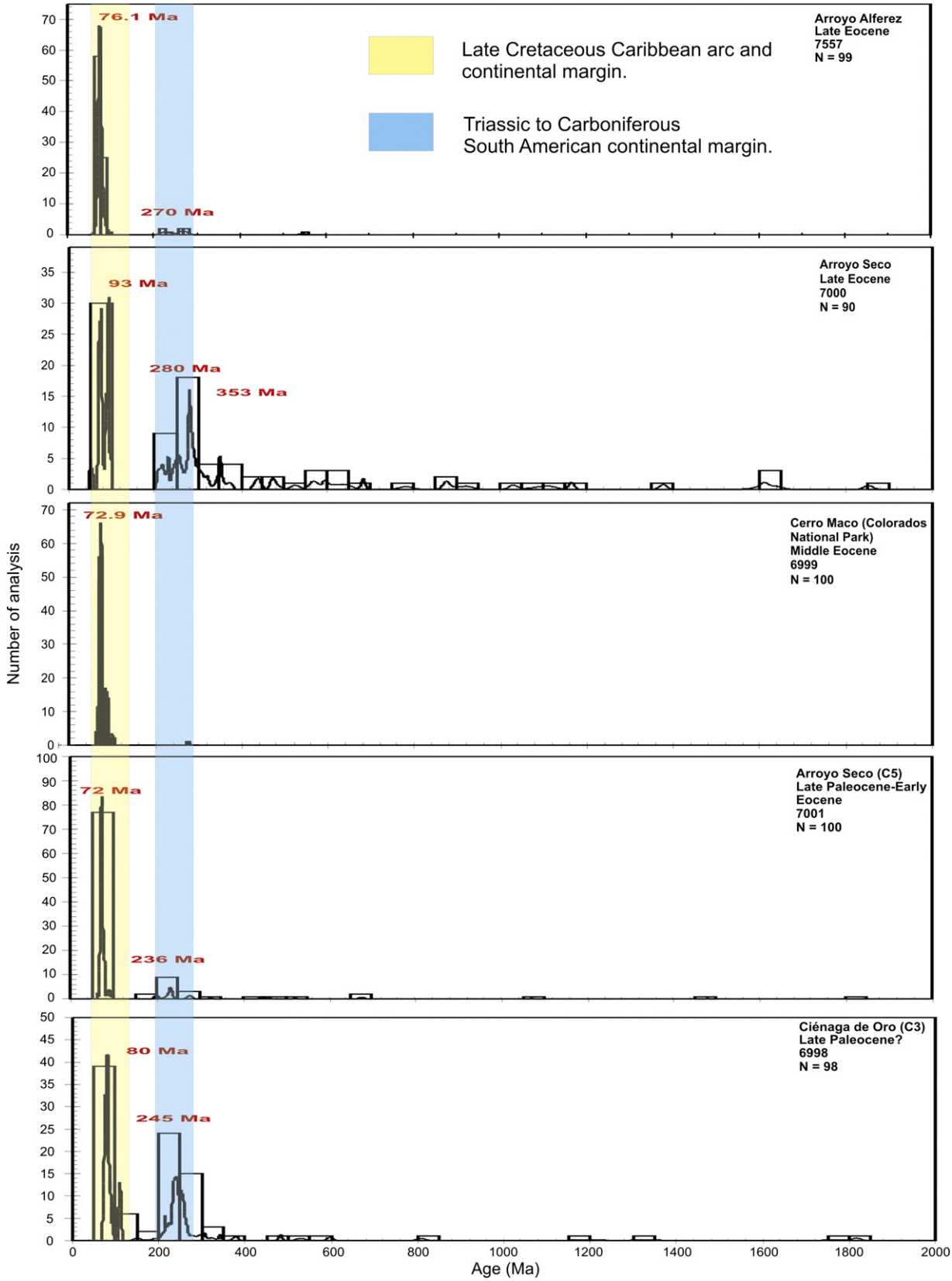

Fig. 8. U–Pb geochronological results from the analyzed samples of the San Jacinto deformed belt. A. Upper Paleocene–lower Eocene. B. Middle Eocene. C. Upper Eocene.

Published biostratigraphic constraints suggest the existence of a depositional gap after de accumulation of the Maastrichtian Cansona Formation and before deposition of the San Cayetano Formation (Duque-Caro et al., 1996; Geotec, 1997; Guzmán, 2007). This early Palocene gap suggests that the intra-oceanic and associated orogenic substrate of the San Jacinto deformed belt was emerged during the collisional event.

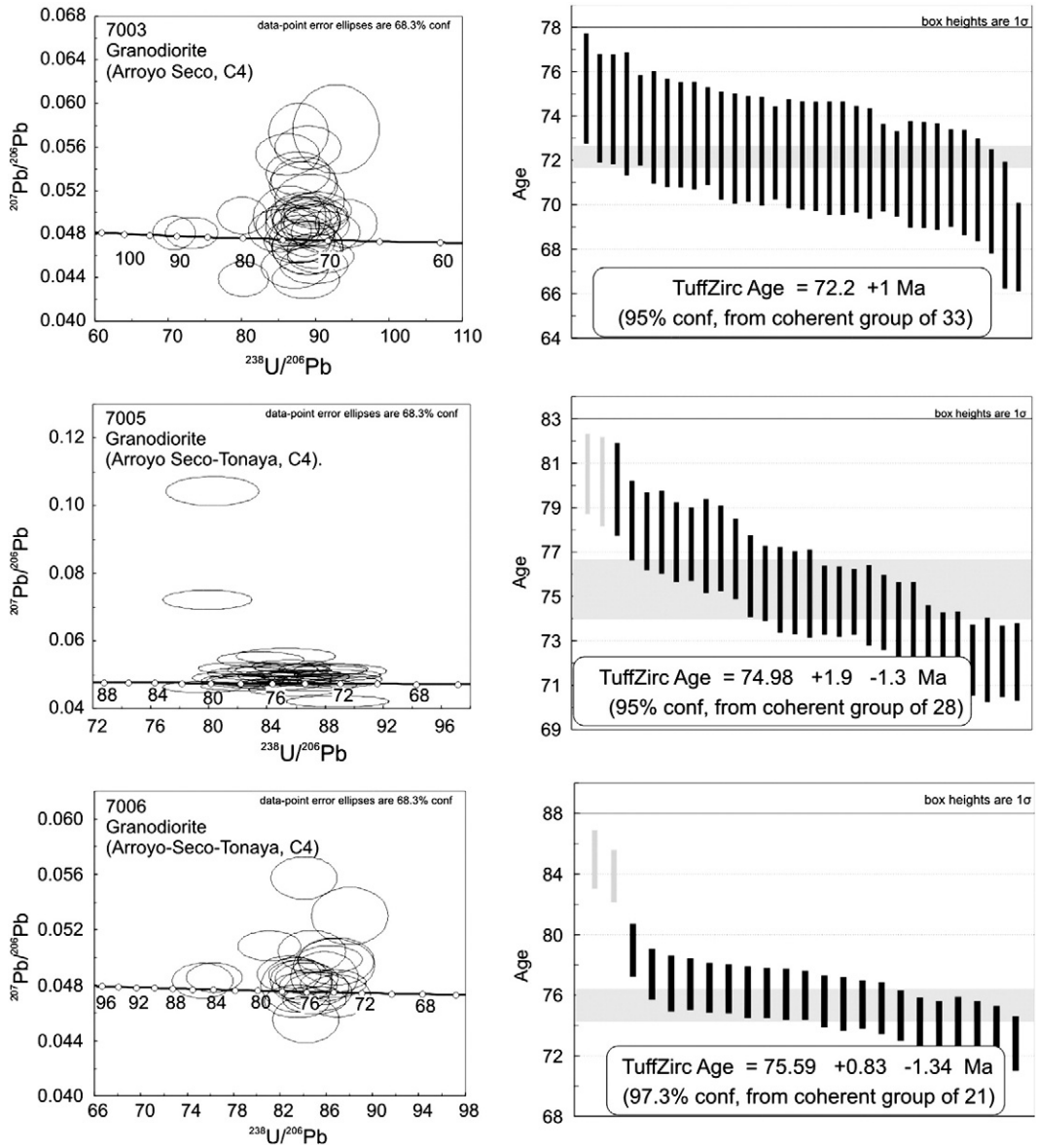

Fig. 9. U–Pb geochronological results of the analyzed plutonic clasts.

Remnants of the accreted arc and the substrate of the San Jacinto Belt include the scarcely studied and highly weathered volcanic rocks associated to the Cretaceous sediments of the Cansona Formation, and some limited serpentinitized remnants exposed in the southeastern segment of the belt.

The presence peridotized serpentinites remnants and as unstable lithic component of the upper Paleocene sediments of San Cayetano–Arroyo Seco formations (Zimmerle, 1968) together with abundant schists and milky quartz clasts as well as heavy minerals such as kyanite and garnet in the conglomerates and sandstones may be a record of the middle pressure collisional metamorphic belt, and ocean closure that accreted the intra-oceanic arc (Chew et al., 2010; Cutts et al., 2011; Dewey and Mange, 1999; Hutchison and Oliver, 1998; Mange et al., 2010; Miyashiro, 1972; Oliver, 2001; Spear, 1995).

Although Albian–Aptian middle pressure rocks have been also found in western Colombia (Villagómez et al., 2011), as already mentioned the mentined absence of Albian–Aptian magmatic zircons which may be link to the evolution of this older metamorphic belt, makes the proposed Late Cretaceous origin of this belt a feasible option.

Volcano-plutonic remnants of Late Cretaceous arc have been found in the Ecuadorian Andes, the western Cordillera of Colombia, Sierra Nevada de Santa Marta, Cabo de la Vela in northeastern Colombia, the Leeward Antilles and Venezuela (Cardona et al., 2010, 2011; Ostos and Sisson, 2005; Thompson et al., 2004; Vallejo et al., 2009; Van del Lelij et al., 2010; Villagómez et al., 2011; Weber et al., 2009, 2011; Wright and Wyld, 2011).

Age estimates for the collision of this Caribbean intra-oceanic arc with the continental margin vary between 80 and 65 Ma (Cardona et al., 2011; Vallejo et al., 2009; Villagómez et al., 2011). Regional paleogeographic models suggest that the oblique advance of the Caribbean plate in relation to the South American results in diachronous collisional events with a single arc formed since ca. 130 Ma (Burke, 1988; Pindell, 1993; Pindell and Kennan, 2009; Pindell et al., 1998, 2005). The new U–Pb detrital record of the San Jacinto deformed belt reveals instead that the magmatic sources were intra-oceanic 90–70 Ma old, precluding the connection with the aforementioned single arc.

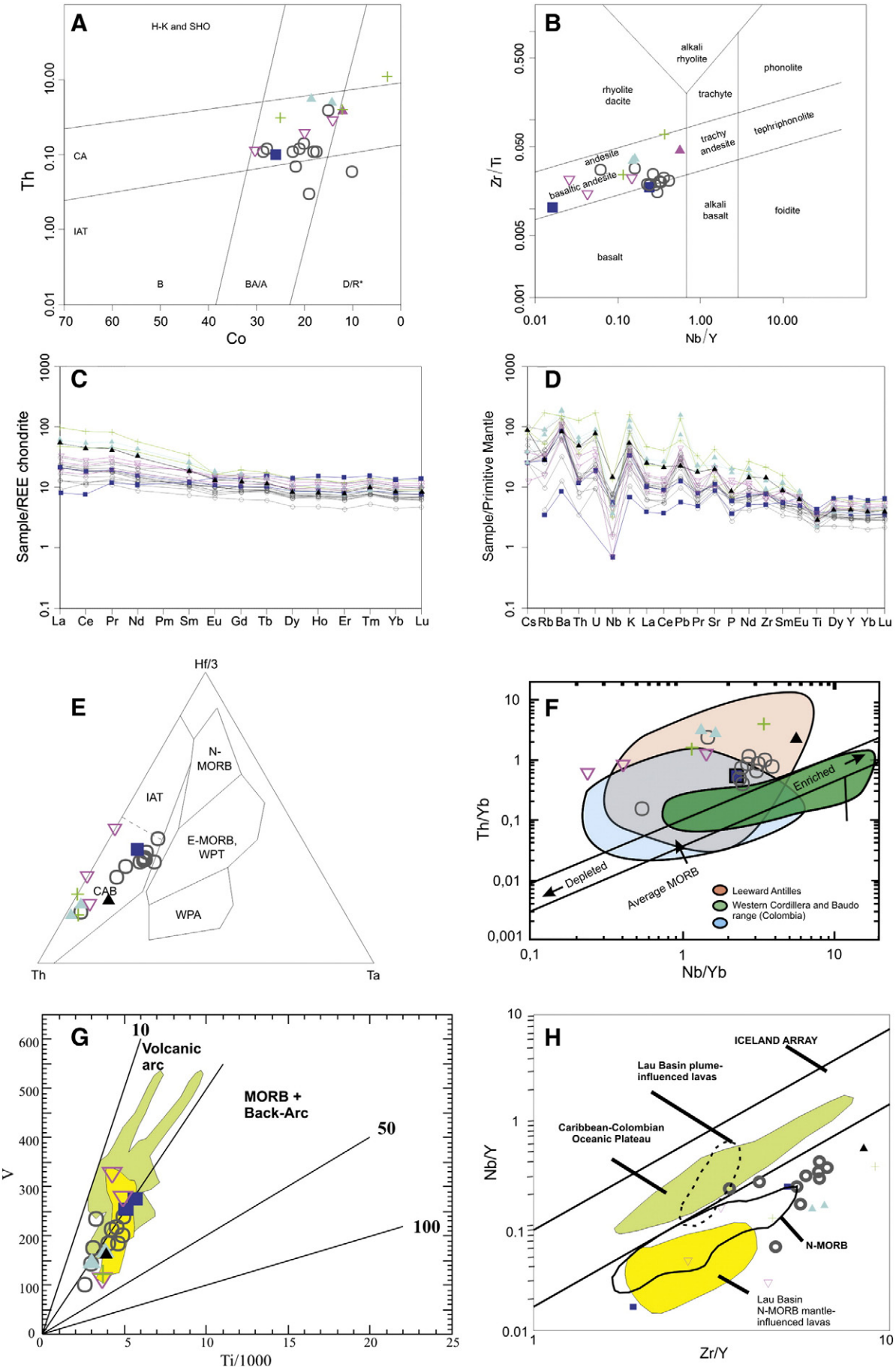
A
H-K and SHO
CA
IAT
B
BA/A
D/R*
Th
Co
B
alkali rhyolite
phonolite
rhyolite dacite
trachyte
trachy andesite
tephriphonolite
andesite
basaltic andesite
alkali basalt
foidite
basalt
Zr/Ti
Nb/Y
C
Sample/REE chondrite
La Ce Pr Nd Pm Sm Eu Gd Tb Dy Ho Er Tm Yb Lu
D
Sample/Primitive Mantle
Cs Rb Ba Th U Nb K La Ce Pb Pr Sr P Nd Zr Sm Eu Ti Dy Y Yb Lu
E
Hf/3
N-MORB
IAT
E-MORB, WPT
CAB
WPA
Th
Ta
F
Th/Yb
Nb/Yb
Enriched
Depleted
Average MORB
Leeward Antilles
Western Cordillera and Baudo range (Colombia)
G
10
Volcanic arc
MORB + Back-Arc
50
100
V
Ti/1000
H
ICELAND ARRAY
Lau Basin plume-influenced lavas
Caribbean-Colombian Oceanic Plateau
N-MORB
Lau Basin N-MORB mantle-influenced lavas
Nb/Y
Zr/Y

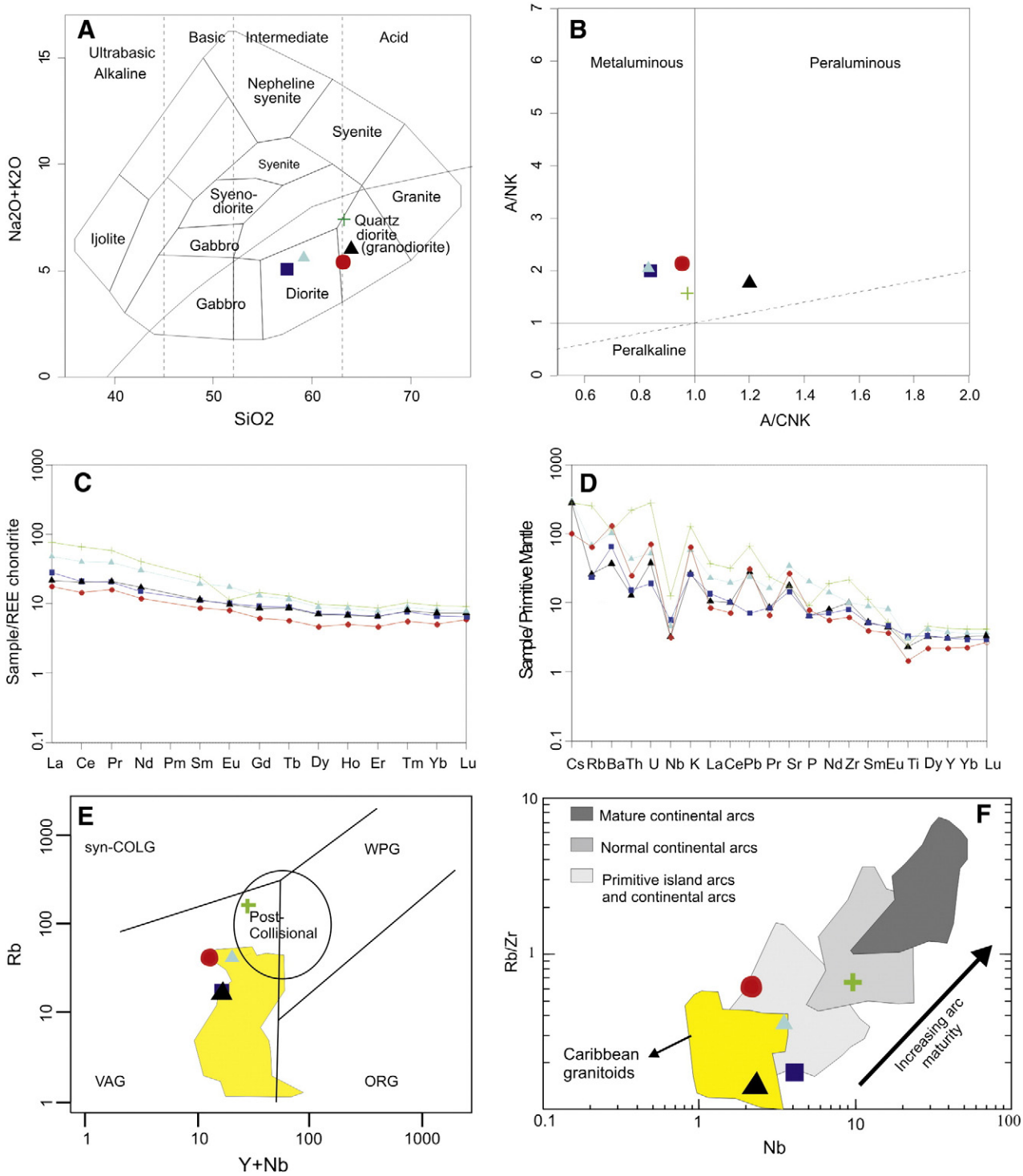

Fig. 11. Geochemical diagrams from the analyzed plutonic clasts. A. TAS classification after Cox et al. (1979). B. A/CNK versus ANK diagram. C. REE Chondrite normalized patterns. D. Trace element normalized to the primitive mantle. E. Rb–Nb–Y tectonic setting discrimination diagram (Pearce et al., 1984). F. Rb/Zr versus Nb granitoid arc maturity diagram.

Recent detailed characterization of the chronology of the orogenic events from different segments of the margins, including the San Jacinto deformed belt, reveals the existence of a contemporaneous collisional event along a relatively long margin segment from Ecuador to northern Colombia (Bustamante et al., 2011; Cardona et al., 2009; Spikings et al., 2001, 2005; Vallejo et al., 2009; Weber et al., 2009, 2010). This, together with the recognition of different type of intra-oceanic units (Cardona et al., 2010; Neill et al., 2011; Weber et al., 2011; Wright and Wyld,

Fig. 10. Geochemical diagrams from the analyzed volcanic clasts. A. Zr/Ti vs. Nb/Y volcanic classification plot after Winchester and Floyd (1977, Pearce, 1996) from the analyzed clasts. B. Th/Co classification diagram of volcanic rocks (Hastie et al., 2007) from the analyzed clasts. C. Rare earth elements chondrite normalized plots of the volcanic clasts. D. Mantle normalized diagram of the analyzed volcanic clasts (Sun and McDonough, 1989). E. Tectonic setting discrimination diagram of volcanic rocks (Wood et al., 1980). F. Th/Yb vs. Nb/Yb discrimination diagram (Pearce and Peate, 1995). G. Nb/Y vs. Zr/Y discrimination of arc rocks derived from depleted mantle wedges from those formed after plume-enriched sources (Fitton et al., 1997; Hastie et al., 2010; Kerr et al., 2009; Neill et al., 2011).

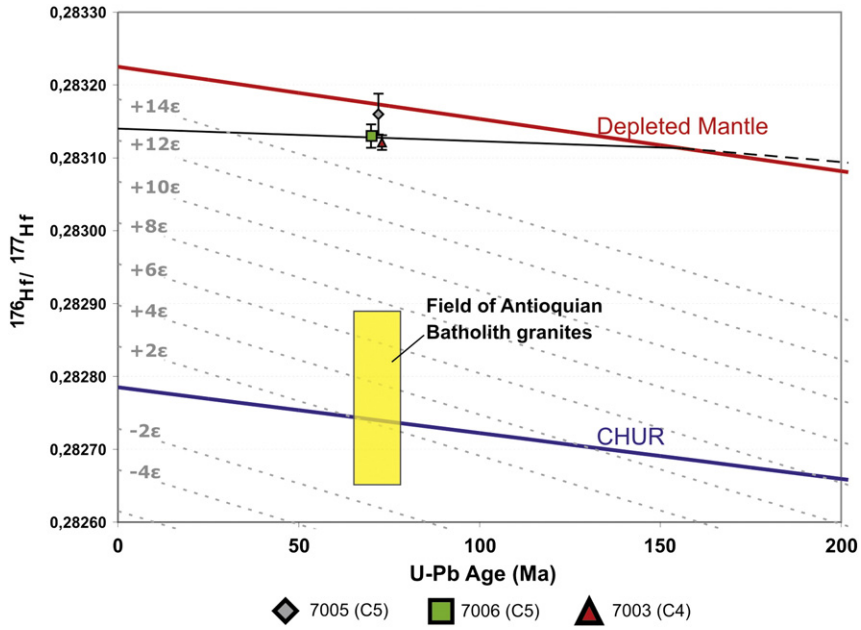

Fig. 12. Hf isotope data including depleted mantle evolution (Vervoort and Blichert-Toft, 1999) and Hf values from the Upper Cretaceous granitoid clasts and results published from Upper Cretaceous granitoids of the Central Cordillera of Colombia.

2011), and the absence of Cretaceous detrital ages older than ca. 90 Ma which will be expected from a single Caribbean built since the Late Jurassic-Early Cretaceous (Burke, 1988; Pindell et al., 2005) favors the existence of various intra-oceanic arc systems formed along the eastern margins of the Caribbean plate that were accreted to the northwestern margin of South America (Bustamante et al., 2011; Cardona et al., 2009; Neill et al., 2011; Wright and Wyld, 2011).

As already discussed the upper Paleocene to Eocene siliciclastic strata of the San Jacinto deformed belt were deposited over remnants of the accreted Late Cretaceous intra-oceanic arc, which are tectonically intermixed with continental rocks (Mantilla-Pimiento et al., 2009), including the slices of serpentinized peridotites. We interpret the late Paleocene basin formation and fill, to the decreasing compressional support of the collisional orogen and its lateral spread and collapse (Fig. 13c, Charlton, 1991; Clift et al., 2008; Dewey, 2005; Teng, 1996). This stage is also related to subduction initiation with the opposite vergence and plate convergence re-initiation causing fore-arc uplift, followed by major subsidence and associated extension (Gurnis et al., 2004; Macpherson, 2008; Whattam and Stern, 2011).

Additional evidences for late Paleocene to early Eocene subduction initiation and renewed convergence in the continental margin of Colombia include the magmatic record in the Central and Eastern Cordillera, the Sierra Nevada de Santa Marta and Guajira region (Aspden et al., 1987; Ayala-Calvo et al., 2010; Bayona et al., 2008, 2011, 2012; Cardona et al., 2011; Leal-Mejía, 2011). Since the time of Late Cretaceous arc-continent collision, oblique to very oblique convergence has taken place between the Caribbean and South American plate and favors the northeastern along strike translation of the San Jacinto belt (Fig. 13d) as a fore-arc type or transcurrente terrane (Gibbons, 1994; Jarrard, 1986) before its re-accretion and deformation near its current position in the Oligocene (Duque-Caro, 1984).

5. Conclusions

The integration of provenance techniques and regional tectonostratigraphic considerations from the upper Paleocene to upper Eocene conglomerates and associated sandstones of the San Jacinto deformed belt in northern Colombia allows to reconstruct the history of this basin the different tectonic events experienced by the continental margin of South America during its interaction with the Caribbean plate: (1) growth of an intra-oceanic arc that was active at least until 73 Ma and may have started activity by 88 Ma; (2) accretion of this arc to the continental margin between 73 and 60 Ma with associated ophiolite obduction and the formation of a middle pressure metamorphic belt, and associated emergence of this belt; (3) formation of a post-collisional basin and submergence of the former orogen due to the decreasing orogen support and the formation of an oblique convergent margin; and (4) isolation of the basin from relief areas either by submergence or by northeast tectonic transport. Although not discussed in this paper this block was deformed in the continental margin during the Oligocene (Duque-Caro, 1984).

The extensive ~90–70 Ma record of the San Jacinto deformed belt together with the limited occurrence of Aptian to Cenomanian magmatic sources, and the margin-scale Late Campanian to Paleocene arc-continent collision in the Northern Andes suggest that not a single, but contemporaneous arc systems were formed along the western and northern segments of the Caribbean plate (Cardona et al., 2009; Hastie et al., 2010; Wright and Wyld, 2011).

Acknowledgements

We thank Ecopetrol (Empresa Colombiana de Petroleos) for their support during a joint research project in the paleogeography of northern Colombia. Additional support from the Smithsonian Institution and Mr. Mark Tupper are also acknowledged. G. Guzman is acknowledged for his support during field work. G. Cañizalez, Y. Villafañez, S. Jaramillo, M. Lara and J. Vanegas are acknowledged for their help on sample preparation, data organization and manuscript edition. D. Buchs and J. Pindell are acknowledged for their constructive reviews that help to improve the manuscript.

Whole-rock geochemistry and Hf isotopic analysis were supported by the Fundación para la Promoción de la Investigación y la Tecnología de la República de Colombia (Project 2570). This is a contribution to the IGCP-546 “Subduction zones of the Caribbean”.

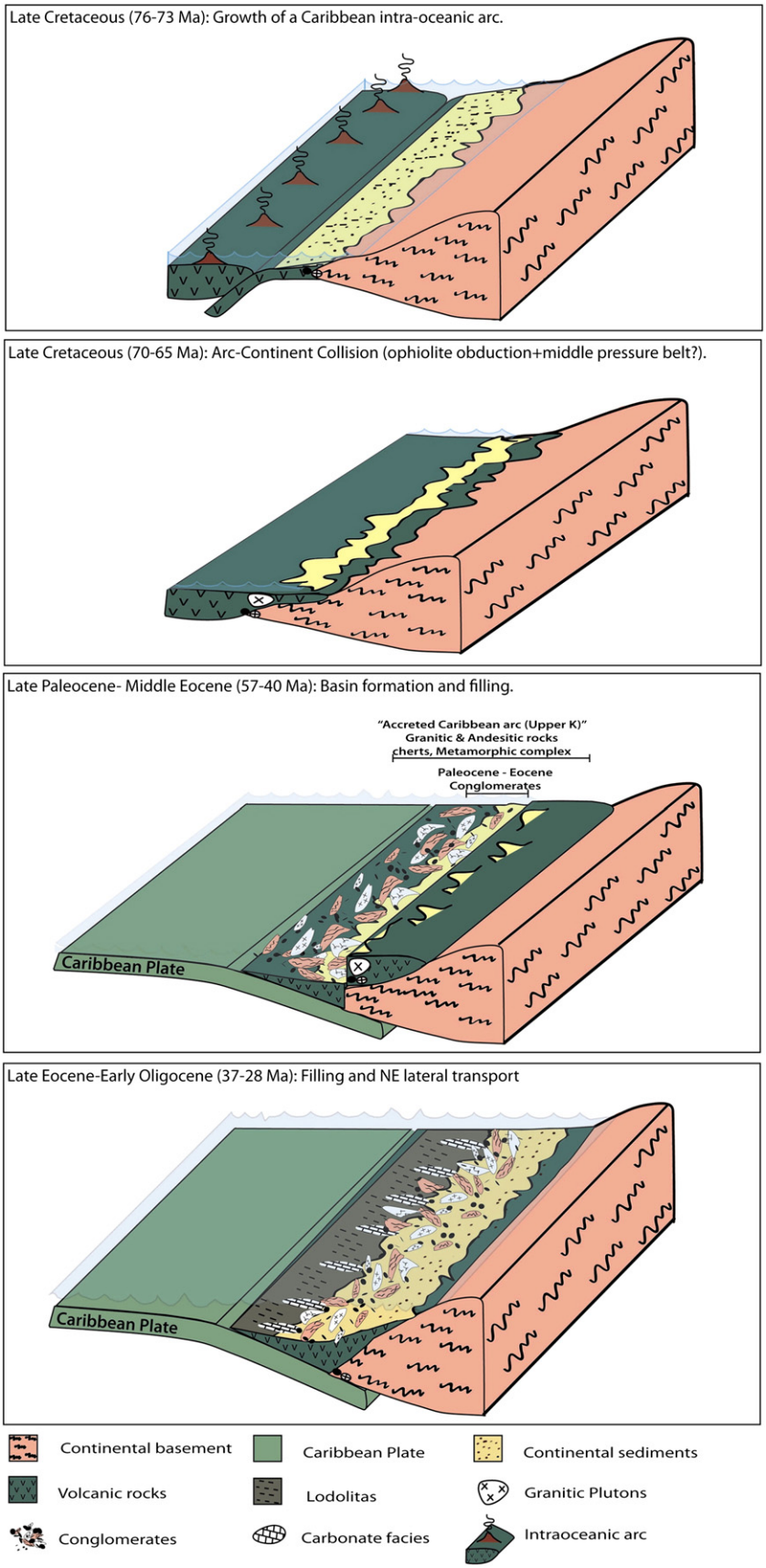

Fig. 13. Tectonic stages recorded by the San Jacinto deformed belt. A. 76–73 intra-oceanic arc growth and approach to the continental margin. B. 70–65 arc-continent collision. C. Basin formation due to orogen collapse. D. Basin filling and northeastern along strike transport.

Appendix Table 1. U–Pb LA-ICP-MS analytical and age results from the analyzed sandstones.

Sample name	238U 206Pb	1 sigma % error	207Pb 206Pb	1 sigma % error	206/238 age	1 sigma err (Ma)	207/206 age	1 sigma err (Ma)	Best age	1 sigma err (Ma)
Locality C6										
<10% discordant										
7557_99	80.74462	1.90%	0.04906	2.08%	79.3	1.5	150.8	48.1	79.3	1.5
7557_98	83.88927	1.79%	0.04861	2.32%	76.4	1.4	128.9	53.7	76.4	1.4
7557_97	75.65518	2.45%	0.04580	2.97%	84.6	2.1	0.0	57.1	84.6	2.1
7557_96	84.61775	2.10%	0.04537	2.61%	75.7	1.6	0.0	26.5	75.7	1.6
7557_95	87.60741	1.86%	0.04918	2.98%	73.2	1.4	156.2	68.3	73.2	1.4
7557_94	11.32381	1.40%	0.05831	1.09%	545.5	7.3	541.6	23.7	545.5	7.3
7557_93	83.96236	2.16%	0.04741	2.98%	76.3	1.6	70.1	69.4	76.3	1.6
7557_92	80.71439	2.36%	0.04892	2.82%	79.4	1.9	144.2	64.8	79.4	1.9
7557_91	85.52371	2.25%	0.04903	2.91%	74.9	1.7	149.4	66.8	74.9	1.7
7557_90	77.58750	1.67%	0.03295	2.59%	82.6	1.4	0.0	0.0	82.6	1.4
7557_89	81.42861	2.10%	0.04877	2.70%	78.7	1.6	136.8	62.1	78.7	1.6
7557_88	86.70375	2.13%	0.04819	2.52%	73.9	1.6	108.7	58.5	73.9	1.6
7557_87	85.77266	2.56%	0.05997	2.71%	74.7	1.9	602.5	57.6	74.7	1.9
7557_86	84.10001	2.50%	0.04675	3.13%	76.2	1.9	36.5	73.3	76.2	1.9
7557_85	83.96708	3.16%	0.04875	3.89%	76.3	2.4	135.6	88.9	76.3	2.4
7557_84	83.31564	2.56%	0.04706	2.60%	76.9	2.0	52.3	60.9	76.9	2.0
7557_83	84.20674	2.42%	0.04783	2.70%	76.1	1.8	90.8	62.8	76.1	1.8
7557_82	74.86730	2.31%	0.04754	1.83%	85.5	2.0	76.7	42.8	85.5	2.0
7557_81	78.14716	2.35%	0.04715	1.86%	82.0	1.9	56.6	43.9	82.0	1.9
7557_80	84.50162	2.70%	0.04783	2.79%	75.8	2.0	90.8	64.8	75.8	2.0
7557_79	86.85361	2.53%	0.04668	2.84%	73.8	1.9	32.9	66.8	73.8	1.9
7557_78	83.93675	2.50%	0.04699	2.31%	76.3	1.9	48.9	54.2	76.3	1.9
7557_77	81.33012	3.88%	0.05504	3.86%	78.8	3.0	414.0	84.1	78.8	3.0
7557_76	81.74789	2.60%	0.04536	3.06%	78.4	2.0	0.0	36.2	78.4	2.0
7557_74	77.10687	2.38%	0.04825	1.96%	83.1	2.0	111.7	45.6	83.1	2.0
7557_73	80.20230	2.43%	0.04599	1.75%	79.9	1.9	0.0	38.9	79.9	1.9
7557_72	85.54831	2.25%	0.04648	1.69%	74.9	1.7	22.4	40.0	74.9	1.7
7557_71	82.01608	2.68%	0.04425	3.47%	78.1	2.1	0.0	0.0	78.1	2.1
7557_70	88.55168	3.70%	0.04624	2.62%	72.4	2.7	0.0	71.9	72.4	2.7
7557_69	86.57076	3.49%	0.04608	1.35%	74.0	2.6	0.0	34.3	74.0	2.6
7557_68	86.59937	3.62%	0.04540	2.41%	74.0	2.7	0.0	23.2	74.0	2.7
7557_67	85.36853	3.80%	0.04937	2.50%	75.1	2.8	165.3	57.3	75.1	2.8
7557_66	87.84881	3.86%	0.04973	2.74%	73.0	2.8	182.4	62.7	73.0	2.8
7557_65	88.03124	3.44%	0.04826	1.98%	72.8	2.5	112.0	46.0	72.8	2.5
7557_64	80.52848	3.57%	0.05300	1.89%	79.6	2.8	328.8	42.3	79.6	2.8
7557_63	84.88410	3.60%	0.04575	2.41%	75.5	2.7	0.0	41.9	75.5	2.7
7557_62	85.33167	3.78%	0.05007	2.41%	75.1	2.8	198.0	55.0	75.1	2.8
7557_61	78.64199	3.77%	0.04478	2.91%	81.5	3.1	0.0	0.0	81.5	3.1
7557_60	85.78963	3.78%	0.06704	3.42%	74.7	2.8	839.0	69.7	74.7	2.8
7557_59	86.10863	3.50%	0.04788	2.23%	74.4	2.6	93.4	51.9	74.4	2.6
7557_58	86.87047	3.66%	0.04835	2.24%	73.8	2.7	116.6	52.0	73.8	2.7
7557_57	83.48083	3.72%	0.04493	2.38%	76.8	2.8	0.0	0.0	76.8	2.8
7557_56	86.55267	3.83%	0.04779	3.81%	74.1	2.8	89.1	87.8	74.1	2.8
7557_55	80.63803	3.12%	0.04810	2.24%	79.5	2.5	104.2	52.2	79.5	2.5
7557_54	68.11049	2.98%	0.04849	1.97%	94.0	2.8	123.3	45.7	94.0	2.8
7557_53	24.05947	2.78%	0.05295	1.02%	262.5	7.1	326.5	23.0	262.5	7.1
7557_52	81.32564	3.16%	0.04580	2.32%	78.8	2.5	0.0	42.5	78.8	2.5
7557_51	84.02425	3.29%	0.04692	2.95%	76.3	2.5	44.9	69.0	76.3	2.5
7557_50	81.52972	3.02%	0.04946	2.00%	78.6	2.4	169.7	45.9	78.6	2.4
7557_49	71.21147	3.11%	0.04374	1.96%	89.9	2.8	0.0	0.0	89.9	2.8
7557_48	86.09000	3.32%	0.04968	2.56%	74.4	2.5	180.0	58.7	74.4	2.5
7557_47	77.79973	3.05%	0.04829	1.81%	82.3	2.5	113.5	42.1	82.3	2.5
7557_46	88.45329	3.09%	0.04565	2.02%	72.5	2.2	0.0	27.4	72.5	2.2
7557_45	85.74248	3.46%	0.04492	2.23%	74.7	2.6	0.0	0.0	74.7	2.6
7557_44	83.78282	3.63%	0.05743	2.47%	76.5	2.8	508.1	53.5	76.5	2.8
7557_43	23.18936	3.20%	0.05268	1.43%	272.2	8.5	315.0	32.2	272.2	8.5
7557_42	26.31168	3.36%	0.05162	1.59%	240.5	7.9	268.7	36.1	240.5	7.9
7557_41	28.09394	3.33%	0.05117	1.52%	225.5	7.4	248.7	34.5	225.5	7.4
7557_39	85.19936	3.29%	0.04782	1.79%	75.2	2.5	90.1	41.9	75.2	2.5
7557_38	81.87664	3.47%	0.05699	2.51%	78.3	2.7	491.3	54.4	78.3	2.7
7557_37	85.41022	3.53%	0.04740	2.70%	75.0	2.6	69.2	63.1	75.0	2.6
7557_35	82.77093	4.14%	0.04989	2.41%	77.4	3.2	189.6	55.0	77.4	3.2
7557_34	86.10568	4.26%	0.04997	3.05%	74.4	3.2	193.4	69.4	74.4	3.2
7557_33	82.19553	4.37%	0.04665	2.65%	78.0	3.4	31.2	62.2	78.0	3.4
7557_32	84.86390	4.33%	0.04753	2.81%	75.5	3.3	75.8	65.5	75.5	3.3
7557_31	84.55766	4.05%	0.04969	2.23%	75.8	3.0	180.6	51.1	75.8	3.0
7557_30	81.96324	4.17%	0.04678	3.09%	78.2	3.2	38.0	72.4	78.2	3.2
7557_29	83.50565	4.29%	0.04944	2.79%	76.7	3.3	168.9	64.0	76.7	3.3
7557_28	85.92791	4.16%	0.04767	2.41%	74.6	3.1	83.0	56.2	74.6	3.1
7557_27	86.03725	4.27%	0.05676	2.70%	74.5	3.2	482.1	58.6	74.5	3.2
7557_26	84.25929	4.30%	0.05389	2.80%	76.1	3.2	366.3	61.8	76.1	3.2
7557_25	83.77590	3.69%	0.04943	2.59%	76.5	2.8	168.4	59.5	76.5	2.8

Appendix Table 1 (*continued*)

Sample name	238U 206Pb	1 sigma % error	207Pb 206Pb	1 sigma % error	206/238 age	1 sigma err (Ma)	207/206 age	1 sigma err (Ma)	Best age	1 sigma err (Ma)
7557_24	75.51075	3.43%	0.05056	2.04%	84.8	2.9	220.7	46.4	84.8	2.9
7557_23	89.43104	3.82%	0.04705	2.57%	71.7	2.7	51.8	60.3	71.7	2.7
7557_22	82.88127	3.42%	0.04770	1.96%	77.3	2.6	84.5	45.9	77.3	2.6
7557_21	89.11810	3.60%	0.04768	1.98%	71.9	2.6	83.3	46.2	71.9	2.6
7557_20	89.37943	3.67%	0.04718	2.99%	71.7	2.6	58.4	69.8	71.7	2.6
7557_19	84.40490	3.66%	0.04819	2.55%	75.9	2.8	108.4	59.2	75.9	2.8
7557_18	23.02297	3.21%	0.05322	1.32%	274.1	8.6	338.0	29.6	274.1	8.6
7557_15	86.45583	4.35%	0.04665	2.78%	74.1	3.2	31.5	65.3	74.1	3.2
7557_14	72.24662	4.47%	0.04897	1.85%	88.6	3.9	146.6	42.9	88.6	3.9
7557_13	24.01023	4.01%	0.05286	0.94%	263.0	10.3	322.7	21.1	263.0	10.3
7557_12	28.38557	4.28%	0.05232	1.35%	223.2	9.4	299.6	30.6	223.2	9.4
7557_11	91.58607	4.49%	0.04870	2.14%	70.0	3.1	133.3	49.6	70.0	3.1
7557_10	89.39390	4.45%	0.04775	1.29%	71.7	3.2	86.7	30.4	71.7	3.2
7557_9	87.40358	4.85%	0.05099	3.47%	73.3	3.5	240.3	78.0	73.3	3.5
7557_6	87.00731	4.38%	0.05154	1.81%	73.7	3.2	265.1	41.1	73.7	3.2
7557_5	97.06172	6.63%	0.04768	2.88%	66.1	4.4	83.2	67.0	66.1	4.4
7557_4	79.05285	6.38%	0.04758	1.99%	81.0	5.1	78.7	46.5	81.0	5.1
7557_3	93.45284	6.42%	0.04722	2.18%	68.6	4.4	60.3	51.2	68.6	4.4
7557_2	91.79408	6.23%	0.04800	1.08%	69.8	4.3	99.4	25.4	69.8	4.3
7557_1	83.61540	6.27%	0.04955	1.70%	76.6	4.8	174.0	39.2	76.6	4.8
Locality C4										
7000_104a	22.97312	1.92%	0.05763	1.36%	274.7	5.2	515.9	29.6	274.7	5.2
7000_102a	5.02732	2.07%	0.10084	0.92%	1169.5	22.1	1639.7	17.0	1639.7	17.0
7000_100a	70.57863	2.10%	0.04976	3.13%	90.7	1.9	183.9	71.4	90.7	1.9
7000_99a	68.50068	1.56%	0.04957	1.30%	93.4	1.4	175.1	30.0	93.4	1.4
7000_96a	25.32585	1.61%	0.05140	1.05%	249.6	3.9	259.0	24.0	249.6	3.9
7000_95a	72.12809	2.16%	0.05559	3.06%	88.8	1.9	435.8	66.7	88.8	1.9
7000_94a	28.86336	2.58%	0.05420	1.07%	219.6	5.6	379.5	23.9	219.6	5.6
7000_93a	82.61472	1.95%	0.05638	2.41%	77.6	1.5	467.2	52.6	77.6	1.5
7000_91a	82.87126	1.55%	0.04836	1.21%	77.3	1.2	117.0	28.3	77.3	1.2
7000_90a	24.82002	1.53%	0.05142	1.09%	254.6	3.8	259.8	24.9	254.6	3.8
7000_89a	90.54053	1.76%	0.05286	1.73%	70.8	1.2	322.8	38.8	70.8	1.2
7000_88a	26.19330	1.48%	0.05243	1.09%	241.5	3.5	304.3	24.7	241.5	3.5
7000_87a	20.18896	1.92%	0.05369	1.10%	311.6	5.8	358.1	24.7	311.6	5.8
7000_86_1a	6.78280	2.25%	0.07278	0.94%	886.6	18.6	1007.8	18.9	886.6	18.6
7000_85a	11.78202	2.05%	0.05841	0.92%	525.2	10.3	545.0	20.1	525.2	10.3
7000_84a	9.60129	2.12%	0.07049	0.99%	638.7	12.9	942.8	20.1	638.7	12.9
7000_83a	87.06302	2.18%	0.04854	1.71%	73.6	1.6	125.5	39.7	73.6	1.6
7000_81a	22.09652	2.08%	0.05229	0.99%	285.3	5.8	298.2	22.3	285.3	5.8
7000_80a	18.30172	3.23%	0.05912	3.16%	342.9	10.8	571.6	67.3	342.9	10.8
7000_79a	6.56656	2.17%	0.07675	0.90%	913.8	18.5	1114.7	17.9	1114.7	17.9
7000_78a	7.75170	2.12%	0.06489	1.03%	782.2	15.6	770.8	21.5	782.2	15.6
7000_77a	25.65048	2.15%	0.05083	1.09%	246.5	5.2	233.2	24.9	246.5	5.2
7000_76a	79.28581	2.44%	0.04950	2.66%	80.8	2.0	171.8	61.0	80.8	2.0
7000_75a	23.90340	2.05%	0.05291	1.02%	264.2	5.3	325.0	23.0	264.2	5.3
7000_74a	21.43720	4.00%	0.06472	4.01%	293.9	11.5	765.2	82.2	293.9	11.5
7000_73a	12.91233	2.06%	0.05849	1.01%	480.9	9.5	548.1	22.0	480.9	9.5
7000_71a	66.82801	1.89%	0.04664	1.29%	95.7	1.8	30.6	30.7	95.7	1.8
7000_70a	21.80223	1.82%	0.05245	0.89%	289.1	5.2	305.0	20.1	289.1	5.2
7000_69a	85.46730	1.95%	0.04954	1.46%	75.0	1.5	173.4	33.8	75.0	1.5
7000_68a	92.81807	2.39%	0.04559	3.38%	69.1	1.6	0.0	55.6	69.1	1.6
7000_67a	2.98842	1.82%	0.11329	0.63%	1860.8	29.4	1852.9	11.3	1852.9	11.3
7000_66a	74.37647	2.57%	0.05228	2.29%	86.1	2.2	297.5	51.4	86.1	2.2
7000_65a	115.14534	3.56%	0.04643	4.67%	55.7	2.0	19.8	108.7	55.7	2.0
7000_64a	10.04121	1.95%	0.06109	0.72%	612.0	11.4	642.4	15.3	612.0	11.4
7000_62a	17.90321	1.89%	0.05393	0.90%	350.4	6.4	368.2	20.1	350.4	6.4
7000_61a	14.26966	1.84%	0.05642	0.66%	436.6	7.8	468.8	14.5	436.6	7.8
7000_60a	85.73285	1.96%	0.04658	1.69%	74.8	1.5	27.5	39.9	74.8	1.5
7000_59a	84.34232	2.43%	0.05019	2.39%	76.0	1.8	203.8	54.5	76.0	1.8
7000_58a	9.55136	4.25%	0.07273	3.59%	641.9	25.9	1006.5	71.2	641.9	25.9
7000_57a	10.83579	2.10%	0.05915	0.81%	569.0	11.4	572.6	17.4	569.0	11.4
7000_56a	90.27224	2.00%	0.04540	3.29%	71.0	1.4	0.0	43.8	71.0	1.4
7000_54a	19.49282	1.20%	0.05494	1.26%	322.5	3.8	409.8	27.8	322.5	3.8
7000_53a	13.14488	1.12%	0.05682	1.15%	472.7	5.1	484.7	25.2	472.7	5.1
7000_52a	20.50705	2.16%	0.05560	1.16%	306.9	6.5	436.6	25.5	306.9	6.5
7000_51a	29.60911	2.70%	0.05341	1.08%	214.1	5.7	346.1	24.3	214.1	5.7
7000_50a	126.07141	2.81%	0.03490	7.93%	50.9	1.4	0.0	0.0	50.9	1.4
7000_49a	22.24679	1.45%	0.05607	1.11%	283.4	4.0	455.3	24.5	283.4	4.0
7000_48a	23.37263	4.67%	0.03955	6.77%	270.1	12.3	0.0	0.0	270.1	12.3
7000_47a	73.75186	1.57%	0.04390	2.59%	86.8	1.4	0.0	0.0	86.8	1.4
7000_45a	22.80442	1.08%	0.05309	1.18%	276.7	2.9	332.7	26.4	276.7	2.9
7000_44a	21.45714	2.75%	0.06210	2.93%	293.6	7.9	677.5	61.4	293.6	7.9
7000_43a	22.02633	1.08%	0.05174	1.21%	286.2	3.0	273.8	27.6	286.2	3.0
7000_41a	10.35045	1.01%	0.06398	1.07%	594.5	5.7	741.0	22.5	594.5	5.7

(*continued on next page*)

Appendix Table 1 (*continued*)

Sample name	238U 206Pb	1 sigma % error	207Pb 206Pb	1 sigma % error	206/238 age	1 sigma err (Ma)	207/206 age	1 sigma err (Ma)	Best age	1 sigma err (Ma)
7000_40a	68.84954	1.15%	0.05197	1.72%	93.0	1.1	284.1	38.8	93.0	1.1
7000_39a	72.93707	1.54%	0.04906	2.95%	87.8	1.3	150.6	67.8	87.8	1.3
7000_37a	68.97346	0.87%	0.05548	1.16%	92.8	0.8	431.8	25.5	92.8	0.8
7000_36a	64.61153	1.44%	0.05362	2.42%	99.0	1.4	355.2	53.7	99.0	1.4
7000_35a	4.91153	0.65%	0.07876	0.33%	1194.6	7.1	1166.0	6.5	1166.0	6.5
7000_34a	4.18848	1.02%	0.08778	0.45%	1380.2	12.6	1377.6	8.6	1377.6	8.6
7000_33a	22.53115	0.71%	0.05135	0.62%	279.9	1.9	256.6	14.1	279.9	1.9
7000_32a	22.42793	0.63%	0.05117	0.71%	281.2	1.7	248.5	16.2	281.2	1.7
7000_31a	5.77679	1.42%	0.07359	0.51%	1029.2	13.5	1030.2	10.4	1030.2	10.4
7000_30a	17.83708	0.69%	0.05348	0.63%	351.6	2.4	349.3	14.2	351.6	2.4
7000_29a	70.31102	0.79%	0.05146	1.36%	91.0	0.7	261.3	30.9	91.0	0.7
7000_28a	8.94510	0.62%	0.06788	0.31%	683.2	4.0	865.0	6.4	683.2	4.0
7000_24a	84.21036	2.51%	0.04694	3.24%	76.1	1.9	46.4	75.8	76.1	1.9
7000_25a	4.52683	2.01%	0.09877	1.23%	1286.7	23.4	1601.1	22.7	1601.1	22.7
7000_23a	27.72189	1.82%	0.05100	1.33%	228.4	4.1	240.8	30.3	228.4	4.1
7000_22a	24.28886	1.81%	0.05178	1.30%	260.1	4.6	275.7	29.5	260.1	4.6
7000_21a	22.03367	2.24%	0.05556	1.23%	286.1	6.3	434.8	27.1	286.1	6.3
7000_19a	10.82886	1.83%	0.06739	1.11%	569.4	10.0	849.9	22.9	569.4	10.0
7000_20a	14.13824	1.71%	0.05617	1.18%	440.6	7.3	459.2	25.9	440.6	7.3
7000_18a	29.17452	1.77%	0.05937	1.52%	217.3	3.8	580.5	32.6	217.3	3.8
7000_17a	16.76013	1.74%	0.05489	1.25%	373.6	6.3	407.7	27.8	373.6	6.3
7000_16a	91.08820	2.12%	0.04694	2.83%	70.4	1.5	46.1	66.4	70.4	1.5
7000_15a	5.47097	1.80%	0.07567	1.24%	1082.2	17.9	1086.4	24.7	1086.4	24.7
7000_14a	21.03584	1.84%	0.05470	1.59%	299.4	5.4	400.1	35.2	299.4	5.4
7000_13a	6.48329	1.79%	0.07363	1.16%	924.7	15.4	1031.3	23.2	924.7	15.4
7000_12a	24.79279	2.08%	0.05228	1.57%	254.9	5.2	297.8	35.4	254.9	5.2
7000_11a	69.40119	1.77%	0.04890	1.74%	92.2	1.6	143.0	40.2	92.2	1.6
7000_10a	83.09886	1.05%	0.04783	1.13%	77.1	0.8	90.8	26.6	77.1	0.8
7000_9a	27.32161	0.80%	0.05183	0.74%	231.7	1.8	277.9	16.8	231.7	1.8
7000_7a	3.47270	0.82%	0.09936	0.50%	1631.3	11.8	1612.1	9.2	1612.1	9.2
7000_8a	30.48973	1.43%	0.05328	0.64%	208.0	2.9	340.6	14.4	208.0	2.9
7000_6a	17.74782	1.99%	0.05791	0.78%	353.4	6.8	526.3	16.9	353.4	6.8
7000_4a	90.21246	1.12%	0.04744	1.68%	71.1	0.8	71.3	39.4	71.1	0.8
7000_5a	6.87565	0.80%	0.07298	0.38%	875.4	6.6	1013.4	7.6	875.4	6.6
7000_3a	87.36860	0.88%	0.04808	0.76%	73.4	0.6	103.4	17.9	73.4	0.6
7000_2a	68.12696	1.29%	0.04827	1.67%	93.9	1.2	112.4	39.0	93.9	1.2
7000_1a	22.46832	0.94%	0.05157	1.03%	280.7	2.6	266.4	23.5	280.7	2.6
Locality C7										
6999_100a	75.34954	2.09%	0.04836	2.57%	85.0	1.8	116.7	59.5	85.0	1.8
6999_98a	86.87282	2.01%	0.04476	2.68%	73.8	1.5	0.0	0.2	73.8	1.5
6999_97a	87.24067	2.16%	0.04608	2.60%	73.5	1.6	2.6	60.5	73.5	1.6
6999_96a	85.79066	2.12%	0.04707	2.74%	74.7	1.6	52.8	64.1	74.7	1.6
6999_95a	89.71132	1.85%	0.04723	1.55%	71.5	1.3	61.1	36.5	71.5	1.3
6999_94a	89.17906	2.30%	0.04777	2.61%	71.9	1.6	88.0	60.7	71.9	1.6
6999_92a	78.38771	2.03%	0.04951	2.52%	81.7	1.6	172.2	57.8	81.7	1.6
6999_91a	84.85072	1.85%	0.04748	2.01%	75.5	1.4	73.7	47.1	75.5	1.4
6999_90	89.54803	1.70%	0.04714	1.88%	71.6	1.2	56.2	44.3	71.6	1.2
6999_89	75.45471	1.87%	0.04856	2.24%	84.9	1.6	126.5	52.0	84.9	1.6
6999_88	87.28795	1.48%	0.04677	1.15%	73.4	1.1	37.5	27.4	73.4	1.1
6999_87	83.43099	2.08%	0.04710	2.93%	76.8	1.6	54.3	68.4	76.8	1.6
6999_86	91.84408	2.43%	0.04918	3.41%	69.8	1.7	156.2	77.9	69.8	1.7
6999_85	86.13612	1.58%	0.04999	1.40%	74.4	1.2	194.7	32.2	74.4	1.2
6999_84	89.50991	1.73%	0.04753	1.24%	71.6	1.2	76.1	29.2	71.6	1.2
6999_82	85.42864	1.84%	0.04899	2.13%	75.0	1.4	147.4	49.2	75.0	1.4
6999_83	90.15056	1.97%	0.04709	2.53%	71.1	1.4	53.8	59.4	71.1	1.4
6999_81	91.42694	1.53%	0.04663	1.55%	70.1	1.1	30.2	36.8	70.1	1.1
6999_80	87.03544	1.71%	0.04944	1.83%	73.6	1.3	168.7	42.1	73.6	1.3
6999_79	91.01562	2.15%	0.05859	3.18%	70.4	1.5	551.9	68.0	70.4	1.5
6999_78	71.90421	1.60%	0.05528	1.48%	89.0	1.4	423.6	32.7	89.0	1.4
6999_77	86.24869	1.56%	0.04673	1.27%	74.3	1.1	35.6	30.2	74.3	1.1
6999_76	88.13924	1.58%	0.05235	2.25%	72.7	1.1	300.9	50.4	72.7	1.1
6999_75	96.27677	1.20%	0.04775	1.87%	66.6	0.8	86.7	43.9	66.6	0.8
6999_74	85.08296	2.21%	0.04641	3.23%	75.3	1.7	18.8	75.9	75.3	1.7
6999_73	91.44144	1.44%	0.05042	2.34%	70.1	1.0	214.4	53.2	70.1	1.0
6999_72	89.17466	1.66%	0.04440	2.62%	71.9	1.2	0.0	0.0	71.9	1.2
6999_71	93.76809	0.87%	0.04785	1.10%	68.4	0.6	91.8	25.9	68.4	0.6
6999_70	80.72602	1.41%	0.04601	2.03%	79.4	1.1	0.0	46.3	79.4	1.1
6999_69	90.70023	1.58%	0.04974	2.72%	70.7	1.1	182.9	62.2	70.7	1.1
6999_68	73.09477	1.40%	0.04635	2.30%	87.6	1.2	16.1	54.4	87.6	1.2
6999_67	86.79713	1.66%	0.05046	2.82%	73.8	1.2	216.2	63.9	73.8	1.2
6999_66	82.51077	1.06%	0.04901	1.44%	77.7	0.8	148.2	33.5	77.7	0.8
6999_65	90.35633	1.23%	0.04879	2.05%	71.0	0.9	138.0	47.5	71.0	0.9
6999_63	87.42154	1.30%	0.04744	2.01%	73.3	1.0	71.4	47.2	73.3	1.0
6999_62	97.57163	0.95%	0.04706	1.03%	65.7	0.6	52.4	24.5	65.7	0.6

Appendix Table 1 (*continued*)

Sample name	238U 206Pb	1 sigma % error	207Pb 206Pb	1 sigma % error	206/238 age	1 sigma err (Ma)	207/206 age	1 sigma err (Ma)	Best age	1 sigma err (Ma)
6999_61	73.44284	1.26%	0.04719	2.02%	87.2	1.1	58.8	47.5	87.2	1.1
6999_60	82.81775	1.41%	0.04767	2.22%	77.4	1.1	82.8	51.9	77.4	1.1
6999_59	74.36814	1.40%	0.05062	2.61%	86.1	1.2	223.6	59.2	86.1	1.2
6999_57	73.79980	1.48%	0.04994	2.62%	86.8	1.3	192.4	59.7	86.8	1.3
6999_56	87.86904	1.30%	0.05105	2.14%	72.9	0.9	242.9	48.5	72.9	0.9
6999_58	94.84058	1.39%	0.04987	2.00%	67.6	0.9	189.0	45.8	67.6	0.9
6999_55	89.26235	1.57%	0.04758	2.58%	71.8	1.1	78.4	60.0	71.8	1.1
6999_54	92.49628	1.39%	0.04767	1.64%	69.3	1.0	83.0	38.4	69.3	1.0
6999_53	87.91228	1.54%	0.04918	2.67%	72.9	1.1	156.5	61.3	72.9	1.1
6999_52	78.47297	0.97%	0.04805	1.37%	81.6	0.8	101.7	32.2	81.6	0.8
6999_51	70.58963	1.46%	0.05614	2.52%	90.7	1.3	458.0	54.8	90.7	1.3
6999_50	94.14180	1.09%	0.04751	1.82%	68.1	0.7	75.1	42.8	68.1	0.7
6999_49	91.61162	1.98%	0.04922	3.07%	70.0	1.4	158.3	70.3	70.0	1.4
6999_48	88.30425	1.97%	0.04847	3.21%	72.6	1.4	122.1	73.9	72.6	1.4
6999_47	87.39263	1.37%	0.04700	2.00%	73.3	1.0	49.1	47.0	73.3	1.0
6999_46	88.67315	1.35%	0.04685	2.23%	72.3	1.0	41.8	52.6	72.3	1.0
6999_45	87.08426	1.47%	0.05374	2.27%	73.6	1.1	360.1	50.5	73.6	1.1
6999_44	87.29385	2.47%	0.05177	3.13%	73.4	1.8	275.3	70.2	73.4	1.8
6999_43	87.17086	1.96%	0.04601	2.98%	73.5	1.4	0.0	68.6	73.5	1.4
6999_42	85.37229	1.47%	0.04733	1.31%	75.1	1.1	65.8	30.9	75.1	1.1
6999_41	75.23913	1.96%	0.04692	2.40%	85.1	1.7	45.0	56.4	85.1	1.7
6999_40	90.85794	1.67%	0.04822	1.47%	70.6	1.2	110.3	34.3	70.6	1.2
6999_39	71.79230	1.84%	0.04709	1.70%	89.2	1.6	53.8	40.0	89.2	1.6
6999_38	84.51546	1.95%	0.04979	2.24%	75.8	1.5	185.2	51.4	75.8	1.5
6999_37	86.77718	2.05%	0.04841	2.56%	73.9	1.5	119.3	59.2	73.9	1.5
6999_35	87.55836	1.60%	0.04612	1.20%	73.2	1.2	3.7	28.8	73.2	1.2
6999_34	85.22740	1.71%	0.04744	2.02%	75.2	1.3	71.3	47.3	75.2	1.3
6999_32	87.18610	1.75%	0.04838	2.15%	73.5	1.3	118.0	50.0	73.5	1.3
6999_33	84.32716	1.77%	0.04907	1.48%	76.0	1.3	151.2	34.2	76.0	1.3
6999_31	96.09569	1.77%	0.04862	1.96%	66.7	1.2	129.3	45.4	66.7	1.2
6999_30a	76.11949	1.49%	0.04724	2.48%	84.1	1.2	61.3	58.1	84.1	1.2
6999_29a	79.97032	1.35%	0.05001	2.57%	80.1	1.1	195.7	58.6	80.1	1.1
6999_28a	93.28956	1.06%	0.04846	1.35%	68.7	0.7	121.8	31.6	68.7	0.7
6999_27a	94.03140	1.16%	0.04952	1.54%	68.2	0.8	172.6	35.6	68.2	0.8
6999_26a	89.59112	1.73%	0.04626	2.99%	71.6	1.2	0.0	81.7	71.6	1.2
6999_25a	90.39486	1.38%	0.04640	1.94%	70.9	1.0	18.5	46.1	70.9	1.0
6999_24a	22.79268	0.87%	0.05290	0.91%	276.8	2.3	324.5	20.5	276.8	2.3
6999_23a	90.67939	1.07%	0.04728	1.52%	70.7	0.8	63.1	35.8	70.7	0.8
6999_22a	90.31903	1.17%	0.04633	1.81%	71.0	0.8	0.0	57.7	71.0	0.8
6999_21a	83.38173	1.09%	0.04796	1.93%	76.9	0.8	97.3	45.0	76.9	0.8
6999_20a	97.36494	1.96%	0.04827	1.76%	65.9	1.3	112.6	41.0	65.9	1.3
6999_19a_4b	87.62636	0.90%	0.04760	1.70%	73.2	0.7	79.7	39.8	73.2	0.7
6999_18a_4b	64.03069	1.16%	0.04718	1.61%	99.9	1.1	58.2	38.0	99.9	1.1
6999_17a_4b	91.76113	0.93%	0.04787	1.19%	69.9	0.6	92.8	27.9	69.9	0.6
6999_16a_4b	90.12918	1.13%	0.05005	1.74%	71.1	0.8	197.4	39.8	71.1	0.8
6999_15a	92.13010	1.04%	0.04802	1.61%	69.6	0.7	100.2	37.7	69.6	0.7
6999_14a	81.26575	1.83%	0.04783	2.08%	78.8	1.4	90.7	48.6	78.8	1.4
6999_13a	90.85554	1.16%	0.04981	1.84%	70.6	0.8	185.9	42.4	70.6	0.8
6999_12a	72.44324	1.10%	0.04913	1.63%	88.4	1.0	154.2	37.8	88.4	1.0
6999_11a	72.60420	1.73%	0.04905	2.66%	88.2	1.5	150.4	61.3	88.2	1.5
6999_10a	72.81314	1.13%	0.05972	1.84%	87.9	1.0	593.3	39.4	87.9	1.0
6999_9a	75.56183	0.97%	0.05946	1.81%	84.8	0.8	584.0	38.8	84.8	0.8
6999_8a	88.56137	1.44%	0.04918	2.23%	72.4	1.0	156.6	51.3	72.4	1.0
6999_7a	83.78244	1.33%	0.04646	2.33%	76.5	1.0	21.7	54.9	76.5	1.0
6999_5a	87.48771	0.91%	0.04762	1.27%	73.3	0.7	80.6	29.8	73.3	0.7
6999_4a	89.88171	1.34%	0.04683	1.94%	71.3	0.9	40.8	45.7	71.3	0.9
6999_3a	64.80660	1.55%	0.05528	2.07%	98.7	1.5	423.7	45.5	98.7	1.5
6999_2a	87.06236	1.11%	0.04879	1.99%	73.6	0.8	0.0	183.9	73.6	0.8
6999_1a	87.61770	1.50%	0.04916	1.96%	73.2	1.1	155.4	45.3	73.2	1.1
Locality C4										
7001_100a	88.40730	1.95%	0.04681	2.62%	72.5	1.4	39.7	61.6	72.5	1.4
7001_99a	93.29052	1.95%	0.04665	2.74%	68.7	1.3	31.1	64.4	68.7	1.3
7001_98a	88.66154	1.89%	0.04526	2.32%	72.3	1.4	0.0	10.6	72.3	1.4
7001_97a	85.51144	1.85%	0.05013	2.28%	74.9	1.4	201.1	52.0	74.9	1.4
7001_95a	86.36506	2.06%	0.04951	3.06%	74.2	1.5	171.8	69.9	74.2	1.5
7001_94a	88.85384	1.82%	0.04748	2.17%	72.1	1.3	73.6	50.7	72.1	1.3
7001_93a	74.71576	1.67%	0.04823	1.71%	85.7	1.4	110.4	39.9	85.7	1.4
7001_92a	66.16604	1.84%	0.06683	2.17%	96.7	1.8	832.5	44.7	96.7	1.8
7001_91a	3.51407	1.49%	0.11091	1.15%	1614.3	21.2	1814.4	20.7	1814.4	20.7
7001_90a	90.26545	1.86%	0.04910	2.52%	71.0	1.3	152.5	57.9	71.0	1.3
7001_89a	89.45134	1.54%	0.04694	1.46%	71.7	1.1	46.2	34.6	71.7	1.1
7001_88a	89.60035	1.90%	0.05196	2.73%	71.5	1.4	283.5	61.2	71.5	1.4
7001_87a	89.61042	2.10%	0.05236	2.97%	71.5	1.5	301.3	66.4	71.5	1.5
7001_86a	81.86776	1.66%	0.04773	1.78%	78.3	1.3	86.1	41.6	78.3	1.3

(*continued on next page*)

Appendix Table 1 (*continued*)

Sample	238U	1 sigma	207Pb	1 sigma	206/238	1 sigma	207/206	1 sigma	Best age	1 sigma
name	206Pb	% error	206Pb	% error	age	err (Ma)	age	err (Ma)		err (Ma)
7001_85a	89.13610	1.84%	0.04770	2.46%	71.9	1.3	84.4	57.4	71.9	1.3
7001_84a	27.31294	1.10%	0.05115	0.77%	231.8	2.5	247.7	17.5	231.8	2.5
7001_83a	92.08334	1.83%	0.04861	2.79%	69.6	1.3	129.0	64.4	69.6	1.3
7001_82a	81.42759	1.38%	0.04727	1.53%	78.7	1.1	62.7	36.0	78.7	1.1
7001_81a	89.73387	1.80%	0.05024	2.91%	71.4	1.3	206.2	66.2	71.4	1.3
7001_80a	27.07666	1.29%	0.05032	1.13%	233.8	3.0	209.8	26.0	233.8	3.0
7001_79a	90.22365	1.50%	0.04815	1.87%	71.1	1.1	106.8	43.6	71.1	1.1
7001_78a	5.80123	1.20%	0.07508	0.58%	1025.2	11.4	1070.5	11.6	1070.5	11.6
7001_77a	87.30846	1.90%	0.04850	3.17%	73.4	1.4	123.6	73.1	73.4	1.4
7001_76a	79.96828	1.40%	0.04755	1.54%	80.1	1.1	76.9	36.3	80.1	1.1
7001_75a	88.60464	1.94%	0.04772	2.98%	72.3	1.4	85.2	69.2	72.3	1.4
7001_74a	86.19837	1.68%	0.04842	2.53%	74.4	1.2	119.7	58.6	74.4	1.2
7001_73a	101.57149	1.85%	0.04931	0.93%	63.2	1.2	162.5	21.5	63.2	1.2
7001_71a	82.03669	1.26%	0.04739	1.37%	78.1	1.0	68.9	32.3	78.1	1.0
7001_70a	13.46700	2.16%	0.05652	0.92%	461.7	9.6	472.8	20.2	461.7	9.6
7001_69a	90.14166	2.46%	0.04823	2.27%	71.1	1.7	110.8	52.8	71.1	1.7
7001_68a	27.28145	2.22%	0.05129	1.07%	232.1	5.1	253.8	24.5	232.1	5.1
7001_67a	19.31492	2.30%	0.05622	1.37%	325.4	7.3	461.2	30.1	325.4	7.3
7001_66a	86.97803	2.80%	0.05150	3.00%	73.7	2.1	263.2	67.4	73.7	2.1
7001_65a	80.91935	2.41%	0.04834	1.99%	79.2	1.9	115.9	46.3	79.2	1.9
7001_64a	71.01314	2.31%	0.04804	1.60%	90.1	2.1	101.2	37.3	90.1	2.1
7001_63a	87.56295	2.40%	0.04878	1.75%	73.2	1.7	137.3	40.7	73.2	1.7
7001_62a	89.66979	2.70%	0.05103	2.64%	71.5	1.9	242.0	59.7	71.5	1.9
7001_61a	88.62164	2.35%	0.04761	1.60%	72.3	1.7	79.8	37.6	72.3	1.7
7001_60a	23.17129	2.26%	0.05084	1.28%	272.4	6.0	233.7	29.2	272.4	6.0
7001_59a	26.78413	2.31%	0.05090	1.16%	236.3	5.4	236.2	26.6	236.3	5.4
7001_58a	88.27773	2.64%	0.04833	2.81%	72.6	1.9	115.2	65.0	72.6	1.9
7001_57a	87.28379	2.64%	0.05143	2.52%	73.4	1.9	260.0	56.9	73.4	1.9
7001_56a	87.64166	2.75%	0.04747	2.76%	73.1	2.0	73.2	64.3	73.1	2.0
7001_55a	87.99579	2.22%	0.04972	2.41%	72.8	1.6	181.9	55.3	72.8	1.6
7001_54a	89.68700	2.22%	0.04954	2.15%	71.5	1.6	173.6	49.5	71.5	1.6
7001_53a	89.69573	2.89%	0.05229	3.67%	71.5	2.1	298.0	81.6	71.5	2.1
7001_52a	91.23695	2.39%	0.05363	2.85%	70.3	1.7	355.5	63.0	70.3	1.7
7001_51a	90.01166	2.03%	0.04758	1.67%	71.2	1.4	78.2	39.1	71.2	1.4
7001_50a	89.99144	2.59%	0.04912	2.90%	71.2	1.8	153.7	66.6	71.2	1.8
7001_49a	87.44470	2.66%	0.04927	3.23%	73.3	1.9	160.8	73.9	73.3	1.9
7001_48a	89.75064	1.90%	0.04803	0.86%	71.4	1.4	100.7	20.2	71.4	1.4
7001_47a	31.48049	2.68%	0.05850	0.98%	201.6	5.3	548.6	21.3	201.6	5.3
7001_46a	27.54894	1.86%	0.05193	0.69%	229.9	4.2	282.5	15.6	229.9	4.2
7001_45a	87.02234	1.85%	0.04803	0.89%	73.7	1.4	100.5	21.0	73.7	1.4
7001_44a	32.00780	2.63%	0.05257	0.97%	198.3	5.1	310.4	21.9	198.3	5.1
7001_44a	32.00780	2.63%	0.05257	0.97%	198.3	5.1	310.4	21.9	198.3	5.1
7001_43a	88.60906	2.33%	0.04970	2.37%	72.3	1.7	180.8	54.3	72.3	1.7
7001_42a	93.37983	2.03%	0.04987	2.06%	68.7	1.4	189.0	47.2	68.7	1.4
7001_41a	87.92793	2.49%	0.05038	2.95%	72.9	1.8	212.6	67.0	72.9	1.8
7001_40a	91.62143	1.66%	0.05065	2.60%	70.0	1.2	224.9	59.1	70.0	1.2
7001_39a	87.91965	1.36%	0.04937	1.44%	72.9	1.0	165.2	33.4	72.9	1.0
7001_38a	88.93114	1.99%	0.05769	2.75%	72.1	1.4	517.8	59.2	72.1	1.4
7001_37a	88.35127	1.57%	0.04711	2.20%	72.6	1.1	54.9	51.8	72.6	1.1
7001_36a	84.40931	1.34%	0.04885	1.35%	75.9	1.0	140.5	31.3	75.9	1.0
7001_35a	14.05089	1.17%	0.05690	0.70%	443.2	5.0	487.8	15.3	443.2	5.0
7001_34a	87.86024	1.46%	0.05040	1.53%	73.0	1.1	213.4	35.2	73.0	1.1
7001_33a	88.95685	1.89%	0.05007	2.70%	72.1	1.4	198.2	61.6	72.1	1.4
7001_32a	89.74308	1.63%	0.04589	2.32%	71.4	1.2	0.0	47.0	71.4	1.2
7001_31a	70.60558	1.27%	0.04914	1.41%	90.7	1.1	154.6	32.7	90.7	1.1
7001_30a	9.05138	1.32%	0.06272	0.89%	675.5	8.5	698.8	18.8	675.5	8.5
7001_30a	9.05138	1.32%	0.06272	0.89%	675.5	8.5	698.8	18.8	675.5	8.5
7001_29a	27.33110	1.23%	0.05158	1.07%	231.7	2.8	266.9	24.4	231.7	2.8
7001_28a	82.20641	1.39%	0.04652	1.42%	77.9	1.1	24.4	33.7	77.9	1.1
7001_27a	82.61599	1.79%	0.04897	2.57%	77.6	1.4	146.5	59.1	77.6	1.4
7001_26a	88.94064	1.90%	0.04574	2.79%	72.1	1.4	0.0	50.1	72.1	1.4
7001_25a	85.29707	2.39%	0.04776	1.55%	75.1	1.8	87.4	36.4	75.1	1.8
7001_23a	89.81715	2.65%	0.04955	2.78%	71.4	1.9	173.9	63.6	71.4	1.9
7001_24a	86.77855	2.45%	0.04592	2.18%	73.9	1.8	0.0	45.3	73.9	1.8
7001_22a	90.30387	2.54%	0.05119	2.47%	71.0	1.8	249.2	55.8	71.0	1.8
7001_21a	90.16888	2.48%	0.04589	2.28%	71.1	1.8	0.0	46.2	71.1	1.8
7001_20a	90.22345	2.50%	0.04921	2.45%	71.1	1.8	157.9	56.3	71.1	1.8
7001_19a	27.82000	2.16%	0.05097	0.72%	227.7	4.8	239.4	16.6	227.7	4.8
7001_18a	28.84875	2.50%	0.05472	1.56%	219.7	5.4	400.7	34.7	219.7	5.4
7001_17a	89.04030	2.47%	0.04550	2.48%	72.0	1.8	0.0	30.4	72.0	1.8
7001_16a	84.71190	2.57%	0.05416	2.57%	75.7	1.9	377.6	56.8	75.7	1.9
7001_15a	80.10496	2.49%	0.04768	2.34%	80.0	2.0	83.6	54.7	80.0	2.0
7001_14a	11.85439	2.16%	0.05821	0.67%	522.1	10.8	537.7	14.6	522.1	10.8
7001_13a	92.17947	2.61%	0.05456	2.72%	69.6	1.8	394.3	59.9	69.6	1.8
7001_12a	86.87707	2.50%	0.05551	2.21%	73.8	1.8	432.7	48.6	73.8	1.8

Appendix Table 1 (*continued*)

Sample name	238U 206Pb	1 sigma % error	207Pb 206Pb	1 sigma % error	206/238 age	1 sigma err (Ma)	207/206 age	1 sigma err (Ma)	Best age	1 sigma err (Ma)
7001_11a	88.55410	2.93%	0.05088	2.91%	72.4	2.1	235.3	65.7	72.4	2.1
7001_10a	87.71218	2.49%	0.04490	3.78%	73.1	1.8	0.0	28.3	73.1	1.8
7001_9a	22.81735	1.67%	0.05286	0.87%	276.5	4.5	323.0	19.6	276.5	4.5
7001_8a	4.22304	2.09%	0.09254	0.62%	1370.0	25.8	1478.6	11.7	1478.6	11.7
7001_7a	22.51818	1.63%	0.05132	1.13%	280.1	4.5	255.4	25.7	280.1	4.5
7001_6a	85.01397	1.97%	0.04538	1.95%	75.4	1.5	0.0	11.3	75.4	1.5
7001_5a	90.91333	1.85%	0.04783	1.65%	70.5	1.3	90.8	38.7	70.5	1.3
7001_4a	87.05556	2.07%	0.04632	2.75%	73.6	1.5	14.3	64.9	73.6	1.5
7001_3a	87.12305	1.86%	0.04860	1.73%	73.6	1.4	128.5	40.1	73.6	1.4
7001_2a	86.65575	2.04%	0.05332	2.28%	74.0	1.5	342.3	50.8	74.0	1.5
7001_1a	73.51093	2.10%	0.04690	2.36%	87.1	1.8	44.2	55.4	87.1	1.8
Locality C3										
6998_102a	6.17172	1.95%	0.0856	1.57%	968.0	17.5	1329.8	30.1	1329.8	30.1
6998_101a	73.67992	2.09%	0.0535	1.85%	86.9	1.8	351.0	41.2	86.9	1.8
6998_100a	77.09133	1.97%	0.0471	1.42%	83.1	1.6	53.8	33.5	83.1	1.6
6998_98a	28.57604	2.12%	0.0523	0.70%	221.7	4.6	297.8	15.8	221.7	4.6
6998_97a	26.09326	1.94%	0.0630	0.90%	242.4	4.6	709.2	19.0	242.4	4.6
6998_96a	19.42711	2.22%	0.0555	0.90%	323.6	7.0	431.9	20.0	323.6	7.0
6998_95a	22.70383	3.48%	0.0674	0.95%	277.9	9.5	850.1	19.7	277.9	9.5
6998_94a	84.83399	2.08%	0.0462	1.58%	75.5	1.6	13.9	32.7	75.5	1.6
6998_93a	25.83324	1.93%	0.0518	0.74%	244.8	4.6	276.4	16.8	244.8	4.6
6998_92a	83.96643	2.13%	0.0476	1.86%	76.3	1.6	81.7	43.2	76.3	1.6
6998_91a	24.89431	1.87%	0.0505	0.83%	253.9	4.7	220.2	19.1	253.9	4.7
6998_90a	79.02077	2.24%	0.0491	2.16%	81.1	1.8	154.8	49.8	81.1	1.8
6998_89a	24.67903	1.88%	0.0506	0.72%	256.1	4.7	223.6	16.5	256.1	4.7
6998_88a	77.97324	2.00%	0.0480	1.30%	82.1	1.6	100.5	30.4	82.1	1.6
6998_87a	26.53430	2.05%	0.0517	1.26%	238.5	4.8	274.0	28.5	238.5	4.8
6998_86a	24.54111	2.15%	0.0596	1.80%	257.5	5.4	588.4	38.6	257.5	5.4
6998_84a	11.68013	1.87%	0.0581	0.67%	529.6	9.5	532.8	14.7	529.6	9.5
6998_83a	24.21604	1.96%	0.0502	0.83%	260.9	5.0	202.6	19.1	260.9	5.0
6998_82a	24.65971	1.90%	0.0515	0.88%	256.3	4.8	261.1	20.1	256.3	4.8
6998_81a	57.69534	1.10%	0.0482	1.38%	110.8	1.2	107.1	32.2	110.8	1.2
6998_80a	68.06890	1.53%	0.0719	2.66%	94.0	1.4	983.3	53.3	94.0	1.4
6998_79a	84.22161	1.23%	0.0465	1.83%	76.1	0.9	27.0	40.6	76.1	0.9
6998_78a	25.98082	0.97%	0.0515	0.86%	243.5	2.3	264.1	19.6	243.5	2.3
6998_77a	74.26975	1.83%	0.0510	2.92%	86.2	1.6	241.6	66.0	86.2	1.6
6998_76a	26.46325	1.12%	0.0504	1.01%	239.1	2.6	215.0	23.3	239.1	2.6
6998_75a	26.00639	1.00%	0.0507	1.00%	243.2	2.4	226.0	23.0	243.2	2.4
6998_74a	26.45730	0.95%	0.0509	1.00%	239.2	2.2	237.4	23.0	239.2	2.2
6998_73a	79.38901	1.36%	0.0494	2.30%	80.7	1.1	167.7	52.9	80.7	1.1
6998_72a	55.91500	1.38%	0.0503	1.85%	114.3	1.6	207.8	42.3	114.3	1.6
6998_71a	23.79943	1.28%	0.0502	0.98%	265.3	3.3	206.0	22.5	265.3	3.3
6998_70a	75.80370	1.44%	0.0467	2.53%	84.5	1.2	36.8	57.4	84.5	1.2
6998_69a	89.92353	1.86%	0.0576	2.70%	71.3	1.3	515.8	58.2	71.3	1.3
6998_68a	83.69603	1.45%	0.0486	1.93%	76.6	1.1	131.0	44.8	76.6	1.1
6998_67a	75.85849	1.41%	0.0482	2.19%	84.4	1.2	109.1	50.8	84.4	1.2
6998_66a	79.01655	1.80%	0.0468	2.31%	81.1	1.5	39.7	54.4	81.1	1.5
6998_65a	87.91650	1.88%	0.0462	2.67%	72.9	1.4	8.3	61.6	72.9	1.4
6998_64a	25.19386	1.33%	0.0524	0.61%	250.9	3.3	301.5	14.0	250.9	3.3
6998_63a	83.98874	1.42%	0.0454	1.46%	76.3	1.1	0.0	2.8	76.3	1.1
6998_62a	28.95272	1.50%	0.0525	0.99%	218.9	3.2	307.5	22.3	218.9	3.2
6998_61a	7.48265	1.31%	0.0706	0.58%	808.6	9.9	945.9	11.8	808.6	9.9
6998_60a	2.69851	1.52%	0.1111	0.52%	2032.1	26.5	1817.0	9.5	1817.0	9.5
6998_59a	76.82269	1.79%	0.0484	2.00%	83.4	1.5	119.2	46.4	83.4	1.5
6998_58a	71.01627	2.02%	0.0451	2.83%	90.1	1.8	0.0	15.6	90.1	1.8
6998_57a	26.63342	1.29%	0.0509	0.79%	237.6	3.0	235.3	18.1	237.6	3.0
6998_56a	16.54381	1.53%	0.0512	1.08%	378.3	5.6	250.6	24.6	378.3	5.6
6998_55a	21.26177	1.50%	0.0557	1.34%	296.3	4.3	438.6	29.5	296.3	4.3
6998_54a	24.96956	1.31%	0.0507	0.92%	253.1	3.3	228.9	21.2	253.1	3.3
6998_53a	25.09662	1.31%	0.0505	0.83%	251.9	3.2	219.8	19.1	251.9	3.2
6998_52a	80.31040	1.44%	0.0478	1.48%	79.8	1.1	89.7	34.7	79.8	1.1
6998_51a	25.43998	1.34%	0.0502	1.13%	248.5	3.3	202.1	26.1	248.5	3.3
6998_50a	22.55055	2.94%	0.0844	1.11%	279.7	8.1	1301.2	21.4	279.7	8.1
6998_49a	82.79017	1.49%	0.0471	1.89%	77.4	1.1	54.1	44.6	77.4	1.1
6998_48a	87.68662	1.16%	0.0479	0.92%	73.1	0.8	93.0	21.6	73.1	0.8
6998_47a	75.60808	1.58%	0.0453	2.59%	84.7	1.3	0.0	20.5	84.7	1.3
6998_45a	27.02447	1.30%	0.0516	0.91%	234.2	3.0	265.7	20.7	234.2	3.0
6998_44a	26.80655	1.21%	0.0506	0.74%	236.1	2.8	224.3	17.1	236.1	2.8
6998_43a	80.09571	1.65%	0.0495	2.71%	80.0	1.3	169.9	62.2	80.0	1.3
6998_42a	81.11525	1.35%	0.0463	1.77%	79.0	1.1	13.4	41.9	79.0	1.1
6998_41a	81.01084	1.53%	0.0493	2.10%	79.1	1.2	162.2	48.5	79.1	1.2
6998_40a	82.20240	1.45%	0.0491	1.91%	77.9	1.1	151.4	44.1	77.9	1.1
6998_39a	24.28174	1.22%	0.0501	0.95%	260.2	3.1	199.5	22.0	260.2	3.1
6998_38a	78.16034	1.53%	0.0485	1.54%	82.0	1.2	125.2	35.8	82.0	1.2

(*continued on next page*)

Appendix Table 1 (*continued*)

Sample name	238U 206Pb	1 sigma % error	207Pb 206Pb	1 sigma % error	206/238 age	1 sigma err (Ma)	207/206 age	1 sigma err (Ma)	Best age	1 sigma err (Ma)
6998_37a	79.77206	1.77%	0.0459	2.54%	80.3	1.4	0.0	50.8	80.3	1.4
6998_36a	25.88857	1.16%	0.0506	0.85%	244.3	2.8	221.4	19.6	244.3	2.8
6998_35a	4.97133	1.10%	0.0799	1.97%	1181.5	11.9	1195.0	38.3	1195.0	38.3
6998_34a	83.73514	1.21%	0.0518	2.46%	76.5	0.9	274.5	55.4	76.5	0.9
6998_33a	81.28831	1.37%	0.0481	2.89%	78.8	1.1	105.1	66.9	78.8	1.1
6998_32a	32.18023	6.21%	0.0732	2.44%	197.3	12.0	1018.8	48.6	197.3	12.0
6998_30a	26.59892	1.22%	0.0507	2.08%	237.9	2.8	226.6	47.3	237.9	2.8
6998_31a	67.91819	1.19%	0.0474	2.32%	94.2	1.1	70.9	54.3	94.2	1.1
6998_29a	25.74675	1.52%	0.0575	1.95%	245.6	3.7	509.0	42.4	245.6	3.7
6998_28a	26.11466	1.14%	0.0514	2.07%	242.2	2.7	257.0	46.8	242.2	2.7
6998_27a	27.02570	1.07%	0.0511	2.05%	234.2	2.5	246.4	46.6	234.2	2.5
6998_26a	27.09480	1.04%	0.0516	2.10%	233.6	2.4	268.7	47.5	233.6	2.4
6998_25a	25.10816	1.11%	0.0528	2.00%	251.8	2.7	321.4	44.8	251.8	2.7
6998_24a	18.28146	1.04%	0.0532	2.04%	343.3	3.5	336.5	45.6	343.3	3.5
6998_23a	42.05353	5.41%	0.0640	2.50%	151.5	8.1	742.8	52.0	151.5	8.1
6998_22a	27.81577	1.99%	0.0648	2.11%	227.7	4.4	766.5	43.8	227.7	4.4
6998_21a	77.41532	1.77%	0.0527	2.83%	82.7	1.5	317.9	63.1	82.7	1.5
6998_20a	30.27692	1.78%	0.0550	1.50%	209.5	3.7	411.4	33.2	209.5	3.7
6998_19a	12.85960	0.80%	0.0617	1.32%	482.8	3.7	663.6	28.0	482.8	3.7
6998_18a	24.55594	0.73%	0.0527	1.53%	257.3	1.8	316.6	34.4	257.3	1.8
6998_17a	72.00766	0.93%	0.0513	2.02%	88.9	0.8	253.0	45.7	88.9	0.8
6998_16a	57.46290	0.88%	0.0517	1.75%	111.2	1.0	271.9	39.5	111.2	1.0
6998_15a	29.47579	0.61%	0.0522	1.34%	215.1	1.3	296.2	30.2	215.1	1.3
6998_14a	59.13702	0.81%	0.0603	1.67%	108.1	0.9	615.7	35.6	108.1	0.9
6998_13a	27.16577	0.76%	0.0536	1.43%	233.0	1.7	354.3	31.9	233.0	1.7
6998_12a	3.40410	0.66%	0.1082	1.29%	1660.3	9.6	1768.7	23.4	1768.7	23.4
6998_10a	78.11313	1.14%	0.0478	2.40%	82.0	0.9	87.6	56.0	82.0	0.9
6998_11a	20.51080	1.01%	0.0600	1.32%	306.9	3.0	601.8	28.3	306.9	3.0
6998_9a	72.69891	1.83%	0.0555	3.50%	88.1	1.6	432.3	76.1	88.1	1.6
6998_8a	28.07386	1.14%	0.0522	1.57%	225.6	2.5	292.2	35.4	225.6	2.5
6998_6a	56.49589	0.92%	0.0497	1.92%	113.1	1.0	178.7	44.1	113.1	1.0
6998_5a	85.30191	0.86%	0.0497	1.71%	75.1	0.6	183.3	39.3	75.1	0.6
6998_4a	10.28615	1.10%	0.0611	0.87%	598.1	6.3	643.0	18.5	598.1	6.3
6998_3a	57.96549	1.49%	0.0524	2.18%	110.3	1.6	302.0	49.0	110.3	1.6
6998_2a	78.81694	1.53%	0.0485	2.09%	81.3	1.2	125.9	48.5	81.3	1.2
6998_1a	77.98256	1.38%	0.0495	1.66%	82.1	1.1	170.8	38.4	82.1	1.1

References

Amelin, Y., Lee, D.-C., Halliday, A.N., 2000. Early-middle Archaean crustal evolution deduced from Lu–Hf and U–Pb isotopic studies of single zircon grains. Geochimica et Cosmochimica Acta 64, 4205–4225.

Aspden, J.A., McCourt, W.J., Brook, M., 1987. Geometrical control of subduction-related magmatism: the Mesozoic and Cenozoic plutonic history of Western Colombia. Journal of the Geological Society 144 (6), 893–905.

Ayala-Calvo, C., Bayona, G., Ojeda-Marulanda Cardona, A., Valencia, V., Padrón, C.E., Yoris, F., Mesa-Salamanca, J., García, A., 2010. Stratigraphy and provenance of Campanian-Paleogene units in Cesar sub-basin: contributions to the regional tectonic evolution. Geologia Colombiana 34, 1–34.

Bahlburg, H., Vervoort, J., DuFrane, S.A., Bock, B., Augustsson, C., 2009. Timing of crust formation and recycling in accretionary orogens: insights learned from the western margin of South America. Earth-Science Reviews 97, 227–253.

Bayona, G., Cortes, M., Jaramillo, C., Ojeda, G., Aristizabal, J., Reyes-Harker, A., 2008. An integrated analysis of an orogen-sedimentary basin pair: latest Cretaceous-Cenozoic evolution of the linked Eastern Cordillera orogen and the Llanos foreland basin of Colombia. Geological Society of America Bulletin 120, 1171–1197.

Bayona, G., Montes, C., Cardona, A., Jaramillo, C., Ojeda, G., Valencia, V., 2011. Intraplate subsidence and basin filling adjacent to an oceanic arc-continental collision; a case from the southern Caribbean–South America plate margin. Basin Research 23. http://dx.doi.org/10.1111/j.1365-2117.2010.00495.x.

Bayona, G., Cardona, A., Jaramillo, C., Montes, C., Mora, A., 2012. Effects of Paleogene Subduction on Basin Segmentation and Oil Migration in NW South America. XI Simposio Bolivariano de Exploración Petrolera en cuencas subandinas. Cartagena. Resúmenes.

Bayona, G., Montes, C., Cardona, A., Jaramillo, C., Ojeda, G., Valencia, V., Ayala-Calvo, C., in press. Intraplate subsidence and basin filling adjacent to an oceanic arc-continent collision: a case from the Southern Caribbean South America plate margin. Basin Res. http://dx.doi.org/10.1111/j.1365-2117.2010.00495.x.

Brown, G.C., Thorpe, R.S., Webb, P.C., 1984. The geochemical characteristics of granitoids in contrasting arcs and comments on magma genesis. Journal of the Geological Society of London 141, 413–426.

Buchs, D.M., Arculus, P.O., Baumgartner, P.O., Baumgartner-Mora, C., Ulianov, A., 2010. Late Cretaceous Arc development on the SW margin of the Caribbean Plate: insights from the Golfito, Costa Rica, and Azuero, Panama, complexes. Geochemistry, Geophysics, Geosystems 11, Q07S24. http://dx.doi.org/10.1029/2009GC002901 (Theme "Central American Subduction System").

Bürgl, H., 1961. Historia Geológica de Colombia Revista de la Academia Colombiana De Ciencias Exactas. Físicas y Naturales 1, 137–191.

Burke, K., 1988. Tectonic evolution of the Caribbean. Annual Reviews on Earth and Planetary Science 16, 201–230.

Bustamante, A., Juliani, C., Hall, C.M., Essene, E.J., 2011. 40Ar/39Ar ages from blueschists of the Jambalo region, Central Cordillera of Colombia: implications for the styles of accretion in the Northern Andes. Geológica Acta 9, 351–362.

Cardona, A., Valencia, V., Bayona, G., Jaramillo, C., Ojeda, G., Ruiz, J., 2009. U/ Pb LA-MC-ICP-MS zircon geochronology and geochemistry from a post-collisional biotite granite of the Baja Guajira basin, Colombia: implications for Late Cretaceous and Neogene Caribbean–South America tectonics. Journal of Geology 117, 685–692.

Cardona, A., Valencia, V., Bustamante, C., García-Casco, A., Ojeda, G., Ruiz, J., Saldarriaga, M., Weber, M., 2010. Tectonomagmatic setting and provenance of the Santa Marta Schists, Northern Colombia: insights on the growth and approach of Cretaceous Caribbean oceanic terranes to the South American continent. Journal of South American Earth Sciences 29, 784–804.

Cardona, A., Valencia, V., Bayona, G., Duque, J., Ducea, M., Gerhels, G., Jaramillo, C., Montes, C., Ojeda, G., Ruiz, J., 2011. Early subduction orogeny in the Northern Andes: Turonian to Eocene magmatic and provenance record in the Santa Marta massif and Rancheria Basin, Northern Colombia. Terranova 23, 26–34.

Cawood, P.A., Kröner, A., Collins, W.J., Kusky, T.D., Mooney, W.D., Windley, B.F., 2009. Accretionary orogens through Earth history. In: Cawood, P.A., Kröner, A. (Eds.), Earth accretionary systems in space and time: Geological Society, London, Special Publications, 318, pp. 1–36.

Cerón, J., Kellogg, J., Ojeda, G.Y., 2007. Basement configuration of the northwestern South America-Caribbean margin from recent geophysical data. Ciencia, Tecnología y Futuro 3, 25–49.

Chang, Z., Vervoort, J.D., McClelland, W.C., Knaack, C., 2006. U–Pb dating of zircon by LA-ICP-MS. Geochemistry, Geophysics, Geosystems 7, 1–14.

Chappell, B.W., White, A.J.R., 1992. I- and S- type granites in the Lachlan Fold belt. Transactions of the Royal Society of Edinburgh: Earth Science 83, 1–26.

Charlton, T.R., 1991. Postcollision extension in arc-continent collision zones, eastern Indonesia. Geology 19, 28–31.

Chew, D.M., Daly, J.S., Magna, T., Page, L.M., Kirkland, C.L., Whitehouse, M.J., Lam, R., 2010. Timing of ophiolite obduction in the Grampian Orogen. Geological Society of America Bulletin 165, 675–685.

Clift, P.D., Carter, A., Krol, M., Kirby, E., 2002. Constraints on India-Eurasia Collision in the Arabian Sea Region taken from the Indus Group, Ladakh Himalaya, India. In: Clift, P.D., Kroon, D., Craig, J., Gaedicke, C. (Eds.), The Tectonic and Climatic Evolution of the Arabian Sea Region: Geological Society of London special publication, 195, pp. 97–116.
Clift, P.D., Lin, A.T.S., Carter, A., Wu, F., Draut, A.E., Lai, T.-H., Fei, L.-Y., Schouten, H., Teng, L., 2008. Orogenic collapse in the Ilan Plain Basin of northern Taiwan. In: Draut, A.E., Clift, P.D., Scholl, D.W. (Eds.), Sedimentation in arc collisional settings: Geological Society of America, special paper, 436, pp. 257–278.
Clift, P.D., Carter, A., Draut, A.E., Hoang, V.L., Chew, D., Schouten, H.A., 2009. Detrital U–Pb Zircon dating of Lower Ordovician syn-arc-continent collision conglomerates in the Irish Caledonides. Tectonophysics 479, 165–174. http://dx.doi.org/10.1016/j.tecto.2008.07.018.
Corfu, F., Hanchar, J.M., Hoskin, P.W.O., Kinny, P., 2003. Atlas of zircon textures. Reviews in Mineralogy and Geochemistry 53, 469–500.
Cox, K., Bell, J., Pankhurst, R., 1979. The interpretation of igenous rocks. George Allen and Inwin, London. 445 pp.
Cutts, K.A., Hand, M., Kelsey, D.E., Strachan, R.A., 2011. P–T constraints and timing of Barrovian metamorphism in the Shetland Islands, Scottish Caledonides: implications for the structural setting of the Unst ophiolite. Journal of the Geological Society 168, 1265–1284. http://dx.doi.org/10.1144/0016-76492010-165 (December).
Dávila, F.M., Astini, R.A., 2007. Cenozoic provenance history of synorogenic conglomerates in western Argentina (Famatina Belt): implications for Central Andean foreland development. Geological Society of America Bulletin 119, 609–622.
DeGraaff–Surpless, K., Wooden, J.L., McWilliams, M.O., 2002. Detrital zircon Provenance analysis of the Great Valley Group, California; Evolution of an arc–forearc system. Geological Society of America Bulletin 114, 1564–1580.
Dewey, J.F., 2005. Orogeny can be very short. PNAS 102, 15286–15293.
Dewey, J.F., Mange, M.A., 1999. Petrography of Ordovician and Silurian sediments in the western Irish Caledonides: tracers of a short-lived Ordovician continent–arc collision orogeny and the evolution of the Laurentian Appalachian–Caledonian margin. In: Mac Niocaill, C., Ryan, P.D. (Eds.), Continental Tectonics: Geological Society, London, Special Publications, 164, pp. 55–107.
Dickinson, W.R., 1985. Interpreting provenance relations from detrital modes of Sandstones. In: Zuffa, G.G. (Ed.), Provenance of Arenites, pp. 333–361.
Dickinson, W.R., Gehrels, G.E., 2003. U–Pb ages of detrital zircons from Permian and Jurassic eolian sandstones of the Colorado Plateau, USA; paleogeographic implications. Sedimentary Geology 163, 29–66.
Dueñas, H., Gómez, C., 2011. Bioestratigrafía y paleogeografía de la Formación Cansona (Quebrada Peñitas, región Caribe colombiana). Memorias XIV Congreso Latinoamericano de Geología y XIII Congreso Colombiano de Geología, Medellín, p. 361.
Dufrane, S.A., Vervoort, J.D., Hart, G.L., 2007. Unertainty of Hf isotope analysis in zircon using LA-MC-ICPMS techniques: full disclosure. 17th annual V.M. Goldschmidt Conference, Cologne, Germany, August 2007. Geochimica et Cosmochimica Acta 71, A241.
Dupuis, C., Malo, M., Bédar, J., Davis, B., Villeneuve, M., 2009. A lost arc-back-arc terrane of the Dunnage oceanic tract recorded in clasts from the Garin Formation and McCrea mélange in the Gaspé Appalachians of Québec. Geological Society of America Bulletting 121, 17–38.
Duque-Caro, H., 1968. Observaciones generales a la bioestratigrafía y geología regional en los departamentos de Bolivar y Cordoba. Boletín de Geología, 24. Universidad Industrial, Santander, pp. 71–87.
Duque-Caro, H., 1972. Ciclos Tectónicos y Sedimentarios en el norte de Colombia y sus relaciones con la Paleoecología. Boletín Geológico, 19, 3. Ingeominas, pp. 1–23.
Duque-Caro, H., 1979a. Major structural elements and evolution of northwestern Colombia. In: Watkins, J.S., Montadert, L., Dickerson, P.W. (Eds.), Geological and geophysical investigations of continental margins: America Association of Petroleum Geologist, Memoir, 29, pp. 329–351.
Duque-Caro, H., 1979b. Major structural elements and evolution of Northwestern Colombia. In: Watkins, J.S., Montadert, L., Dickerson, P.W. (Eds.), Geological and -Geophysical Investigations of Continental Margins: American Association of Petroleum Geologist Memoir, 29, pp. 239–351.
Duque-Caro, H., 1980. Geotectónica de la Región Noroccidental Colombiana. Boletín de Geología Ingeominas 23, 4–37.
Duque-Caro, H., 1984. Structural style, diapirism and accretionary episodes of the Sinu-San Jacinto terrane, southwestern Caribbean borderland. In: Bonini, W.E., Hargraves, R.B., Shagam, R. (Eds.), The Caribbean–South American plate boundary and regional tectonics: Geological Society of America Memoir, 162, pp. 303–316.
Duque-Caro, H., Guzmán, G., Hernández, R., 1996. Geología de la Plancha 38–Carmen de Bolívar. INGEOMINAS, Bogotá, p. 45.
Eggins, S.M., Kinsley, L.P.J., Shelly, J.M.G., 1998. Deposition and elemental fractionation processes during atmospheric pressure laser ablation sampling for analysis by ICP-MS. Applied Surface Science 127, 278–286.
Escalona, A., Mann, P., 2010. Tectonics, basin subsidence mechanism and paleogeography of the Caribbean-South American plate boundary zone. Marine and Petroleum Geology 28, 8–39.
Escalona, A., Mann, P., 2011. Tectonics, basin subsidence mechanisms, and paleogeography of the Caribbean–South American plate boundary zone. Marine and Petroleum Geology 28, 8–39. http://dx.doi.org/10.1016/j.marpetgeo.2010.01.016.
Ferguson, R., Hoey, T., Wathen, S., Werritty, A., 1996. Field evidence for rapid downstream fining of river gravels through selective transport. Geology 24, 179–182.
Fitton, J.G., Saunders, A.D., Norry, M.J., Hardarson, B.S., Taylor, R.N., 1997. Thermal and chemical structure of the Iceland plume. Earth and Planetary Science Letters 153, 197–208.
Flinch, J.F., 2003. Structural evolution of the Sinú-Lower Magdalena Area (Northern Colombia). In: Bartolini, C., Buffl er, R.T., Blickwede, J. (Eds.), The circum-Gulf of Mexico and the Caribbean: hydrocarbon habitats, basin formation, and plate tectonics: AAPG Memoir, 79, pp. 776–796.
Folk, R., 1980. Petrology of Sedimentary Rocks. Hemphill Publishing Co(184 pp.).
Foster, D.A., Gray, D.R., Spaggiari, C., Kamenov, G., Bierlein, F.P., 2009. Palaeozoic Lachlan Orogen, Australia; accretion and construction of continental crust in a marginal ocean setting: isotopic evidence from Cambrian metavolcanic rocks. In: Cawood, P.A., Kroner, A. (Eds.), Earth Accretionary Systems in Space and Time: Geological Society, London, Special Publications, 318, pp. 329–349. http://dx.doi.org/10.1144/SP318.12.
Gehrels, G., Valencia, V., Pullen, A., 2006. Detrital zircon geochronology by Laser-Ablation Multicollector ICPMS at the Arizona LaserChron Center. In: Olszewski, T.D. (Ed.), Geochronology Emerging Opportunities, vol. 12. Paleontological Society, pp. 67–76.
Geotec, 1997. Cartografía geológica de la Región del Sinú (Noroeste de Colombia). Planchas 50, 51, 59, 60, 61, 69, 70, 71, 79 y 80., 3 volúmenes (Bogotá).
Gibbons, W., 1994. Suspect terranes. In: Hackock, P. (Ed.), Continental deformation. Pergamon Press, pp. 305–319.
Gomez, E., Jordan, T., Allmendinger, R.W., Hegarty, K., Kelley, S., 2005. Syntectonic Cenozoic sedimentation in the northern middle Magdalena Valley Basin of Colombia and implications for exhumation of the Northern Andes. Geological Society of America Bullettin 117, 547–569.
Gray, D.R., Foster, D.A., Maas, R., Spaggiari, C.V., Gregory, R.T., Goscombe, B., Hoffmann, K.H., 2007. Continental growth and recycling by accretion of deformed turbidite fans and remnant ocean basins: examples from Neoproterozoic and Phanerozoic orogens. In: Hatcher Jr., R.D., Carlson, M.P., McBride, J.H., Martínez Catalán, J.R. (Eds.), 4-D Framework of Continental Crust: Geological Society of America Memoir, 200. http://dx.doi.org/10.1130/2007.1200(05).
Gurnis, M., Hall, C.H., Lavier, L., 2004. Evolving force balance during incipient subduction. Geochemisty, Geophysics and Geosystems 5, vQ07001. http://dx.doi.org/10.1029/2003GC000681.
Guzmán, G., 2007, Stratigraphy and sedimentary environment and implicationsin the Plato basin and the San Jacinto belt, northwestern Colombia. [Ph.D.Thesis], University of Liège, Belgium, 275 p.
Guzman, G., Gómez, E., Serrano, B. E., 2004. Geología de los cinturones del Sinú, San Jacinto y borde Occidental del Magdalena, Caribe Colombiano. Escala 1:500.000. INGEOMINAS. 134p.
Hall, R., 2002. Cenozoic geological and plate tectonic evolution of SE Asia and the SW Pacific: computer-based reconstructions, model and animations. Journal of Asian Earth Sciences 20, 353–431.
Hastie, A.R., Kerr, A.C., Pearce, J.A., Mitchell, S.F., 2007. Classification of altered volcanic island arc rocks using immobile trace elements: development of the Co-Th discrimination diagram. Journal of Petrology 48, 2341–2357.
Hastie, A.R., Ramsook, R., Mitchell, S.F., Kerr, A.C., Millar, I.L., Mark, D.F., 2010. Geochemistry of Compositionally Distinct Late Cretaceous Back-Arc Basin Lavas: Implications for the Tectonomagmatic Evolution of the Caribbean Plate. Journal of Geology 118, 655–676.
Horton, B.K., Saylor, J.E., Nie, J., Mora, A., Parra, M., Reyes-Harker, A., Stockli, 2010. Linking sedimentation in the northern Andes to basement configuration, Mesozoic extension, and Cenozoic shortening: Evidence from detrital zircon U-Pb ages, Eastern Cordillera, Colombia. Geological Society of America Bulletin 123, 1423–1442.
Howard, J.L., 1993. The statistics of counting clasts in rudites: a review, with examples from the upper Palaeogene of southern California, USA. Sedimentology 40, 157–174.
Hughes, R.A., Pilatasig, L.F., 2002. Cretaceous and Tertiary terrane accretion in the Cordillera Occidental of the Andes of Ecuador. Tectonophysics 345, 29–48.
Hutchison, A.R., Oliver, G.J.H., 1998. Garnet provenance studies, juxtaposition of Laurentian marginal terranes and timing of the Grampian Orogeny in Scotland. Journal of the Geological Society of London 155, 541–550.
Ibañez-Mejia, M., Tassinari, C.C.G., Jaramillo-Mejia, J.M., 2007. U–Pb zircon ages of the "Antioquian Batholith". Geochronological constraints of Late Cretaceous magmatism in the Central Andes of Colombia: 11th Colombian Geological Congress, extended abstracts, 11.
Ibañez-Mejía, M., Vinasco, C., Cardona, A., Valencia, V., Weber, M., 2010. Permian–Triassic orogenesis in the northern andes: a record of arc magmatism, accretion, anatexis and relaxation of a continental terrane in the Proto-Andes in the wake of Pangea. Geological Society of America, Annual meeting, p. 197-1 (Paper).
Ingersoll, R.V., Graham, S.A., Dickinson, W.R., 1995. Remnant ocean basins. In: Busby, C.J., Ingersoll, R.V. (Eds.), Tectonics of Sedimentary Basins: Cambridge. Blackwell Science, Massachusetts, pp. 363–391.
Ingersoll, R.V., Dickinson, W.R., Graham, S.A., 2003. Remnant-ocean submarine fans: largest sedimentary systems on Earth. In: Chan, M.A., Archer, A.W. (Eds.), Extreme Depositional Environments: Mega End Members in Geologic Time: Geol. Soc. Am. Spec. Pap., 370, pp. 191–208.
Jaillard, E., Bengtson, P., Ordoñez, M., Vaca, W., Dhondt, A., Suarez, J., Toro, J., 2008. Sedimentary record of terminal Cretaceous accretions in Ecuador: the Yunguilla Group in the Cuenca area. Journal of South American Earth Sciences 25, 133–144.
Jaillard, E., Lapierre, H., Ordoñez, M., Toro-Alava, J., Amórtegui, A., Vanmelle, J., 2009. Accreted oceanic terranes in Ecuador: southern edge of the Caribbean plate? In: James, K.H., Lorente, M.A., Pindell, J. (Eds.), The origin and evolution of the Caribbean plate: Geol. Soc. Lond. Spec. Publ., 328, pp. 469–485.
Jarrard, R.D., 1986. Terrane motion by strike-slip faulting of forearc slivers. Geology 14, 780–783.
Kennan, L., Pindell, J., 2009. Dextral shear, terrane accretion and basin formation in the Northern Andes: best explained by interaction with a Pacific-derived Caribbean Plate? In: James, K.H., Lorente, M.A., Pindell, J. (Eds.), The Origin and Evolution of the Caribbean Plate: Geological Society of London, Special Publication, 328, pp. 487–532.
Kerr, A.C., Marriner, G.F., Tarney, J., Nivia, A., Saunders, A.D., Thirlwall, M.F., Sinton, C.W., 1997. Cretaceous basaltic terranes in western Colombia: elemental, chronological and Sr-Nd constraints on petrogenesis. Journal of Petrology 38, 677–702.

Kerr, A.C., White, R.V., Thompson, P.M.E., Tarney, J., Saunders, A.D., 2003. No oceanic plateau – no Caribbean Plate? The seminal role of anoceanic plateau in Caribbean plate evolution. In: Bartolini, C., Buffler, R.T., Blickwede, J. (Eds.), The Gulf of Mexico and Caribbean Region: Hydrocarbon Habitats, Basin Formation and Plate Tectonics: America Association of Petroleum Geologist, Memoir, 79, pp. 126–168.

Kerr, A.C., Pearson, D.G., Nowell, G.M., 2009. Magma source evolution beneath the Caribbean oceanic plateau: New insights from elemental and Sr-Nd-Pb-Hf isotopic studies of ODP Leg 165 Site 1001 basalts. In: James, K., Lorente, M.A., Pindell, J.L. (Eds.), The Origin and Evolution of the Caribbean Plate: Special Publication of the Geological Society of London, 328, pp. 805–824.

Kosler, J., Sylvester, P., 2003. Present trends and the future of zircon in geochronology: laser ablation ICPMS. Reviews in Mineralogy and Geochemistry 53, 243–275.

Kusky, T.M., Bradley, D.C., Haeussler, P., Karl, S., 1997. Controls on accretion of flysch and melange belts at convergent margins: evidence from Chugach Bay thrust and Iceworm Melange, Chugach Terrane, Alaska. Tectonics 16, 855–878.

Lamus-Ochoa, F., Bayona, G., Cardona, A., Montenegro, O., Mora, A., Caballero, V., Moreno, N., 2012. Aproximación a la proveniencia sedimentaria de unidades Paleógenas de la Cordillera Oriental mediante el uso de minerales pesados. XI Simposio Bolivariano de Exploración Petrolera en cuencas subandinas. Cartagena. Resúmenes.

Leal-Mejía, I., 2011. Phanerozoic gold metallogeny in the Colombian andes: a tectonomagmatic approach. PhD Thesis, University of Barcelona, Spain. 1000p.

Ludwig, K.J., 2007. Isoplot 3.62. Special Publication. Berkeley Geochonology Center, Berkeley (70 pp.).

Luzieux, L.D.A., Heller, F., Spikings, R., Vallejo, C.F., Winkler, W., 2006. Origin and Cretaceous tectonic history of the coastal Ecuadorian forearc Between 1°S-4°S: paleomagnetic, radiometric and fossil evidence. Earth Planet. Science Letters 249, 400–414.

Macpherson, C.G., 2008. Lithosphere erosion and crustal growth in subduction zones: insights from initiation of the nascent East Philippine Arc. Geology 36, 311–314.

Mange, M.A., Maurer, H., 1991. Heavy Minerals in Colour. Springer-Verlag.

Mange, M., Idleman, B., Yin, Q.-Z., Hidacke, H., Dewey, J., 2010. Detrital heavy minerals, white mica and zircon geochronology in the Ordovician South Mayo Trough, western Ireland: signatures of the Laurentian basement and the Grampian orogeny. Journal of the Geological Society of London 167, 1147–1160.

Mantilla-Pimiento, A., Jentzsch, G., Kley, J., Pava, A., 2009. Configuration of the Colombia Caribbean Margin: Constraints from 2D seismic Reflection data Potencial Fields Interpretation. In: Lallemand, S., Funiciello, F. (Eds.), Subduction Zone Geodynamics. Springer- Verlag, Berlin Heidelberg, pp. 247–272. http://dx.doi.org/10.1007/978-3-540-87974-9.

Marresh, W.V., Kluge, R., Baumann, A., Pindell, J.L., Kru¨ ckhans-Lueder, G., Stanek, K., 2009. The occurrence and timing of high-pressure metamorphism on Margarita Island, Venezuela: a constraint on Caribbean–South American interaction. In: James, K.H., Lorente, M.A., Pindell, J. (Eds.), The Geology and Evolution of the Region Between North and South America: Geological Society of London. Special Publication, 328, pp. 705–742.

Marsaglia, K.M., 2003. Sandstone detrital modes support Magdalena fan displacement from mouth of Gulf of California. Geology 32, 45–48.

Martens, U., Restrepo, J.J., Ordoñez, U., 2011. In–situ U/Pb geochronology reveals distinct crustal domains in the western flank of Colombia's Central Cordillera. Memorias XIV Congreso Latinoamericano de Geología y XIII Congreso Colombiano de Geología, Medellín, 322.

McCourt, W.J., Feininger, T., Brook, M., 1984. New geological and geochronological data from the Colombian Andes: continental growth by multiple accretion. Journal of the Geological Society of London 141, 831–845.

Miyashiro, A., 1972. Pressure and temperature conditions and tectonic significance of regional and ocean floor metamorphism. Tectonophysics 13, 141–159.

Montes, C., Hatcher, R.D., Restrepo-Pace, P., 2005. Tectonic reconstruction of the northern Andean blocks: oblique convergence and rotations derived from the kinematics of the Piedras-Girardot area, Colombia. Tectonophysics 399, 221–250.

Montes, C., Guzmán, G., Bayona, G., Cardona, A., Valencia, V., Jaramillo, C., 2010. Clockwise rotation of the Santa Marta Massif and simultaneous paleogene to neogene deformation of the Plato-San Jorge and Cesar-Ranchería Basins. Journal of South American Earth Sciences 29, 832–848.

Mora, A., Horton, B.K., Mesa, A., Rubiano, J., Ketcham, R.A., Parra, M., Blnaco, V., García, D., Stockli, 2010. Migration of Cenozoic deformation in the Eastern Cordillera of Colombia interpreted from fission track results and structural relationships: implications for petroleum systems. American Association of Petroleum Bulletin 94, 1543–1580.

Müller, R.D., Royer, J.-Y., Cande, S.C., Roest, W.R., Maschenkov, S., 1999. New constraints on the Late Cretaceous-Tertiary Plate tectonic evolution of the Caribbean. In: Mann, P. (Ed.), Caribbean Basins: Sedimentary Basins of the World, 4. Elsevier Science, Amsterdam, pp. 33–59.

Neill, I., Kerr, A.C., Hastie, A., Stanek, K.-P., Millar, I.L., 2011. Origin of the Aves Ridge and Dutch–Venezuelan Antilles: interaction of the Cretaceous "Great Arc" and Caribbean-Colombian Oceanic Plateau? Journal of the Geologycal Society, London 168, 333–347.

Nivia, A., Marrimer, G.F., Kerr, A.C., Tarney, J., 2006. The Quebradagrande Complex: A Lower Cretaceous ensialic marginal basin in the Central Cordillera of the Colombian Andes. Journal of South American Earth Sciences 21, 423–436.

Oliver, G.J.H., 2001. Reconstruction of the Grampian episode in Scotland: its place in the Caledonian Orogeny. Tectonophysics 332, 23–49.

Onishi, C.T., Kimura, G., 1995. Melange fabric and relative convergence in subduction zones. Tectonics 4, 1273–1289.

Ordóñez-Carmona, O., Pimentel, M.M., 2002. Rb-Sr and Sm-Nd isotopic study of the Puquí complex, Colombian Andes. Journal of South American Earth Sciences 15 (2), 173–182.

Ostos, M., Sisson, V.B., 2005. Geochemistry and tectonic setting of igneous and metaigneous rocks of northern Venezuela. In: Avé Lallemant, H.G., Sisson, V.B. (Eds.), Caribbean/ South American plate interactions, Venezuela: Geological Society of America Special Publication, 394, pp. 119–155.

Paces, J.B., Miller, J.D., 1993. Precise U–Pb ages of Duluth Complex and related mafic intrusions, northeastern Minnesota: geochronological insights to physical, petrogenetic, paleomagnetic, and tectonomagmatic process associated with the Ga Midcontinent Rift System. Journal of Geophysical Research 98, 13997–14013.

Parra, M., Mora, A., Sobel, E.R., Strecker, M.R., González, R., 2009. Episodic orogenic front migration in the northern Andes: constraints from low- temperature thermochronology in the Eastern Cordillera, Colombia. Tectonics 28, TC4004. http://dx.doi.org/10.1029/2008TC002423.

Pearce, J.A., Harris, N.B.W., Tindle, A.G., 1984. Trace element discrimination diagrams for the tectonic interpretation of granitic rocks. Journal of Petrology 25, 956–983.

Pearce, J.A., 1996. A user's guide to basalt discrimination diagrams. Geological Association of Canada, Short Course Notes 12, 79–113.

Pearce, J.A., Peate, D.W., 1995. Tectonic implications of the composition of volcanic arc magmas. Annual Reviews Earth Sciences 23, 251–285.

Pindell, J.L., 1993. Evolution of the Gulf of Mexico and the Caribbean: An Introduction. In: Donovan, S.K., Jackson, T.A. (Eds.), University of the West Indies Publisher's Association Caribbean Geology, pp. 13–39.

Pindell, J., Kennan, L., 2009. Tectonic evolution of the Gulf of Mexico, Caribbean and northern South America in the mantle reference frame: an update. In: James, K.H., Lorente, M.A., Pindell, J. (Eds.), The Origin and Evolution of the Caribbean Plate: Geol. Soc. [Lond.] Spec. Publ., 328, pp. 1–56.

Pindell, J.L., Higgs, R., Dewey, J.F., 1998. Cenozoic palinspastic reconstruction, paleogeographic evolution, and hydrocarbon setting of the northern margin of South America. In: Pindell, J.L., Drake, C.L. (Eds.), Paleogeographic Evolution and Non-Glacial Eustasy, Northern South America: SEPM Special Publication, 58, pp. 45–86.

Pindell, J., Kennan, L., Maresch, W.V., Stanek, K.-P., Draper, G., Higgs, R., 2005. Plate kinematic and crustal dynamics of circum-Caribbean arc- Continent interactions: tectonics controls on basin development in the Proto- Caribbean margins. In: Avé Lallemant, H.G., Sisson, V.B. (Eds.), Caribbean–South American Plate Interactions: Geological Society of America Special Paper, 394, pp. 7–52.

Restepo-Moreno, S., Foster, D.A., Kamenov, G., 2007. Formation age and magma sources for the Antioqueño Batholith derived from LA-ICP-MS Uranium–Lead dating and Hafnium-isotope analysis of zircon grains. Geological Society of America, Annual Meeting, Abstracts, p. 181-28 (Paper).

Restrepo-Moreno, S.A., Foster, D.A., Stockli, D.F., Parra-Sánchez, L.-N., 2009. Long-term erosion and exhumation of the Altiplano Antioqueño, Northern Andes (Colombia) from apatite (U–Th) /He thermochronology. Earth and Planetary Science Letters 278, 1–12.

Rincón, D., Arenas, J.E., Cuartas, C.H., Cárdenas, A.L., Molinares, C.E., Caicedo, C., Jaramillo, C., 2007. Eoocene–Pliocene planktonic foraminifera biostratigraphy from the continental margin of the southwest Caribbean. Stratigraphy 4, 261–311.

Rollinson, H.R., 1993. Using Geochemical Data: Evaluation, Presentation Interpretation. Prentice Hall, Singapore. 352 pp.

Rubio, M.A., Herrera, J.M., Navarrete, R.E., Bermudez, H.D., Calderón, J.E., Parra, F.J., Sarmiento, G., Vega, F., Perrilliat, 2009. Cartografía geológica, levantamiento de columnas estratigráficas, toma de muestras y análisis. Sector de Chalán (Cuenca Sinú-San Jacinto). Informe Agencia Nacional de Hidrocarburos 93 pp.

Shervais, J.W., 1982. Ti–V plots and the petrogenesis of modern and ophiolitic lavas. Earth and Planetary Science Letters 59, 101–118.

Sisson, V.B., Avá Lallemant, H.G., Ostos, M., Blythe, A.E., Snee, L.W., Copeland, P., Wright, J.E., Donelick, R.A., Guth, L.R., 2005. Overview of radiometric ages in three allochthonous belts of northern Venezuela: Old ones, new ones, and their impact on regional geology. In: Avé Lallemant, H.G., Sisson, V.B. (Eds.), Caribbean–South American Plate Interactions, Venezuela: Geological Society of America Special Paper, 394, pp. 91–118.

Snyder, D.B., Clowes, R.M., Cook, F.A., Erdmer, P., Evenchich, C.A., Van Der Velden, A.J., Hall, K.W., 2002. Proterozoic prism arrests suspect terranes: insights into the ancient Cordilleran margin from seismic reflection data. GSA Today 12, 4–9.

Spadea, P., Espinosa, A., 1996. Petrology and chemistry of late Cretaceous volcanic rocks from the southernmost segment of the Western Cordillera of Colombia (South America). Journal of South American Earth Sciences. 9, 79–90.

Spear, F.S., 1995. Metamorphic phase equilibria and pressure-temperature-time paths. Mineralogical Society of America Monograph. (Second printing. 799 pp.).

Spikings, R.A., Winkler, W., Seward, D., Handler, R., 2001. Along-strike variations in the thermal and tectonic response of the continental Ecuadorian Andes to the collision with heterogeneous oceanic crust. Earth and Planetary Science Letters 186, 57–73.

Spikings, R.A., Winkler, W., Hughes, R.A., Handler, R., 2005. Thermochronology of Allochthonous Terranes in Ecuador: unraveling the accretionary and post- accretionary history of the Northern Andes. Tectonophysics 399, 195–220.

Sun, S.S., McDonough, W.F., 1989. Chemical and isotopic systematics of oceanic basalts: implications for mantle composition and processes. In: Saunders, A.D., Norry, M.J. (Eds.), Magmatism in the Ocean Basins: Geological Society, Special Publication, 42, pp. 313–345.

Teng, L.S., 1996. Extensional collapse of the northern Taiwan mountain belt. Geology 24, 949–952.

Thompson, P.M.E., Kempton, P.D., White, R.V., Saunders, A.D., Kerr, A.C., Tarney, J., Pringle, M.S., 2004. Elemental, Hf–Nd isotopic and geochronological constraints on an island arc sequence associated with the Cretaceous Caribbean plateau: Bonaire, Dutch Antilles. Lithos 74, 91–116.

Toto, E., Kellogg, J., 1992. Structure of the Sinú-San Jacinto fold belt: an active accretionary prism in northern Colombia. Journal of South American Earth Sciences 5, 211–222.

Trop, J.M., Ridgway, K.D., Spell, T.L., 2003. Synorogenic sedimentation and forearc basin development along a transpressional plate boundary, Matanuska Valley-Talkeetna Mountains, southern Alaska. In: Sisson, V.B., Roeske, S., Pavlis, T.L. (Eds.), Geology

of a transpressional orogen developed during ridge-trench interaction along the north Pacific margin: Geological Society of America Special Paper, 371, pp. 89–118.
Valencia, V.A., Ruiz, J., Barra, F., Gehrels, G., Ducea, M., Titley, S.M., Ochoa-Landin, L., 2005. U–Pb single zircon and Re-Os geochronology from La Caridad Porphyry Copper deposit: insights for the duration of magmatism and mineralization in the Nacozari District, Sonora, Mexico. Mineralium Deposita 40, 175–191.
Vallejo, C., Spikings, R.A., Winkler, W., Luzieux, L., Chew, D., Page, L., 2006. The early interaction between the Caribbean Plateau and the NW South American plate. Terra Nova 18, 264–269.
Vallejo, C., Winkler, W., Spikings, R., Luzieux, L., Heller, F., Bussy, F., 2009. Mode and timing of terrane accretion in the forearc of the Andes in Ecuador. In: Kay, S.M., Ramos, V.A., Dickinson, W.E. (Eds.), Backbone of the Americas: Shallow Subduction, Plateau Uplift, and Ridge and Terrane Collision: Geological Society of America Memoir, 204, pp. 197–216.
Van del Lelij, R., Spikings, R.A., Kerr, A.C., Kounov, A., Cosca, M., Chew, D., 2010. Thermochronology and tectonics of the Leeward Antilles: evolution of the southern Caribbean Plate boundary zone. Tectonics 29, TC6003. http://dx.doi.org/10.1029/2009TC002654.
Vervoort, J.D., Blichert-Toft, J., 1999. Evolution of the depleted mantle: Hf isotope evidence from juvenile rocks through time. Geochimica et Cosmochimica Acta 63, 533–556.
Vervoort, J.D., Patchett, P.J., 1996. Behavior of hafnium and neodymium isotopes in the crust: constraints from Precambrian crustally derived granites. Geochimica et Cosmochimica Acta 60, 3717–3733.
Vervoort, J.D., Patchett, P.J., Soderlund, U., Baker, M., 2004. Isotopic composition of Yb and the determination of Lu concentrations and Lu/Hf ratios by isotope dilution using MC-ICPMS. Geochemistry, Geophysics, Geosystems 5. http://dx.doi.org/10.1029/2004GC000721 (15 pp.).
Villagómez, D., 2010. Thermochronology, geochronology and geochemistry of the Western and Central cordilleras and Sierra Nevada de Santa Marta, Colombia: The tectonic evolution of NW South America. PhD. Thesis de l'Université de Genève. Genève. 123p.
Villagómez, D., Spikings, R., Magna, T., Kammer, A., Winkler, W., Beltrán, A., 2011. Geochronology, geochemistry and tectonic evolution of the Western and Central cordilleras of Colombia. Lithos 125, 875–896.
Vinasco, C.J., Cordani, U.G., González, H., Weber, M., Pelaez, C., 2006. Geochronological, isotopic, and geochemical data from Permo-Triassic granitic gneisses and granitoids of the Colombian Central Andes. Journal of South American Earth Sciences 21, 355–371.
Wanders, A.M., Bradshaw, J.D., Weaver, S., Maas, R., Ireland, T., Eby, N., 2004. Provenance analysis using conglomerate clast lithologies: a case study from the Pahau terrane of New Zealand. Sedimentary Geology 167, 57–89.
Weber, M.B.I., Cardona, A., Paniagua, F., Cordani, U., Sepúlveda, L., Wilson, R., 2009. The Cabo de la Vela maficultramafic complex, Northeastern Colombian Caribbean region – a record of multi stage evolution of a Late Cretaceous intra- oceanic arc. In: James, K.H., Lorente, M.A., Pindell, J.L. (Eds.), Caribbean– South American Plate Interactions, Venezuela: Geol. Soc. [Lond.] Spec. Publ., 394, pp. 549–568.
Weber, M., Cardona, A., Valencia, V., Garcia-Casco, A., Tobón, M., Zapata, S., 2010. U/Pb detrital zircon provenance from Late Cretaceous metamorphic units of the Guajira Peninsula, Colombia: tectonic implications on the collision between the Caribbean arc and the South American margin. Journal of South American Earth Sciences 29, 805–816.
Weber, M., Cardona, A., Valencia, V., Altenberger, U., López-Martinez, M., Tobón, M., Zapata, G., Concha, A.E., 2011. Geochemistry and Geochronology of the Guajira Eclogites, northern Colombia – evidence of a metamorphosed primitive Cretaceous Caribbean Island-arc. Geologica Acta 9, 425–443.
Whattam, S.A., Stern, R.J., 2011. The subduction initiation rule: a key for linking ophiolits, intra-oceanic forearcs, and subduction initiation. Contributions to Mineralogy and Petrology 162, 1031–1045.
Winchester, J.A., Floyd, P.A., 1977. Geochemical discrimination of different magma series and their differentiation products using immobile elements. Chemical Geology 20, 325–343.
Williams, I.S., 1998. U-Th-Pb geochronology by ion microprobe. Reviews in Economic Geology 7, 1–35.
Wood, D.A., 1980. The application of a Th-Hf-Ta diagram to problems of tectonomagmatic classification and to establishing the nature of crustal contamination of basaltic lavas of the British Tertiary volcanic province. Earth and Planetary Science Letters 50, 11–30.
Wright, J.E., Wyld, S.J., 2011. Late Cretaceous subduction initiation on the eastern margin of the Caribbean-Colombian Oceanic Plateau: one Great Arc of the Caribbean (?). Geosphere 7, 468–493. http://dx.doi.org/10.1130/GES00577.1.
Zimmerle, W., 1968. Serpentine greywackes from the North Coast basin, Colombia, and their geotectonic significance. Neues Jahrbuch für Mineralogie (Abhandlungen) 109, 156–182.